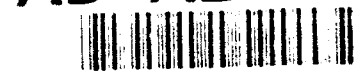

Highly Transient Elastodynamic Crack Growth in a Bimaterial Interface: Higher Order Asymptotic Analysis and Optical Experiments

by

Cheng Liu[1]
John Lambros[1]
Ares J. Rosakis[2]

CALIFORNIA INSTITUTE OF TECHNOLOGY
PASADENA, CALIFORNIA

SM Report 92-37

St-A per Dr. Rajapakse, ONR/Code 1132SM.
Arl., VA 22217.
7-6-93 JK

Highly Transient Elastodynamic Crack Growth in a Bimaterial Interface: Higher Order Asymptotic Analysis and Optical Experiments

by

Cheng Liu[1]
John Lambros[1]
Ares J. Rosakis[2]

December 20, 1992

GRADUATE AERONAUTICAL LABORATORIES
CALIFORNIA INSTITUTE OF TECHNOLOGY
PASADENA, CALIFORNIA 91125

[1]Graduate Research Assistant
[2]Associate Professor of Aeronautics and Applied Mechanics

Abstract

A higher order asymptotic analysis of the transient deformation field surrounding the tip of a crack running dynamically along a bimaterial interface is presented. An asymptotic methodology is used to reduce the problem to one of the Riemann-Hilbert type. Its solution furnishes displacement potentials which are used to explicitly evaluate the near-tip transient stress field. Crack-tip fields corresponding to crack speeds up to the lower of the two shear wave speeds are investigated. An experimental study of dynamic crack growth in PMMA/steel interfaces using the optical method of CGS and high speed photography, is also described. Transonic terminal speeds (up to $1.4c_s^{PMMA}$) and initial accelerations ($\sim 10^8 \mathrm{m/sec}^2$) are reported and discussed. Transient effects are found to be severe and more important than in homogeneous dynamic fracture. For subsonic crack growth, these experiments are used to demonstrate the necessity of employing a fully transient expression in the analysis of optical data to accurately predict the complex dynamic stress intensity factor history.

1 Introduction

Advanced multiphase materials such as fiber or whisker reinforced composites have seen widespread applications in recent years. It has been recognized that interfacial fracture may play an important role in determining the overall mechanical response of such multiphase systems. It is the low fracture toughness of these materials, which may result from debonding between different phases, that limits their use in engineering applications. Therefore, the scientific understanding of the mechanics of crack formation, initiation, and crack growth in bimaterial interfaces is essential for the effective study of failure processes of these advanced composite materials.

The earliest study of interfacial fracture appears to be by WILLIAMS (1959), who examined the local fields near the tip of a traction free semi-infinite interfacial crack, lying between two otherwise perfectly bonded elastic halfspaces. He observed that, unlike in homogeneous materials, the interfacial crack exhibits an oscillatory stress singularity. Since then, SIH and RICE (1964), and RICE and SIH (1965) have provided explicit expressions for the near-tip stresses and related them to remote elastic stress fields. The works of ERDOGAN (1965), ENGLAND (1965), and MALYSHEV and SALGANIK (1965) have also further examined two-dimensional singular models for single or multiple crack configurations in bimaterial systems. Recent progress in static interfacial fracture includes work by RICE (1988), HUTCHINSON and SUO (1991), and SHIH (1991).

Depending on the nature of loads that the composite structure is subjected to, the debonding process may take place dynamically. If the interface is already weakened by pre-existing flaws, these flaws may serve as sites of initiation of cracks which propagate unstably along the interface under the right circumstances. Such situations have motivated attempts to analyze dynamic crack propagation in interfaces. However, due to the complexity of the problem, thus far, only a few theoretical results of dynamic bimaterial

crack growth have been obtained. Among others, GOL'DSHTEIN (1967), BROCK and ACHENBACH (1973), WILLIS (1971, 1973), and ATKINSON (1977) have provided crack line solutions of particular fracture problems. Although these analytical results have provided some insights of the near-tip dynamic behavior, in order to effectively formulate and apply crack initiation and growth criteria in bimaterial systems, we need knowledge about the complete spatial structure of the field surrounding the moving interfacial crack-tip.

More recently, experimental investigations of interfacial crack-tip deformation fields have been carried out by TIPPUR and ROSAKIS (1991) and ROSAKIS *et al.* (1991) using the optical method of Coherent Gradient Sensor (CGS) (ROSAKIS, 1993) and high speed photography. The bimaterial system they used was a PMMA/aluminum combination. They observed substantial crack-tip speeds (up to $90\% c_R^{\text{PMMA}}$) associated with crack initiation and growth. Motivated by these observations, YANG *et al.* (1991) provided the asymptotic structure of the most singular term of the steady state elastodynamic bimaterial crack-tip fields. In the work of WU (1991), similar conclusions were reached. In addition, DENG (1992) obtained the asymptotic series representation of the stress field near the tip of a running interfacial crack in a bimaterial system under steady state conditions. Also motivated by the experiments of TIPPUR and ROSAKIS (1991), LO *et al.* (1992) have performed a numerical analysis of the same bimaterial system as was used in the experiments.

The question of whether there exists a K^d-dominant region surrounding the crack-tip (i.e. a region where the stress field can be well described by the leading singular term only), or in fact whether steady state crack propagation constitutes a good assumption in analysis, are issues to be verified by experimental observations. New experimental evidence, described in this paper, emphasize the existence of substantial crack-tip accelerations in addition to very high crack-tip speeds. The existence of high accelerations

violates the conditions under which the steady state assumption may confidently be applied. Motivated by the above experimental evidence, in this paper, we investigate the asymptotic structure of the near-tip field in a bimaterial system, where a highly transient elastodynamic crack growth history has occured. To do so, we employ the asymptotic procedure proposed by FREUND (1990) and utilized by FREUND and ROSAKIS (1992) in studying the transient growth of a mode-I crack in a homogeneous isotropic material. The same procedure was employed by LIU and ROSAKIS (1992) in studying the mixed-mode transient growth of a crack along an arbitrary curved path in a homogeneous isotropic solid. For anisotropic solids, transient crack growth under mode-I conditions was recently explored by WILLIS (1992).

In section 2 of the present study, the general formulation and properties of the asymptotic procedure are described. By using this asymptotic methodology, the equation of motion is reduced to a series of coupled partial differential equations. In section 3, the solution for the higher order transient problem is obtained. By imposing the boundary conditions along the surface of the interfacial crack and the bonding conditions along the interface ahead of the crack-tip, our problem can be further recasted into a Riemann-Hilbert problem. Upon solving the Riemann-Hilbert equation and evaluating the Stieltjes transforms, the higher order near-tip transient elastodynamic asymptotic field can be obtained. In section 4, the asymptotic elastodynamic stress field surrounding the interfacial crack-tip is studied. The first stress invariant is provided explicitly. The properties of the interfacial mismatch parameters are studied in section 5. These depend on the properties of the bimaterial combination and the crack-tip speed. In some of the available experiments by ROSAKIS *et al.* (1991), and the experimental evidence described in this paper, it has been observed that an interfacial crack can reach speeds amounting to a considerable fraction, or even exceeding the lower Rayleigh wave speed of the two constituents of the interface. Recognizing that our analysis need not be limited to a velocity regime below the lower Rayleigh wave speed, in section 6, we extend our solution to the

case when the crack is travelling at a speed between the lower Rayleigh and shear wave speeds. Finally, in section 7, recent experimental evidence of a transient higher order stress field in bimaterial fracture specimens is presented. The transient theoretical fields obtained in previous sections are used to quantitatively analyze optical interferograms obtained in real time high speed photography of dynamic bimaterial experiments in a PMMA/steel system. In addition, we present experimental evidence of transonic crack growth histories involving maximum speeds between 60% and 80% of the *dilatational* wave speed of PMMA. For comparison purposes, one should note that typical terminal crack-tip speeds in homogeneous PMMA are of the order of only 20% of the dilatational wave speed.

2 General formulation

Consider a planar body composed of two homogeneous, isotropic, and linearly elastic materials which are bonded along a straight line interface. A crack propagates non-uniformly along the interface, see Figure 1. Introduce a fixed orthonormal Cartesian coordinate system (x_1, x_2) so that the x_1-axis lies on the interface and coincides with the direction of the propagating crack. Suppose that the crack propagates with a non-uniform speed, $v(t)$, and the crack faces satisfy traction free boundary conditions. At a time $t = 0$, the crack-tip happens to be at the origin of the system, so the growth of the interfacial crack at any $t > 0$ is characterized by the length $l(t)$ ($v(t) = \dot{l}(t)$), which is the distance from the origin to the moving crack-tip. If the deformation is assumed to be plane strain, for each of the two materials comprising the interface, the displacement field may be generated from two displacement potentials, $\phi_k(x_1, x_2, t)$ and $\psi_k(x_1, x_2, t)$, where $k \in \{1, 2\}$. Here, the integer k is assigned to distinguish between the two different materials. In Figure 1, material–1 is the one shown above while material–2 is the one shown below the interface. Then, in either one of the two materials, the two non-zero

displacement components can be expressed as

$$u_\alpha(x_1,x_2,t) = \phi_{,\alpha}(x_1,x_2,t) + e_{\alpha\beta}\psi_{,\beta}(x_1,x_2,t)\ , \tag{2.1}$$

where $\alpha,\ \beta \in \{1,2\}$ and the summation convention has been used. $e_{\alpha\beta}$ is the two-dimensional alternator defined by

$$e_{12} = -e_{21} = 1\ , \qquad e_{11} = e_{22} = 0\ .$$

The components of stress for each material can be expressed in terms of the displacement potentials by

$$\left.\begin{aligned} \sigma_{11} &= \mu\left[\frac{c_l^2}{c_s^2}\phi_{,\alpha\alpha} - 2\phi_{,22} + 2\psi_{,12}\right] \\ \sigma_{22} &= \mu\left[\frac{c_l^2}{c_s^2}\phi_{,\alpha\alpha} - 2\phi_{,11} - 2\psi_{,12}\right] \\ \sigma_{12} &= \mu\left[2\phi_{,12} + \psi_{,22} - \psi_{,11}\right] \end{aligned}\right\}\ , \tag{2.2}$$

where μ is the shear modulus, and c_l, c_s are the longitudinal and shear wave speeds of each elastic material above or below the interface, respectively. In terms of the shear modulus μ, mass density ρ, and Poisson's ratio ν, for each of the two materials, c_l and c_s are given by

$$c_l = \left\{\frac{\kappa+1}{\kappa-1}\frac{\mu}{\rho}\right\}^{1/2}\ , \qquad c_s = \left\{\frac{\mu}{\rho}\right\}^{1/2}\ , \tag{2.3}$$

where

$$\kappa = \begin{cases} 3-4\nu, & \text{Plane strain} \\ \dfrac{3-\nu}{1+\nu}, & \text{Plane stress} \end{cases}$$

The corresponding plane stress solution can be obtained by changing the definition for the longitudinal wave speed in equation (2.3). Meanwhile, c_l and c_s in both plane strain and plane stress, are related by

$$\frac{c_s}{c_l} = \left\{\frac{\kappa-1}{\kappa+1}\right\}^{1/2}\ . \tag{2.4}$$

The equation of motion in the absence of body forces in the fixed coordinate system, in terms of $\phi(x_1, x_2, t)$ and $\psi(x_1, x_2, t)$, reduces to

$$\left.\begin{aligned} \phi_{,\alpha\alpha}(x_1, x_2, t) - \frac{1}{c_l^2}\ddot{\phi}(x_1, x_2, t) &= 0 \\ \psi_{,\alpha\alpha}(x_1, x_2, t) - \frac{1}{c_s^2}\ddot{\psi}(x_1, x_2, t) &= 0 \end{aligned}\right\} . \tag{2.5}$$

Equations (2.5) hold for each material above or below the interface.

We further introduce a new moving coordinate system, (ξ_1, ξ_2), by

$$\xi_1 = x_1 - l(t) , \qquad \xi_2 = x_2 . \tag{2.6}$$

This system is such that its origin is translating with the crack-tip. In this new system, the equations (2.5) for $\phi(\xi_1, \xi_2, t)$ and $\psi(\xi_1, \xi_2, t)$ become (FREUND, 1990)

$$\left.\begin{aligned} \left(1 - \frac{v^2(t)}{c_l^2}\right)\phi_{,11} + \phi_{,22} + \frac{\dot{v}(t)}{c_l^2}\phi_{,1} + \frac{2v(t)}{c_l^2}\phi_{,1t} - \frac{1}{c_l^2}\phi_{,tt} &= 0 \\ \left(1 - \frac{v^2(t)}{c_s^2}\right)\psi_{,11} + \psi_{,22} + \frac{\dot{v}(t)}{c_s^2}\psi_{,1} + \frac{2v(t)}{c_s^2}\psi_{,1t} - \frac{1}{c_s^2}\psi_{,tt} &= 0 \end{aligned}\right\} . \tag{2.7}$$

Notice that in equations (2.7), the differentiation with respect to time, t, is distinct to that in equations (2.5). Here, (ξ_1, ξ_2) are held fixed, whereas in (2.5), (x_1, x_2) are held fixed. Throughout this study, we will use $\partial/\partial t$, or $\{\ \}_{,t}$ to denote differentiation with respect to time, t, when the moving spatial coordinates (ξ_1, ξ_2) are held fixed. The notation $\dot{\{\ \}}$ denotes the same operation when the spatial coordinates (x_1, x_2) are held fixed.

At this point, we employ the standard asymptotic device used by FREUND and ROSAKIS (1992) for the analysis of transient crack growth in homogeneous materials. We assume that $\phi(\xi_1, \xi_2, t)$ and $\psi(\xi_1, \xi_2, t)$, for each material, can be asymptotically expanded as

$$\left.\begin{aligned} \phi(\xi_1, \xi_2, t) &= \sum_{m=0}^{\infty} \varepsilon^{p_m}\phi_m(\eta_1, \eta_2, t) \\ \psi(\xi_1, \xi_2, t) &= \sum_{m=0}^{\infty} \varepsilon^{p_m}\psi_m(\eta_1, \eta_2, t) \end{aligned}\right\} , \tag{2.8}$$

as $r = (\xi_1^2 + \xi_2^2)^{1/2} \to 0$, where $\eta_\alpha = \xi_\alpha/\varepsilon$, $\alpha \in \{1, 2\}$, and ε is a small arbitrary positive number. The parameter ε is used here so that the region around the crack-tip is expanded to fill the entire field of observation. As ε is chosen to be infinitely small, all points in the (ξ_1, ξ_2) plane except those very close to the crack-tip, are pushed out of the field of observation in the (η_1, η_2) plane, and the crack line occupies the whole negative η_1-axis. By taking $\varepsilon = 1$, the above equations will provide the asymptotic representation of the displacement potentials in the unscaled physical plane for each of the materials, respectively.

In the asymptotic representation (2.8), the powers of ε are such that

$$p_{m+1} = p_m + \frac{1}{2} , \qquad m = 0, 1, 2, \cdots . \tag{2.9}$$

Since the displacement should be bounded throughout the region, but the stress may be singular at the crack-tip, p_0 is expected to be in the range $1 < p_0 < 2$ (FREUND, 1990). We also should have

$$\frac{\varepsilon^{p_{m+n}} \phi_{m+n}(\eta_1, \eta_2, t)}{\varepsilon^{p_m} \phi_m(\eta_1, \eta_2, t)} \to 0 , \qquad \text{as} \quad \varepsilon \to 0 , \tag{2.10}$$

for any positive integer n. Returning to the unscaled physical plane, we will have

$$\frac{\phi_{m+n}(\xi_1, \xi_2, t)}{\phi_m(\xi_1, \xi_2, t)} \to 0 , \qquad \text{as} \quad r = \sqrt{\xi_1^2 + \xi_2^2} \to 0 , \tag{2.11}$$

for any positive integer n, so that in the physical plane, (ξ_1, ξ_2), $\phi_m(\xi_1, \xi_2, t)$ are ordered according to their contributions to the near-tip deformation field. The above properties for ϕ_m hold for ψ_m as well.

Substituting the asymptotic representations for $\phi(\xi_1, \xi_2, t)$ and $\psi(\xi_1, \xi_2, t)$, (2.8), into the equations of motion, (2.7), we obtain two equations whose left hand side is an infinite power series in ε and whose right hand side vanishes. Since ε is an arbitrary number, the coefficient of each power of ε should be zero. Therefore, the equations of motion reduce

to a series of coupled differential equations for $\phi_m(\eta_1, \eta_2, t)$ and $\psi_m(\eta_1, \eta_2, t)$ as follows (ROSAKIS *et al.*, 1991, FREUND and ROSAKIS, 1992):

$$\left.\begin{aligned} \phi_{m,11} + \frac{1}{\alpha_l^2(t)}\phi_{m,22} &= -\frac{2v^{1/2}(t)}{\alpha_l^2(t)c_l^2}\left\{v^{1/2}(t)\phi_{m-2,1}\right\}_{,t} + \frac{1}{\alpha_l^2(t)c_l^2}\phi_{m-4,tt} \\ \psi_{m,11} + \frac{1}{\alpha_s^2(t)}\psi_{m,22} &= -\frac{2v^{1/2}(t)}{\alpha_s^2(t)c_s^2}\left\{v^{1/2}(t)\psi_{m-2,1}\right\}_{,t} + \frac{1}{\alpha_s^2(t)c_s^2}\psi_{m-4,tt} \end{aligned}\right\}, \quad (2.12)$$

for $m = 0, 1, 2, \cdots$, and the quantities α_l and α_s depend on the crack-tip speed, and therefore on time t through

$$\alpha_{l,s}^2(t) = 1 - \frac{v^2(t)}{c_{l,s}^2}\,. \quad (2.13)$$

Also

$$\phi_m = \begin{cases} \phi_m & \text{for } m \geq 0 \\ 0 & \text{for } m < 0 \end{cases}, \qquad \psi_m = \begin{cases} \psi_m & \text{for } m \geq 0 \\ 0 & \text{for } m < 0 \end{cases}. \quad (2.14)$$

In what will follow, for our convenience, we drop the subscript which is used to distinguish between the two materials. However, we should keep in mind that the above asymptotic form of the equations of motion (2.12) hold for each of the materials with the appropriate elastic constants. The term "coupled" is used above in the sense that the higher order solutions for ϕ_m and ψ_m will depend on the lower order solutions for the same quantities. It is noted that, for the special case of *steady state* crack growth, the crack-tip speed, v, will be a constant, and at the same time, $\phi_{m,t} = \psi_{m,t} = 0$, for $m = 0, 1, 2, \cdots$. This means that ϕ_m and ψ_m depend on t only through the spatial scaled coordinate η_1. In such a case, the equations in (2.12) are not coupled anymore, and each one reduces to Laplace's equation in the coordinates $(\eta_1, \alpha_l\eta_2)$ for ϕ_m and $(\eta_1, \alpha_s\eta_2)$ for ψ_m. For steady state conditions, the functions ϕ_m and ψ_m are independent of time in the moving coordinate system. For the transient case, however, the crack-tip speed, $v(t)$, may be an arbitrary smooth function of time, and also ϕ_m and ψ_m may depend on time explicitly in the moving coordinate system. The only uncoupled equations are those for $m = 0$ and $m = 1$. For $m > 1$, we can see from (2.12) that the solutions for ϕ_m, and ψ_m are composed of two parts. One is the particular solution which is wholely determined

by lower order solutions for ϕ_{m-1} and ψ_{m-1}. The other part is the homogeneous solution which satisfies Laplace's equation in the corresponding scaled coordinate plane. The combination of the particular and homogeneous solutions should satisfy the traction free conditions on the crack faces as well as the bonding conditions along the interface. In the following sections, we will solve for ϕ_m and ψ_m for the most general transient situation, and for both materials.

It should be noted that the steady state problem could be solved using the efficient Stroh formulation. This formulation reduces the two spatial and one temporal variables to only two spatial variables and takes advantage of a well known formalism to solve the steady state crack problem (YANG *et al.*, 1991). However, this approach, although it can be easily be extended to anisotropic solids, is strictly restricted to steady state conditions and cannot be used for our present purposes.

3 Solution for the higher order transient problem

As we have discussed in the previous section, the only uncoupled equations in (2.12) are those for $m = 0$ and $m = 1$. For $m > 1$, the solutions for ϕ_m and ψ_m will be affected by the solutions with smaller m. In this section, we consider the situation of $m = 0$ and $m = 1$ first. After we get solutions for $m = 0$, and 1, we will subsequently solve for higher order ϕ_m and ψ_m.

3.1 Solutions for $\phi_m(\eta_1, \eta_2, t)$ and $\psi_m(\eta_1, \eta_2, t)$ for $m = 0$ and 1

For $m = 0$, or 1, (2.12) reduce to

$$\left.\begin{aligned} \phi_{m,11}(\eta_1, \eta_2, t) + \frac{1}{\alpha_l^2(t)}\phi_{m,22}(\eta_1, \eta_2, t) &= 0 \\ \psi_{m,11}(\eta_1, \eta_2, t) + \frac{1}{\alpha_s^2(t)}\psi_{m,22}(\eta_1, \eta_2, t) &= 0 \end{aligned}\right\} . \tag{3.1}$$

The above equations are Lapalace's equations in the corresponding scaled planes $(\eta_1, \alpha_l\eta_2)$ for ϕ_m, and $(\eta_1, \alpha_s\eta_2)$ for ψ_m. As we have mentioned earlier, the subscript k is omitted here, but the above equations hold for both materials that constitute the bimaterial body.

The most general solutions for equations (3.1) can be expressed as

$$\phi_m(\eta_1, \eta_2, t) = \mathrm{Re}\{F_m(z_l; t)\} , \qquad \psi_m(\eta_1, \eta_2, t) = \mathrm{Im}\{G_m(z_s; t)\} , \tag{3.2}$$

where the two complex variables z_l and z_s are given by

$$z_l = \eta_1 + i\alpha_l\eta_2 , \qquad z_s = \eta_1 + i\alpha_s\eta_2 ,$$

and $i = \sqrt{-1}$. For the bimaterial system, $F_{mk}(z_l; t)$ and $G_{mk}(z_s; t)$ are analytic in the upper half complex z_{lk}-, or z_{sk}-planes for $k = 1$ (upper material), and analytic in the lower half complex z_{lk}-, or z_{sk}-planes for $k = 2$ (lower material). The complex conjugates of these functions are also analytic on the plane obtained by reflection along the real axis,

e.g. $\overline{F}_{m1}(\overline{z}_l;t)$ is an analytic function on the $\overline{z}_l$ plane. Since α_l and α_s are different for each material, the scaled complex variables z_l and z_s will also be different. For fully transient problems, in the analytic functions $F_{mk}(z_l;t)$ and $G_{mk}(z_s;t)$, time t appears as a parameter. This suggests that these functions will depend on time t not only through the complex variables, z_l and z_s, but also directly through time t itself.

The displacement and stress components associated with these ϕ_m and ψ_m, are given by

$$\left.\begin{aligned} u_1^{(m)} &= \mathrm{Re}\left\{F_m'(z_l;t) + \alpha_s G_m'(z_s;t)\right\} \\ u_2^{(m)} &= -\mathrm{Im}\left\{\alpha_l F_m'(z_l;t) + G_m'(z_s;t)\right\} \end{aligned}\right\}, \tag{3.3}$$

and

$$\left.\begin{aligned} \sigma_{11}^{(m)} &= \mu\mathrm{Re}\left\{\left(1+2\alpha_l^2-\alpha_s^2\right)F_m''(z_l;t) + 2\alpha_s G_m''(z_s;t)\right\} \\ \sigma_{22}^{(m)} &= -\mu\mathrm{Re}\left\{\left(1+\alpha_s^2\right)F_m''(z_l;t) + 2\alpha_s G_m''(z_s;t)\right\} \\ \sigma_{12}^{(m)} &= -\mu\mathrm{Im}\left\{2\alpha_l F_m''(z_l;t) + \left(1+\alpha_s^2\right)G_m''(z_s;t)\right\} \end{aligned}\right\}, \tag{3.4}$$

where primes denote the derivative with respect to the corresponding complex arguments.

For any analytic function $\Omega(z)$, define the following,

$$\left.\begin{aligned} \lim_{\eta_2\to 0^+}\Omega(z) &= \Omega^+(\eta_1) \\ \lim_{\eta_2\to 0^-}\Omega(z) &= \Omega^-(\eta_1) \end{aligned}\right\}, \qquad z = \eta_1 + i\eta_2 \ .$$

For $\eta_1 < 0$ and $\eta_2 \to 0^+$, the traction free condition on the upper crack face gives

$$\left\{\sigma_{22}^{(m)}\right\}_1 = \left\{\sigma_{12}^{(m)}\right\}_1 = 0 \ ,$$

or, in terms of the complex displacement potentials $F_m(z_l;t)$ and $G_m(z_s;t)$,

$$\left.\begin{aligned} &\left\{\mu(1+\alpha_s^2)\left[F_m''^{+}(\eta_1;t) + \overline{F}_m''^{-}(\eta_1;t)\right] + 2\mu\alpha_s\left[G_m''^{+}(\eta_1;t) + \overline{G}_m''^{-}(\eta_1;t)\right]\right\}_1 = 0 \\ &\left\{2\mu\alpha_l\left[F_m''^{+}(\eta_1;t) - \overline{F}_m''^{-}(\eta_1;t)\right] + \mu(1+\alpha_s^2)\left[G_m''^{+}(\eta_1;t) - \overline{G}_m''^{-}(\eta_1;t)\right]\right\}_1 = 0 \end{aligned}\right\}, \tag{3.5}$$

For $\eta_1 < 0$ and $\eta_2 \to 0^-$, the traction free condition on the lower crack face gives

$$\left\{\sigma_{22}^{(m)}\right\}_2 = \left\{\sigma_{12}^{(m)}\right\}_2 = 0 \ ,$$

or

$$\left.\begin{aligned}&\left\{\mu(1+\alpha_s^2)\left[F_m''^-(\eta_1;t)+\overline{F}_m''^+(\eta_1;t)\right]+2\mu\alpha_s\left[G_m''^-(\eta_1;t)+\overline{G}_m''^+(\eta_1;t)\right]\right\}_2=0\\&\left\{2\mu\alpha_l\left[F_m''^-(\eta_1;t)-\overline{F}_m''^+(\eta_1;t)\right]+\mu(1+\alpha_s^2)\left[G_m''^-(\eta_1;t)-\overline{G}_m''^+(\eta_1;t)\right]\right\}_2=0\end{aligned}\right\}. \quad (3.6)$$

The above equations, (3.5) and (3.6), hold for $\eta_1 < 0$.

Along the interface, or $\eta_1 > 0$ and $\eta_2 = 0$, the bonding conditions should be satisfied, which implies that

$$\left.\begin{aligned}&\left\{\sigma_{22}^{(m)}\right\}_1-\left\{\sigma_{22}^{(m)}\right\}_2=0,\quad\left\{\sigma_{12}^{(m)}\right\}_1-\left\{\sigma_{12}^{(m)}\right\}_2=0\\&\left\{u_1^{(m)}\right\}_1-\left\{u_1^{(m)}\right\}_2=0,\quad\left\{u_2^{(m)}\right\}_1-\left\{u_2^{(m)}\right\}_2=0\end{aligned}\right\},\ \forall\ \eta_1>0,\ \eta_2=0\ ,$$

or, in terms of $F_m(z_l;t)$ and $G_m(z_s;t)$, from traction continuity,

$$\left.\begin{aligned}&\left\{\mu(1+\alpha_s^2)\left[F_m''^+(\eta_1;t)+\overline{F}_m''^-(\eta_1;t)\right]+2\mu\alpha_s\left[G_m''^+(\eta_1;t)+\overline{G}_m''^-(\eta_1;t)\right]\right\}_1\\&-\left\{\mu(1+\alpha_s^2)\left[F_m''^-(\eta_1;t)+\overline{F}_m''^+(\eta_1;t)\right]+2\mu\alpha_s\left[G_m''^-(\eta_1;t)+\overline{G}_m''^+(\eta_1;t)\right]\right\}_2=0\\&\left\{2\mu\alpha_l\left[F_m''^+(\eta_1;t)-\overline{F}_m''^-(\eta_1;t)\right]+\mu(1+\alpha_s^2)\left[G_m''^+(\eta_1;t)-\overline{G}_m''^-(\eta_1;t)\right]\right\}_1\\&-\left\{2\mu\alpha_l\left[F_m''^-(\eta_1;t)-\overline{F}_m''^+(\eta_1;t)\right]+\mu(1+\alpha_s^2)\left[G_m''^-(\eta_1;t)-\overline{G}_m''^+(\eta_1;t)\right]\right\}_2=0\end{aligned}\right\}, \quad (3.7)$$

and from displacement continuity,

$$\left.\begin{aligned}&\left\{\left[F_m'^+(\eta_1;t)+\overline{F}_m'^-(\eta_1;t)\right]+\alpha_s\left[G_m'^+(\eta_1;t)+\overline{G}_m'^-(\eta_1;t)\right]\right\}_1\\&-\left\{\left[F_m'^-(\eta_1;t)+\overline{F}_m'^+(\eta_1;t)\right]+\alpha_s\left[G_m'^-(\eta_1;t)+\overline{G}_m'^+(\eta_1;t)\right]\right\}_2=0\\&\left\{\alpha_l\left[F_m'^+(\eta_1;t)-\overline{F}_m'^-(\eta_1;t)\right]+\left[G_m'^+(\eta_1;t)-\overline{G}_m'^-(\eta_1;t)\right]\right\}_1\\&-\left\{\alpha_l\left[F_m'^-(\eta_1;t)-\overline{F}_m'^+(\eta_1;t)\right]+\left[G_m'^-(\eta_1;t)-\overline{G}_m'^+(\eta_1;t)\right]\right\}_2=0\end{aligned}\right\}. \quad (3.8)$$

The above equations, (3.7) and (3.8), hold for $\eta_1 > 0$.

For simplicity, define the following matrices for each material, $k \in \{1,2\}$,

$$\boldsymbol{P}_k=\begin{bmatrix}\mu(1+\alpha_s^2) & 2\mu\alpha_s\\ 2\mu\alpha_l & \mu(1+\alpha_s^2)\end{bmatrix}_k,\qquad \boldsymbol{Q}_k=\begin{bmatrix}\mu(1+\alpha_s^2) & 2\mu\alpha_s\\ -2\mu\alpha_l & -\mu(1+\alpha_s^2)\end{bmatrix}_k,$$

$$\boldsymbol{U}_k = \begin{bmatrix} 1 & \alpha_s \\ \alpha_l & 1 \end{bmatrix}_k , \qquad \boldsymbol{V}_k = \begin{bmatrix} 1 & \alpha_s \\ -\alpha_l & -1 \end{bmatrix}_k .$$

Also define the following complex vector for each material,

$$\boldsymbol{f}_{mk}(z;t) = (\ F_{mk}(z;t),\ G_{mk}(z;t)\ )^{\top} ,$$

where $z = \eta_1 + i\eta_2$. From above definitions, the boundary and bonding conditions, equations (3.5), (3.6), (3.7), and (3.8), can be rewritten as

$$\left.\begin{aligned} \boldsymbol{P}_1 \boldsymbol{f}''^{+}_{m1}(\eta_1;t) + \boldsymbol{Q}_1 \overline{\boldsymbol{f}}''^{-}_{m1}(\eta_1;t) = \mathbf{o} \\ \boldsymbol{P}_2 \boldsymbol{f}''^{-}_{m2}(\eta_1;t) + \boldsymbol{Q}_2 \overline{\boldsymbol{f}}''^{+}_{m2}(\eta_1;t) = \mathbf{o} \end{aligned}\right\} , \qquad \forall\, \eta_1 < 0 , \tag{3.9}$$

and

$$\left.\begin{aligned} \boldsymbol{P}_1 \boldsymbol{f}''^{+}_{m1}(\eta_1;t) + \boldsymbol{Q}_1 \overline{\boldsymbol{f}}''^{-}_{m1}(\eta_1;t) - \boldsymbol{P}_2 \boldsymbol{f}''^{-}_{m2}(\eta_1;t) - \boldsymbol{Q}_2 \overline{\boldsymbol{f}}''^{+}_{m2}(\eta_1;t) = \mathbf{o} \\ \boldsymbol{U}_1 \boldsymbol{f}'^{+}_{m1}(\eta_1;t) + \boldsymbol{V}_1 \overline{\boldsymbol{f}}'^{-}_{m1}(\eta_1;t) - \boldsymbol{U}_2 \boldsymbol{f}'^{-}_{m2}(\eta_1;t) - \boldsymbol{V}_2 \overline{\boldsymbol{f}}'^{+}_{m2}(\eta_1;t) = \mathbf{o} \end{aligned}\right\} , \ \forall\, \eta_1 > 0. \tag{3.10}$$

Further, the bonding conditions in (3.10) can be rearranged as

$$\left.\begin{aligned} \boldsymbol{P}_1 \boldsymbol{f}''^{+}_{m1}(\eta_1;t) - \boldsymbol{Q}_2 \overline{\boldsymbol{f}}''^{+}_{m2}(\eta_1;t) = \boldsymbol{P}_2 \boldsymbol{f}''^{-}_{m2}(\eta_1;t) - \boldsymbol{Q}_1 \overline{\boldsymbol{f}}''^{-}_{m1}(\eta_1;t) \\ \boldsymbol{U}_1 \boldsymbol{f}'^{+}_{m1}(\eta_1;t) - \boldsymbol{V}_2 \overline{\boldsymbol{f}}'^{+}_{m2}(\eta_1;t) = \boldsymbol{U}_2 \boldsymbol{f}'^{-}_{m2}(\eta_1;t) - \boldsymbol{V}_1 \overline{\boldsymbol{f}}'^{-}_{m1}(\eta_1;t) \end{aligned}\right\} , \qquad \forall\, \eta_1 > 0 . \tag{3.11}$$

In the above equations (3.11), the left hand sides are the limiting values of functions which are analytic in the *upper* half plane. The right hand sides are the limiting values of functions which are analytic in the *lower* half plane. Since the limiting values are the same along the positive real axis, the function $\boldsymbol{P}_2 \boldsymbol{f}''_{m2}(z;t) - \boldsymbol{Q}_1 \overline{\boldsymbol{f}}''_{m1}(z;t)$ defined in the lower half plane, is the analytic continuation of the function $\boldsymbol{P}_1 \boldsymbol{f}''_{m1}(z;t) - \boldsymbol{Q}_2 \overline{\boldsymbol{f}}''_{m2}(z;t)$ which is defined in the upper half plane, and vice versa. This results from the continuation propertities of analytic functions. As a result, we can write

$$\left.\begin{aligned} \boldsymbol{P}_1 \boldsymbol{f}''_{m1}(z;t) - \boldsymbol{Q}_2 \overline{\boldsymbol{f}}''_{m2}(z;t) = \boldsymbol{\kappa}_m(z;t) , \qquad z \in S^+ \\ \boldsymbol{P}_2 \boldsymbol{f}''_{m2}(z;t) - \boldsymbol{Q}_1 \overline{\boldsymbol{f}}''_{m1}(z;t) = \boldsymbol{\kappa}_m(z;t) , \qquad z \in S^- \end{aligned}\right\} , \tag{3.12}$$

and

$$\left.\begin{aligned} \boldsymbol{U}_1 \boldsymbol{f}'_{m1}(z;t) - \boldsymbol{V}_2 \overline{\boldsymbol{f}}'_{m2}(z;t) &= \boldsymbol{\theta}_m(z;t)\ , \qquad z \in S^+ \\ \boldsymbol{U}_2 \boldsymbol{f}'_{m2}(z;t) - \boldsymbol{V}_1 \overline{\boldsymbol{f}}'_{m1}(z;t) &= \boldsymbol{\theta}_m(z;t)\ , \qquad z \in S^- \end{aligned}\right\}\ , \tag{3.13}$$

where

$$S^{\pm} = \begin{cases} \{\ (\eta_1,\ i\eta_2)\ |\ -\infty < \eta_1 < \infty,\ \eta_2 \geq 0\ \} - C \\ \{\ (\eta_1,\ i\eta_2)\ |\ -\infty < \eta_1 < \infty,\ \eta_2 \leq 0\ \} - C \end{cases},$$

$$C = \{\ (\eta_1,\ i\eta_2)\ |\ -\infty < \eta_1 \leq 0,\ \eta_2 = 0\ \}\ .$$

$\boldsymbol{\kappa}_m(z;t)$ and $\boldsymbol{\theta}_m(z;t)$ are analytic functions throughout the z-plane except along the cut C which is the entire non-positive real axis. From the above equations, it can be seen immediately that equations (3.10) are satisfied identically. So, the question now is to find the analytic functions $\boldsymbol{\kappa}_m(z;t)$ and $\boldsymbol{\theta}_m(z;t)$ in the cut-plane $S^+ \cup S^-$.

Solving for $\boldsymbol{f}''_{mk}(z;t)$ and $\overline{\boldsymbol{f}}''_{mk}(z;t)$ from equations (3.12) and (3.13), we get

$$\left.\begin{aligned} \boldsymbol{f}''_{m1}(z;t) &= \boldsymbol{P}_1^{-1}\boldsymbol{H}^{-1}\left\{\boldsymbol{\theta}'_m(z;t) - \overset{*}{\boldsymbol{L}}_2\,\boldsymbol{\kappa}_m(z;t)\right\} \\ \overline{\boldsymbol{f}}''_{m2}(z;t) &= \boldsymbol{Q}_2^{-1}\boldsymbol{H}^{-1}\left\{\boldsymbol{\theta}'_m(z;t) - \boldsymbol{L}_1\boldsymbol{\kappa}_m(z;t)\right\} \end{aligned}\right\}\ , \qquad z \in S^+\ , \tag{3.14}$$

and

$$\left.\begin{aligned} \boldsymbol{f}''_{m2}(z;t) &= -\boldsymbol{P}_2^{-1}\,\overset{*}{\boldsymbol{H}}^{-1}\left\{\boldsymbol{\theta}'_m(z;t) - \overset{*}{\boldsymbol{L}}_1\,\boldsymbol{\kappa}_m(z;t)\right\} \\ \overline{\boldsymbol{f}}''_{m1}(z;t) &= -\boldsymbol{Q}_1^{-1}\,\overset{*}{\boldsymbol{H}}^{-1}\left\{\boldsymbol{\theta}'_m(z;t) - \boldsymbol{L}_2\boldsymbol{\kappa}_m(z;t)\right\} \end{aligned}\right\}\ , \qquad z \in S^-\ . \tag{3.15}$$

The definitions of matrices $\boldsymbol{L}_k$, $\overset{*}{\boldsymbol{L}}_k$, $\boldsymbol{H}$, and $\overset{*}{\boldsymbol{H}}$, as well as the properties of these matrices are given in Appendix I. Matrices $\boldsymbol{P}_k$ and $\boldsymbol{Q}_k$ have been defined above. In obtaining (3.14) and (3.15), we have assumed that the inverse matrices $\boldsymbol{P}_k^{-1}$ and $\boldsymbol{Q}_k^{-1}$ exist. Notice that the determinants of $\boldsymbol{P}_k$ and $\boldsymbol{Q}_k$ are both equal to $D_k(v)$, where

$$D_k(v) = \left\{4\alpha_l\alpha_s - \left(1+\alpha_s^2\right)^2\right\}_k\ .$$

Therefore, in this analysis, we exclude the situation where the interfacial crack propagates with either of the two Rayleigh wave speeds of the bimaterial system which are the real roots of $D_k(v) = 0$. This ensures the existence of $\boldsymbol{P}_k^{-1}$ and $\boldsymbol{Q}_k^{-1}$.

Substituting equations (3.14) and (3.15) into the traction free conditions on the crack faces, (3.9), we get

$$\left.\begin{aligned} \dot{\boldsymbol{H}}\left\{\boldsymbol{\theta}_m'^{+}(\eta_1;t)-\dot{\boldsymbol{L}}_2\,\boldsymbol{\kappa}_m^{+}(\eta_1;t)\right\}-\boldsymbol{H}\left\{\boldsymbol{\theta}_m'^{-}(\eta_1;t)-\boldsymbol{L}_2\boldsymbol{\kappa}_m^{-}(\eta_1;t)\right\}&=\mathbf{o}\\ \boldsymbol{H}\left\{\boldsymbol{\theta}_m'^{-}(\eta_1;t)-\dot{\boldsymbol{L}}_1\,\boldsymbol{\kappa}_m^{-}(\eta_1;t)\right\}-\dot{\boldsymbol{H}}\left\{\boldsymbol{\theta}_m'^{+}(\eta_1;t)-\boldsymbol{L}_1\boldsymbol{\kappa}_m^{+}(\eta_1;t)\right\}&=\mathbf{o}\end{aligned}\right\},\forall\eta_1<0. \quad (3.16)$$

Adding the two equations in (3.16), and using the fact that $\dot{\boldsymbol{H}}\,\boldsymbol{H}\neq\mathbf{o}$ for a crack propagating with a nonzero speed, we obtain

$$\boldsymbol{\kappa}_m^{+}(\eta_1;t)-\boldsymbol{\kappa}_m^{-}(\eta_1;t)=\mathbf{o}\,,\qquad\forall\,\eta_1<0\,. \quad (3.17)$$

This implies that $\boldsymbol{\kappa}_m(z;t)$ is continuous across the cut except at the crack-tip and therefore $\boldsymbol{\kappa}_m(z;t)$ is analytic in the entire complex plane except at $z=0$. However, the condition of bounded displacement requires that $|\,\boldsymbol{\kappa}_m(z;t)\,|=O\,(\,|z|^{\alpha}\,)$ for some $\alpha>-1$, as $|z|\to 0$, so that any singularity of $\boldsymbol{\kappa}_m(z;t)$ at the crack-tip is removable. Therefore, $\boldsymbol{\kappa}_m(z;t)$ is an entire function. Now, both equations in (3.16) become

$$\dot{\boldsymbol{H}}\,\boldsymbol{\theta}_m'^{+}(\eta_1;t)-\boldsymbol{H}\boldsymbol{\theta}_m'^{-}(\eta_1;t)=\boldsymbol{R}\boldsymbol{\kappa}_m(\eta_1;t)\,,\qquad\forall\,\eta_1<0\,, \quad (3.18)$$

where

$$\left.\begin{aligned}\boldsymbol{\kappa}_m(\eta_1;t)&=\boldsymbol{\kappa}_m^{+}(\eta_1;t)=\boldsymbol{\kappa}_m^{-}(\eta_1;t)\\ \boldsymbol{R}&=\dot{\boldsymbol{H}}\dot{\boldsymbol{L}}_2-\boldsymbol{H}\boldsymbol{L}_2=\dot{\boldsymbol{H}}\,\boldsymbol{L}_1-\boldsymbol{H}\,\dot{\boldsymbol{L}}_1\end{aligned}\right\}.$$

Equation (3.18) constitutes a Riemann-Hilbert problem. Its solution $\boldsymbol{\theta}_m'(z;t)$ is analytic in the cut-plane $S^{+}\cup S^{-}$. Along the cut, $\boldsymbol{\theta}_m'(z;t)$ satisfies equation (3.18) for some arbitrary entire function $\boldsymbol{\kappa}_m(z;t)$. Also, from the requirement of bounded displacements at the crack-tip, as $|z|\to 0$,

$$|\,\boldsymbol{\theta}_m'(z;t)\,|=O\,(\,|z|^{\alpha}\,)\,, \quad (3.19)$$

for some $\alpha>-1$.

In equation (3.18), the solution $\boldsymbol{\theta}'_m(z;t)$ is composed of two parts, the homogeneous solution $\overset{\circ}{\boldsymbol{\theta}}{}'_m(z;t)$, and the particular solution $\hat{\boldsymbol{\theta}}'_m(z;t)$. We will consider these two solutions separately.

HOMOGENEOUS SOLUTION:

The homogeneous solution is obtained by solving

$$\overset{*}{\boldsymbol{H}}\overset{\circ}{\boldsymbol{\theta}}{}'^{+}_m(\eta_1;t) - \boldsymbol{H}\overset{\circ}{\boldsymbol{\theta}}{}'^{-}_m(\eta_1;t) = \mathbf{o}\,, \qquad \forall\,\eta_1 < 0\,. \tag{3.20}$$

By using the solution given in Appendix II and by imposing restriction (3.19), we can write the solution to the above equation as follows:

$$\overset{\circ}{\boldsymbol{\theta}}{}'_m(z;t) = z^{-\frac{1}{2}+i\epsilon}\,\overset{\circ}{A}_m(z;t)\boldsymbol{\zeta} + z^{-\frac{1}{2}-i\epsilon}\,\overset{\circ}{B}_m(z;t)\,\overset{*}{\boldsymbol{\zeta}}\,, \tag{3.21}$$

where

$$\left.\begin{aligned} &\epsilon = \frac{1}{2\pi}\ln\frac{1-\beta}{1+\beta},\quad \beta = \frac{h_{11}}{\sqrt{h_{12}h_{21}}},\\ &\boldsymbol{\zeta} = (\,1,\,\eta\,)^{\mathsf{T}},\qquad \overset{*}{\boldsymbol{\zeta}} = (\,1,\,-\eta\,)^{\mathsf{T}},\quad \eta = \sqrt{\frac{h_{21}}{h_{12}}} \end{aligned}\right\},$$

and $\overset{\circ}{A}_m(z;t)$, $\overset{\circ}{B}_m(z;t)$ are arbitrary entire functions. The parameters ϵ and η defined here are known functions of crack-tip speed, v, and material properties. Their functional dependence on these variables is discussed in Appendix I and section 5. For $v = 0$, $\epsilon(v)$ reduces to ϵ_0 which is the oscillatory index that appears in the quasi-static interfacial crack problems (WILLIAMS, 1959; RICE, 1988).

By substituting equation (3.21) into equations (3.14) and (3.15), we get

$$\left.\begin{aligned} \overset{\circ}{\boldsymbol{f}}{}''_{m1}(z;t) &= \boldsymbol{P}_1^{-1}\boldsymbol{H}^{-1}\left\{z^{-\frac{1}{2}+i\epsilon}\,\overset{\circ}{A}_m(z;t)\boldsymbol{\zeta} + z^{-\frac{1}{2}-i\epsilon}\,\overset{\circ}{B}_m(z;t)\,\overset{*}{\boldsymbol{\zeta}}\right\}\\ \overline{\overset{\circ}{\boldsymbol{f}}{}''_{m2}}(z;t) &= \boldsymbol{Q}_2^{-1}\boldsymbol{H}^{-1}\left\{z^{-\frac{1}{2}+i\epsilon}\,\overset{\circ}{A}_m(z;t)\boldsymbol{\zeta} + z^{-\frac{1}{2}-i\epsilon}\,\overset{\circ}{B}_m(z;t)\,\overset{*}{\boldsymbol{\zeta}}\right\} \end{aligned}\right\},\ z\in S^+, \tag{3.22}$$

and

$$\left.\begin{aligned} \overset{\circ}{f}{}''_{m2}(z;t) &= -\boldsymbol{P}_2^{-1}\,\overset{*}{\boldsymbol{H}}{}^{-1}\left\{z^{-\frac{1}{2}+ic}\,\overset{\circ}{A}_m(z;t)\boldsymbol{\zeta}+z^{-\frac{1}{2}-ic}\,\overset{\circ}{B}_m(z;t)\,\overset{*}{\boldsymbol{\zeta}}\right\}\\ \overline{\overset{\circ}{f}}{}''_{m1}(z;t) &= -\boldsymbol{Q}_1^{-1}\,\overset{*}{\boldsymbol{H}}{}^{-1}\left\{z^{-\frac{1}{2}+ic}\,\overset{\circ}{A}_m(z;t)\boldsymbol{\zeta}+z^{-\frac{1}{2}-ic}\,\overset{\circ}{B}_m(z;t)\,\overset{*}{\boldsymbol{\zeta}}\right\}\end{aligned}\right\},\ z\in S^-. \quad (3.23)$$

Notice that the following identities hold,

$$\left.\begin{aligned} \boldsymbol{H}^{-1}\boldsymbol{\zeta} &= -\frac{\sqrt{h_{12}h_{21}}}{h_{11}^2-h_{12}h_{21}}(1-\beta)\boldsymbol{\zeta}, \quad \boldsymbol{H}^{-1}\,\overset{*}{\boldsymbol{\zeta}} = \frac{\sqrt{h_{12}h_{21}}}{h_{11}^2-h_{12}h_{21}}(1+\beta)\,\overset{*}{\boldsymbol{\zeta}}\\ \overset{*}{\boldsymbol{H}}{}^{-1}\boldsymbol{\zeta} &= \frac{\sqrt{h_{12}h_{21}}}{h_{11}^2-h_{12}h_{21}}(1+\beta)\boldsymbol{\zeta}, \quad \overset{*}{\boldsymbol{H}}{}^{-1}\,\overset{*}{\boldsymbol{\zeta}} = -\frac{\sqrt{h_{12}h_{21}}}{h_{11}^2-h_{12}h_{21}}(1-\beta)\,\overset{*}{\boldsymbol{\zeta}}\end{aligned}\right\},$$

and

$$1+\beta=\frac{e^{-\epsilon\pi}}{\cosh\epsilon\pi}\,, \qquad 1-\beta=\frac{e^{\epsilon\pi}}{\cosh\epsilon\pi}\,.$$

Without losing generality, we may absorb the factor $\sqrt{h_{12}h_{21}}/(h_{11}^2-h_{12}h_{21})$ into the entire functions, $\overset{\circ}{A}_m(z;t)$ and $\overset{\circ}{B}_m(z;t)$. By taking the conjugate of the function $\overline{\overset{\circ}{f}}{}''_{m1}(z;t)$ in equation (3.23) and comparing it with the function $\overset{\circ}{f}{}''_{m1}(z;t)$ in equation (3.22), and also by using the properties of matrices $\boldsymbol{P}_k$ and $\boldsymbol{Q}_k$, we can obtain a relationship between the entire functions $\overset{\circ}{A}_m(z;t)$ and $\overset{\circ}{B}_m(z;t)$ as follows,

$$\overset{\circ}{B}_m(z;t)=-\overline{\overset{\circ}{A}}_m(z;t)\,.$$

Meanwhile, by using the fact that

$$\boldsymbol{P}_k^{-1}\,\overset{*}{\boldsymbol{\zeta}}=\boldsymbol{Q}_k^{-1}\boldsymbol{\zeta}\,, \qquad \boldsymbol{Q}_k^{-1}\,\overset{*}{\boldsymbol{\zeta}}=\boldsymbol{P}_k^{-1}\boldsymbol{\zeta}\,,$$

we can get the solutions,

$$\left.\begin{aligned} \overset{\circ}{f}{}''_{m1}(z;t) &= \left\{\frac{e^{\epsilon\pi}\boldsymbol{P}_1^{-1}\boldsymbol{\zeta}}{\cosh\epsilon\pi}z^{-\frac{1}{2}+ic}\,\overset{\circ}{A}_m(z;t)+\frac{e^{-\epsilon\pi}\boldsymbol{Q}_1^{-1}\boldsymbol{\zeta}}{\cosh\epsilon\pi}z^{-\frac{1}{2}-ic}\,\overline{\overset{\circ}{A}}_m(z;t)\right\},\ z\in S^+\\ \overset{\circ}{f}{}''_{m2}(z;t) &= \left\{\frac{e^{-\epsilon\pi}\boldsymbol{P}_2^{-1}\boldsymbol{\zeta}}{\cosh\epsilon\pi}z^{-\frac{1}{2}+ic}\,\overset{\circ}{A}_m(z;t)+\frac{e^{\epsilon\pi}\boldsymbol{Q}_2^{-1}\boldsymbol{\zeta}}{\cosh\epsilon\pi}z^{-\frac{1}{2}-ic}\,\overline{\overset{\circ}{A}}_m(z;t)\right\},\ z\in S^-\end{aligned}\right\}, \quad (3.24)$$

or, in terms of $F_m(z_l;t)$ and $G_m(z_s;t)$, for the material above the interface,

$$\left.\begin{aligned}
\overset{\circ}{F}{}''_m(z_l;t) &= -\frac{[(1+\alpha_s^2)-2\eta\alpha_s]\,e^{\epsilon\pi}}{\mu D(v)\cosh\epsilon\pi} z_l^{-\frac{1}{2}+i\epsilon}\,\overset{\circ}{A}_m(z_l;t) \\
&\quad - \frac{[(1+\alpha_s^2)+2\eta\alpha_s]\,e^{-\epsilon\pi}}{\mu D(v)\cosh\epsilon\pi} z_l^{-\frac{1}{2}-i\epsilon}\,\overline{\overset{\circ}{A}}_m(z_l;t) \\
\overset{\circ}{G}{}''_m(z_s;t) &= \frac{[2\alpha_l-\eta(1+\alpha_s^2)]\,e^{\epsilon\pi}}{\mu D(v)\cosh\epsilon\pi} z_s^{-\frac{1}{2}+i\epsilon}\,\overset{\circ}{A}_m(z_s;t) \\
&\quad + \frac{[2\alpha_l+\eta(1+\alpha_s^2)]\,e^{-\epsilon\pi}}{\mu D(v)\cosh\epsilon\pi} z_s^{-\frac{1}{2}-i\epsilon}\,\overline{\overset{\circ}{A}}_m(z_s;t)
\end{aligned}\right\}. \tag{3.25}$$

For the material below the interface, the solution is also given by equation (3.25) with the parameter $\epsilon\pi$ changed to $-\epsilon\pi$.

PARTICULAR SOLUTION:

Since $\boldsymbol{\kappa}_m(z;t)$ is an entire function, the particular solution $\hat{\boldsymbol{\theta}}'_m(z;t)$ can be easily constructed. Suppose $\hat{\boldsymbol{\theta}}'_m(z;t)$ is also an entire function, which implies that

$$\hat{\boldsymbol{\theta}}'^{+}_m(\eta_1;t) = \hat{\boldsymbol{\theta}}'^{-}_m(\eta_1;t) = \hat{\boldsymbol{\theta}}'_m(\eta_1;t),$$

then from equation (3.18), we get

$$\hat{\boldsymbol{\theta}}'_m(\eta_1;t) = \left\{\overset{*}{\boldsymbol{H}} - \boldsymbol{H}\right\}^{-1} \boldsymbol{R}\boldsymbol{\kappa}_m(\eta_1;t)\,, \qquad \forall\ \eta_1 < 0\,. \tag{3.26}$$

By using the identity theorem for analytical functions, it can be shown that for any z,

$$\hat{\boldsymbol{\theta}}'_m(z;t) = \left\{\overset{*}{\boldsymbol{H}} - \boldsymbol{H}\right\}^{-1} \boldsymbol{R}\boldsymbol{\kappa}_m(z;t)\,. \tag{3.27}$$

By substituting this particular solution into equations (3.14) and (3.15), we have

$$\left.\begin{aligned}
\hat{\boldsymbol{f}}''_{m1}(z;t) &= \boldsymbol{P}_1^{-1}\left\{\overset{*}{\boldsymbol{H}} - \boldsymbol{H}\right\}^{-1}\left\{\overset{*}{\boldsymbol{L}}_2 - \boldsymbol{L}_2\right\}\boldsymbol{\kappa}_m(z;t) \\
\overline{\hat{\boldsymbol{f}}}''_{m2}(z;t) &= -\boldsymbol{Q}_2^{-1}\left\{\overset{*}{\boldsymbol{H}} - \boldsymbol{H}\right\}^{-1}\left\{\overset{*}{\boldsymbol{L}}_1 - \boldsymbol{L}_1\right\}\boldsymbol{\kappa}_m(z;t)
\end{aligned}\right\}, \qquad z \in S^+, \tag{3.28}$$

and

$$\left.\begin{aligned}\hat{\boldsymbol{f}}''_{m2}(z;t) &= \boldsymbol{P}_2^{-1}\left\{\mathring{\boldsymbol{H}}-\boldsymbol{H}\right\}^{-1}\left\{\mathring{\boldsymbol{L}}_1-\boldsymbol{L}_1\right\}\boldsymbol{\kappa}_m(z;t)\\ \overline{\hat{\boldsymbol{f}}}''_{m1}(z;t) &= -\boldsymbol{Q}_1^{-1}\left\{\mathring{\boldsymbol{H}}-\boldsymbol{H}\right\}^{-1}\left\{\mathring{\boldsymbol{L}}_2-\boldsymbol{L}_2\right\}\boldsymbol{\kappa}_m(z;t)\end{aligned}\right\}, \qquad z\in S^-. \tag{3.29}$$

Notice that

$$\left\{\mathring{\boldsymbol{H}}-\boldsymbol{H}\right\}^{-1}\left\{\mathring{\boldsymbol{L}}_k-\boldsymbol{L}_k\right\} = \begin{bmatrix}\dfrac{(l_{21})_k}{h_{21}} & 0\\ 0 & \dfrac{(l_{12})_k}{h_{12}}\end{bmatrix}, \qquad k\in\{1,2\}\,.$$

If the entire function $\boldsymbol{\kappa}_m(z;t)$ is expressed as

$$\boldsymbol{\kappa}_m(z;t) = \left(\ \kappa_m^{(1)}(z;t),\ \kappa_m^{(2)}(z;t)\ \right)^{\mathsf{T}}\,,$$

then, it can be shown that by comparing the conjugate of $\overline{\hat{\boldsymbol{f}}}''_{m1}(z;t)$ in equation (3.29) with $\hat{\boldsymbol{f}}''_{m1}(z;t)$ in equation (3.28), we have

$$\kappa_m^{(1)}(z;t)+\overline{\kappa}_m^{(1)}(z;t)=0\,, \qquad \kappa_m^{(2)}(z;t)-\overline{\kappa}_m^{(2)}(z;t)=0\,.$$

Define a new entire function $\hat{A}_m(z;t)$ by

$$\hat{A}_m(z;t) = \frac{1}{4}\left\{\left[\kappa_m^{(1)}(z;t)-\overline{\kappa}_m^{(1)}(z;t)\right]+\left[\kappa_m^{(2)}(z;t)+\overline{\kappa}_m^{(2)}(z;t)\right]\right\}\,.$$

Also let

$$\boldsymbol{w}_k = \left(\frac{(l_{21})_k}{h_{21}},\ \frac{(l_{12})_k}{h_{12}}\right)^{\mathsf{T}}\,.$$

By relating $\boldsymbol{\kappa}_m(z;t)$ to $\hat{A}_m(z;t)$, and by using the above definition, equations (3.28) and (3.29) give

$$\left.\begin{aligned}\hat{\boldsymbol{f}}''_{m1}(z;t) &= \boldsymbol{P}_1^{-1}\boldsymbol{w}_2\hat{A}_m(z;t)-\boldsymbol{Q}_1^{-1}\boldsymbol{w}_2\overline{\hat{A}}_m(z;t)\,, \quad z\in S^+\\ \hat{\boldsymbol{f}}''_{m2}(z;t) &= \boldsymbol{P}_2^{-1}\boldsymbol{w}_1\hat{A}_m(z;t)-\boldsymbol{Q}_2^{-1}\boldsymbol{w}_1\overline{\hat{A}}_m(z;t)\,, \quad z\in S^-\end{aligned}\right\}. \tag{3.30}$$

In order to express the particular solution in terms of $F_m(z_l;t)$ and $G_m(z_s;t)$, we need to define two parameters, ω_l and ω_s that only depend on the crack-tip speed,

$$\omega_l = \frac{\left\{\dfrac{\alpha_l(1-\alpha_s^2)}{\mu D(v)}\right\}_1}{\left\{\dfrac{\alpha_l(1-\alpha_s^2)}{\mu D(v)}\right\}_2}, \qquad \omega_s = \frac{\left\{\dfrac{\alpha_s(1-\alpha_s^2)}{\mu D(v)}\right\}_1}{\left\{\dfrac{\alpha_s(1-\alpha_s^2)}{\mu D(v)}\right\}_2}.$$

Then, for the material above the interface, the particular solution can be expressed as

$$\left.\begin{aligned}
\hat{F}''_m(z_l;t) &= -\frac{1}{\mu D(v)}\left\{\left(\frac{1+\alpha_s^2}{1+\omega_l}-\frac{2\alpha_s}{1+\omega_s}\right)\hat{A}_m(z_l;t)\right. \\
&\quad \left.-\left(\frac{1+\alpha_s^2}{1+\omega_l}+\frac{2\alpha_s}{1+\omega_s}\right)\overline{\hat{A}}_m(z_l;t)\right\} \\
\hat{G}''_m(z_s;t) &= \frac{1}{\mu D(v)}\left\{\left(\frac{2\alpha_l}{1+\omega_l}-\frac{1+\alpha_s^2}{1+\omega_s}\right)\hat{A}_m(z_s;t)\right. \\
&\quad \left.-\left(\frac{2\alpha_l}{1+\omega_l}+\frac{1+\alpha_s^2}{1+\omega_s}\right)\overline{\hat{A}}_m(z_s;t)\right\}
\end{aligned}\right\}. \tag{3.31}$$

For the material below the interface, the particular solution is also given by equations (3.31) with ω_l and ω_s changed to ω_l^{-1} and ω_s^{-1}, respectively.

By adding the expressions in equations (3.25) and (3.31), and by integrating with respect to the corresponding arguments, the final solutions of $F_m(z_l;t)$ and $G_m(z_s;t)$ for the material above the interface, for $m = 0,\ 1$, can be obtained as

$$\left.\begin{aligned}
F_m(z_l;t) &= -\frac{\left[(1+\alpha_s^2)-2\eta\alpha_s\right]e^{\epsilon\pi}}{\mu D(v)\cosh\epsilon\pi} z_l^{\frac{3}{2}+i\epsilon} A_m(z_l;t) \\
&+\frac{\left[(1+\alpha_s^2)+2\eta\alpha_s\right]e^{-\epsilon\pi}}{\mu D(v)\cosh\epsilon\pi} z_l^{\frac{3}{2}-i\epsilon}\overline{A}_m(z_l;t) \\
&-\frac{1}{\mu D(v)}\left\{\left(\frac{1+\alpha_s^2}{1+\omega_l}-\frac{2\alpha_s}{1+\omega_s}\right)B_m(z_l;t)-\left(\frac{1+\alpha_s^2}{1+\omega_l}+\frac{2\alpha_s}{1+\omega_s}\right)\overline{B}_m(z_l;t)\right\} z_l^2
\end{aligned}\right\}, \tag{3.32}$$

and

$$\left.\begin{aligned} G_m(z_s;t) \;=\; & \frac{[2\alpha_l-\eta(1+\alpha_s^2)]\,e^{\epsilon\pi}}{\mu D(v)\cosh\epsilon\pi} z_s^{\frac{3}{2}+i\epsilon} A_m(z_s;t) \\ & + \frac{[2\alpha_l+\eta(1+\alpha_s^2)]\,e^{-\epsilon\pi}}{\mu D(v)\cosh\epsilon\pi} z_s^{\frac{3}{2}-i\epsilon} \overline{A}_m(z_s;t) \\ & + \frac{1}{\mu D(v)} \left\{ \left(\frac{2\alpha_l}{1+\omega_l} - \frac{1+\alpha_s^2}{1+\omega_s} \right) B_m(z_s;t) - \left(\frac{2\alpha_l}{1+\omega_l} + \frac{1+\alpha_s^2}{1+\omega_s} \right) \overline{B}_m(z_s;t) \right\} z_s^2 \end{aligned} \right\}, \tag{3.33}$$

where the entire functions, $A_m(z;t)$ and $B_m(z;t)$ are defined by

$$\frac{\mathrm{d}^2}{\mathrm{d}z^2}\left\{ z^{\frac{3}{2}+i\epsilon} A_m(z;t) \right\} = z^{-\frac{1}{2}+i\epsilon}\, \mathring{A}_m\,(z;t)\,, \qquad \frac{\mathrm{d}^2}{\mathrm{d}z^2}\left\{ z^2 B_m(z;t) \right\} = \hat{A}_m(z;t)\,,$$

and they can only be determined by the far field conditions. The solutions for the two displacement potentials, $\phi_m(\eta_1,\eta_2,t)$ and $\psi_m(\eta_1,\eta_2,t)$, will be given by equations (3.2).

Since $A_m(z;t)$ and $B_m(z;t)$ are entire functions, they can be expanded into Taylor series,

$$\left.\begin{aligned} A_0(z;t) &= \sum_{n=0}^{\infty} A_0^{(n)}(t) z^n\,, \quad B_0(z;t) = \sum_{n=0}^{\infty} B_0^{(n)}(t) z^n \\ A_1(z;t) &= \sum_{n=0}^{\infty} A_1^{(n)}(t) z^n\,, \quad B_1(z;t) = \sum_{n=0}^{\infty} B_1^{(n)}(t) z^n \end{aligned} \right\}. \tag{3.34}$$

As we have mentioned in the previous section, in the unscaled physical plane, (ξ_1,ξ_2), $\phi_m(\xi_1,\xi_2,t)$ and $\psi_m(\xi_1,\xi_2,t)$ should be ordered according to their contributions to the near-tip deformation field. By imposing this property, i.e. equation (2.11), to the representations of $\phi_m(\eta_1,\eta_2,t)$ and $\psi_m(\eta_1,\eta_2,t)$, for $m=0$ and 1, we can obtain restrictions on the entire functions $A_m(z;t)$ and $B_m(z;t)$. In the Taylor expansion (3.34), $A_0^{(0)}(t) \neq 0$ and $B_1^{(0)}(t) \neq 0$, but $A_1^{(0)}(t) = 0$. In other words, the leading terms of ϕ_0 and ψ_0 are of order $z^{3/2}$, whereas the leading terms of ϕ_1 and ψ_1 are of order z^2. Meanwhile, it can be shown that the coefficient of the leading term, $A_0^{(0)}(t)$, in (3.32) and (3.33), is directly related to the complex dynamic stress intensity factor $K^d(t)$ defined by YANG *et*

al. (1991) through the relation

$$A_0^{(0)}(t) = -\frac{1}{2\sqrt{2\pi}} \frac{K^d(t)}{\left(\frac{3}{2}+i\epsilon\right)\left(\frac{1}{2}+i\epsilon\right)} \,. \tag{3.35}$$

As a matter of fact, in the unscaled plane, (ξ_1, ξ_2), and for $m = 0$, equations (3.32) and (3.33) are identical in spatial structure to the complete solution for the *steady state* propagating interfacial crack in a bimaterial. By using an entirely different methodologies, the most singular solution of the steady state problem was obtained by YANG *et al.* (1991) and the complete solution of the steady state problem was given by DENG (1992). However, in the present analysis the functions $A_m^{(n)}(t)$ and $B_m^{(n)}(t)$ are allowed to be functions of time.

3.2 Solutions for $\phi_m(\eta_1, \eta_2, t)$ and $\psi_m(\eta_1, \eta_2, t)$ for $m = 2$

For $m = 2$, the equations of motion (2.12) are coupled. They take the form,

$$\left.\begin{aligned} \phi_{2,11}(\eta_1,\eta_2,t) + \frac{1}{\alpha_l^2}\phi_{2,22}(\eta_1,\eta_2,t) &= -\frac{2v^{1/2}}{\alpha_l^2 c_l^2}\mathrm{Re}\left\{v^{1/2}F_0'(z_l;t)\right\}_{,t} \\ \psi_{2,11}(\eta_1,\eta_2,t) + \frac{1}{\alpha_s^2}\psi_{2,22}(\eta_1,\eta_2,t) &= -\frac{2v^{1/2}}{\alpha_s^2 c_s^2}\mathrm{Im}\left\{v^{1/2}G_0'(z_s;t)\right\}_{,t} \end{aligned}\right\}, \tag{3.36}$$

where $F_0(z_l;t)$ and $G_0(z_s;t)$ correspond to the solution of (2.12) for $m = 0$ and are given by equations (3.32) and (3.33).

In order to obtain the next most singular term in $\phi_2(\eta_1, \eta_2, t)$ and $\psi_2(\eta_1, \eta_2, t)$, we should only consider the most singular terms in $F_0(z_l;t)$ and $G_0(z_s;t)$. Therefore, for the material above the interface,

$$\left.\begin{aligned} F_0(z_l;t) &= a_0(t)A_0(t)z_l^{\frac{3}{2}+i\epsilon} + b_0(t)\overline{A}_0(t)z_l^{\frac{3}{2}-i\epsilon} \\ G_0(z_s;t) &= c_0(t)A_0(t)z_s^{\frac{3}{2}+i\epsilon} + d_0(t)\overline{A}_0(t)z_s^{\frac{3}{2}-i\epsilon} \end{aligned}\right\}, \tag{3.37}$$

where $A_0(t) = A_0^{(0)}(t)$, given in (3.35), and

$$a_0(t) = -\frac{\left[(1+\alpha_s^2) - 2\eta\alpha_s\right]e^{\epsilon\pi}}{\mu D(v)\cosh\epsilon\pi} \,,$$

$$
\begin{aligned}
b_0(t) &= -\frac{[(1+\alpha_s^2)+2\eta\alpha_s]\,e^{-\epsilon\pi}}{\mu D(v)\cosh\epsilon\pi}\,, \\
c_0(t) &= \frac{[2\alpha_l-\eta(1+\alpha_s^2)]\,e^{\epsilon\pi}}{\mu D(v)\cosh\epsilon\pi}\,, \\
d_0(t) &= \frac{[2\alpha_l+\eta(1+\alpha_s^2)]\,e^{-\epsilon\pi}}{\mu D(v)\cosh\epsilon\pi}\,.
\end{aligned}
$$

For the material below the interface, we need to change the parameter $\epsilon\pi$ to $-\epsilon\pi$.

Substituting (3.37) into (3.36) and carrying out the differentiation with respect to time, (3.36) becomes

$$
\left.
\begin{aligned}
&\phi_{2,11}(\eta_1,\eta_2,t)+\frac{1}{\alpha_l^2}\phi_{2,22}(\eta_1,\eta_2,t)= \\
&-\frac{2\sqrt{v}}{\alpha_l^2 c_l^2}\mathrm{Re}\left\{i\dot{\epsilon}\sqrt{v}\left[\hat{A}_0(t)a_0(t)z_l^{i\epsilon}-\overline{\hat{A}}_0(t)b_0(t)z_l^{-i\epsilon}\right]z_l^{\frac{1}{2}}\ln z_l\right. \\
&-\frac{\sqrt{v}\dot{\alpha}_l}{2\alpha_l}\left[\hat{B}_0(t)a_0(t)z_l^{i\epsilon}+\overline{\hat{B}}_0(t)b_0(t)z_l^{-i\epsilon}\right]z_l^{-\frac{1}{2}}\overline{z}_l \\
&+\left[\frac{\mathrm{d}}{\mathrm{d}t}\left(\sqrt{v}\hat{A}_0(t)a_0(t)\right)+\frac{\sqrt{v}\dot{\alpha}_l}{2\alpha_l}\hat{B}_0(t)a_0(t)\right]z_l^{\frac{1}{2}+i\epsilon} \\
&\left.+\left[\frac{\mathrm{d}}{\mathrm{d}t}\left(\sqrt{v}\overline{\hat{A}}_0(t)b_0(t)\right)+\overline{\hat{B}}_0(t)b_0(t)\right]z_l^{\frac{1}{2}-i\epsilon}\right\}
\end{aligned}
\right\}\,, \qquad (3.38)
$$

and

$$
\left.
\begin{aligned}
&\psi_{2,11}(\eta_1,\eta_2,t)+\frac{1}{\alpha_s^2}\psi_{2,22}(\eta_1,\eta_2,t)= \\
&-\frac{2\sqrt{v}}{\alpha_s^2 c_s^2}\mathrm{Im}\left\{i\dot{\epsilon}\sqrt{v}\left[\hat{A}_0(t)c_0(t)z_s^{i\epsilon}-\overline{\hat{A}}_0(t)d_0(t)z_s^{-i\epsilon}\right]z_s^{\frac{1}{2}}\ln z_s\right. \\
&-\frac{\sqrt{v}\dot{\alpha}_s}{2\alpha_s}\left[\hat{B}_0(t)c_0(t)z_s^{i\epsilon}+\overline{\hat{B}}_0(t)d_0(t)z_s^{-i\epsilon}\right]z_s^{-\frac{1}{2}}\overline{z}_s \\
&+\left[\frac{\mathrm{d}}{\mathrm{d}t}\left(\sqrt{v}\hat{A}_0(t)c_0(t)\right)+\frac{\sqrt{v}\dot{\alpha}_s}{2\alpha_s}\hat{B}_0(t)c_0(t)\right]z_s^{\frac{1}{2}+i\epsilon} \\
&\left.+\left[\frac{\mathrm{d}}{\mathrm{d}t}\left(\sqrt{v}\overline{\hat{A}}_0(t)d_0(t)\right)+\frac{\sqrt{v}\dot{\alpha}_s}{2\alpha_s}\overline{\hat{B}}_0(t)d_0(t)\right]z_s^{\frac{1}{2}-i\epsilon}\right\}
\end{aligned}
\right\}\,, \qquad (3.39)
$$

where

$$\hat{A}_0(t) = \left(\frac{3}{2} + i\epsilon\right) A_0(t) \ , \qquad \hat{B}_0(t) = \left(\frac{3}{2} + i\epsilon\right)\left(\frac{1}{2} + i\epsilon\right) A_0(t) \ .$$

The most general solutions to equations (3.38) and (3.39) are

$$\left.\begin{aligned} \phi_2(\eta_1, \eta_2, t) &= \mathrm{Re}\left\{F_2(z_l; t) - \overline{z}_l \hat{F}(z_l; t) - \overline{z}_l^2 \tilde{F}(z_l; t)\right\} \\ \psi_2(\eta_1, \eta_2, t) &= \mathrm{Im}\left\{G_2(z_s; t) - \overline{z}_s \hat{G}(z_s; t) - \overline{z}_s^2 \tilde{G}(z_s; t)\right\} \end{aligned}\right\} , \tag{3.40}$$

where

$$\left.\begin{aligned} \hat{F}(z;t) &= D_l\{a_0(t)\} z^{\frac{3}{2}+i\epsilon} + \overline{D}_l\{b_0(t)\} z^{\frac{3}{2}-i\epsilon} \\ &+ \dot{\epsilon}\left\{K_l(t) a_0(t) z^{\frac{3}{2}+i\epsilon} + \overline{K}_l(t) b_0(t) z^{\frac{3}{2}-i\epsilon}\right\} \ln z \\ \hat{G}(z;t) &= D_s\{c_0(t)\} z^{\frac{3}{2}+i\epsilon} + \overline{D}_s\{d_0(t)\} z^{\frac{3}{2}-i\epsilon} \\ &+ \dot{\epsilon}\left\{K_s(t) c_0(t) z^{\frac{3}{2}+i\epsilon} + \overline{K}_s(t) d_0(t) z^{\frac{3}{2}-i\epsilon}\right\} \ln z \end{aligned}\right\} ,$$

and

$$\left.\begin{aligned} \tilde{F}(z;t) &= B_l(t) a_0(t) z^{\frac{1}{2}+i\epsilon} + \overline{B}_l(t) b_0(t) z^{\frac{1}{2}-i\epsilon} \\ \tilde{G}(z;t) &= B_s(t) c_0(t) z^{\frac{1}{2}+i\epsilon} + \overline{B}_s(t) d_0(t) z^{\frac{1}{2}-i\epsilon} \end{aligned}\right\} .$$

The two operators $D_l\{\cdot\}$ and $D_s\{\cdot\}$ are given by

$$\left.\begin{aligned} D_{l,s}\{p(t)\} &= \frac{v^{1/2}}{2\alpha_{l,s}^2 c_{l,s}^2}\left\{\left(\frac{3}{2} + i\epsilon\right)^{-1} \frac{\mathrm{d}}{\mathrm{d}t}\left[v^{1/2} p(t)\left(\frac{3}{2} + i\epsilon\right) A_0(t)\right]\right. \\ &+ \left.\frac{v^{1/2}\dot{\alpha}_{l,s}}{2\alpha_{l,s}} p(t)\left(\frac{1}{2} + i\epsilon\right) A_0(t) \ + \ i\,\dot{\epsilon} v^{1/2} p(t) A_0(t)\right\} \end{aligned}\right\} ,$$

where $p(t)$ is a real function of time t. Also

$$\left.\begin{aligned} B_{l,s}(t) &= -\frac{v\dot{\alpha}_{l,s}}{8\alpha_{l,s}^3 c_{l,s}^2}\left(\frac{3}{2} + i\epsilon\right) A_0(t) \\ K_{l,s}(t) &= \frac{iv A_0(t)}{2\alpha_{l,s}^2 c_{l,s}^2} \end{aligned}\right\} .$$

In (3.40), $\hat{F}(z_l;t)$, $\tilde{F}(z_l;t)$, $\hat{G}(z_s;t)$, and $\tilde{G}(z_s;t)$ are totally determined by $F_0(z_l;t)$ and $G_0(z_s;t)$, given in equation (3.37). The coefficients of functions $\hat{F}(z_l;t)$, $\tilde{F}(z_l;t)$, $\hat{G}(z_s;t)$, and $\tilde{G}(z_s;t)$ are related to the crack-tip acceleration, the time derivative of $A_0(t)$, as well

as the crack-tip speed and $A_0(t)$ themselves through the definitions of $D_{l,s}\{A_0(t)\}$, $B_{l,s}(t)$, and $K_{l,s}(t)$. It should be noted at this point that these definitions reduce to the equivalent ones corresponding to the transient crack growth in homogeneous materials. Indeed, if ϵ is set to be zero, the expressions for $D_{l,s}\{A_0(t)\}$ and $B_{l,s}(t)$ that appear in FREUND and ROSAKIS (1992) are obtained. Once again, it is clear that for the steady state situation, functions $\hat{F}(z_l;t)$, $\tilde{F}(z_l;t)$, $\hat{G}(z_s;t)$, and $\tilde{G}(z_s;t)$ will vanish. The undetermined functions $F_2(z_l;t)$ and $G_2(z_s;t)$ are analytic in the upper half plane for the material above the interface, and in the lower half for the material below the interface. These functions are at the moment unknown and will be determined below by using the boundary and bonding conditions.

Associated with $\phi_2(\eta_1,\eta_2,t)$ and $\psi_2(\eta_1,\eta_2,t)$, the components of displacement will be

$$\left.\begin{aligned} u_1^{(2)} &= \mathrm{Re}\Big\{ F_2'(z_l;t) + \alpha_s G_2'(z_s;t) \\ &- \left[\overline{z}_l \hat{F}'(z_l;t) + \overline{z}_l^2 \tilde{F}'(z_l;t) + \hat{F}(z_l;t) + 2\overline{z}_l \tilde{F}(z_l;t)\right] \\ &- \alpha_s \left[\overline{z}_s \hat{G}'(z_s;t) + \overline{z}_s^2 \tilde{G}'(z_s;t) - \hat{G}(z_s;t) - 2\overline{z}_s \tilde{G}(z_s;t)\right]\Big\} \\ u_2^{(2)} &= \mathrm{Im}\Big\{ \alpha_l F_2'(z_l;t) + G_2'(z_s;t) \\ &- \alpha_l \left[\overline{z}_l \hat{F}'(z_l;t) + \overline{z}_l^2 \tilde{F}'(z_l;t) - \hat{F}(z_l;t) - 2\overline{z}_l \tilde{F}(z_l;t)\right] \\ &- \left[\overline{z}_s \hat{G}'(z_s;t) + \overline{z}_s^2 \tilde{G}'(z_s;t) + \hat{G}(z_s;t) + 2\overline{z}_s \tilde{G}(z_s;t)\right]\Big\} \end{aligned}\right\}, \tag{3.41}$$

and the components of stress

$$\left.\begin{aligned} \sigma_{11}^{(2)} &= \mu \mathrm{Re}\Big\{ \left(1 + 2\alpha_l^2 - \alpha_s^2\right) F_2''(z_l;t) + 2\alpha_s G_2''(z_s;t) \\ &- \left(1 + 2\alpha_l^2 - \alpha_s^2\right) \left[\overline{z}_l \hat{F}''(z_l;t) + \overline{z}_l^2 \tilde{F}''(z_l;t) + 2\tilde{F}(z_l;t)\right] \\ &- 2\left[\left(1 - \alpha_s^2\right) + \frac{2\alpha_l^2\left(\alpha_l^2 - \alpha_s^2\right)}{1 - \alpha_l^2}\right] \left[\hat{F}'(z_l;t) + 2\overline{z}_l \tilde{F}'(z_l;t)\right] \\ &- 2\alpha_s \left[\overline{z}_s \hat{G}''(z_s;t) + \overline{z}_s^2 \tilde{G}''(z_s;t) - 2\tilde{G}(z_s;t)\right]\Big\} \end{aligned}\right\}, \tag{3.42}$$

$$\left.\begin{aligned}\sigma_{22}^{(2)} &= -\mu \mathrm{Re}\Big\{ \left(1+\alpha_s^2\right) F_2''(z_l;t) + 2\alpha_s G_2''(z_s;t) \\ &- \left(1+\alpha_s^2\right)\left[\overline{z}_l \hat{F}''(z_l;t) + \overline{z}_l^2 \tilde{F}''(z_l;t) + 2\tilde{F}(z_l;t)\right] \\ &- 2\left[\left(1-\alpha_s^2\right) - \frac{2\left(\alpha_l^2-\alpha_s^2\right)}{1-\alpha_l^2}\right]\left[\hat{F}'(z_l;t) + 2\overline{z}_l \tilde{F}'(z_l;t)\right] \\ &- 2\alpha_s\left[\overline{z}_s \hat{G}''(z_s;t) + \overline{z}_s^2 \tilde{G}''(z_s;t) - 2\tilde{G}(z_s;t)\right]\Big\}\end{aligned}\right\}, \tag{3.43}$$

and

$$\left.\begin{aligned}\sigma_{12}^{(2)} &= -\mu \mathrm{Im}\Big\{ 2\alpha_l F_2''(z_l;t) + \left(1+\alpha_s^2\right) G_2''(z_s;t) \\ &- 2\alpha_l\left[\overline{z}_l \hat{F}''(z_l;t) + \overline{z}_l^2 \tilde{F}''(z_l;t) - 2\tilde{F}(z_l;t)\right] \\ &- \left(1+\alpha_s^2\right)\left[\overline{z}_s \hat{G}''(z_s;t) + \overline{z}_s^2 \tilde{G}''(z_s;t) + 2\tilde{G}(z_s;t)\right] \\ &- 2\left(1-\alpha_s^2\right)\left[\hat{G}'(z_s;t) + 2\overline{z}_s \tilde{G}'(z_s;t)\right]\Big\}\end{aligned}\right\}. \tag{3.44}$$

To produce a more compact form for the boundary and bonding conditions, one needs to define the following quantities: First let $\overset{*}{\boldsymbol{P}}_k$, $\overset{*}{\boldsymbol{Q}}_k$, $\overset{*}{\boldsymbol{U}}_k$, and $\overset{*}{\boldsymbol{V}}_k$ be obtained from matrices $\boldsymbol{P}_k$, $\boldsymbol{Q}_k$, $\boldsymbol{U}_k$, and $\boldsymbol{V}_k$, respectively, by changing the sign of the off-diagonal elements, and let

$$\boldsymbol{M}_k = \begin{bmatrix} \mu m(v) & 0 \\ 0 & \mu n(v) \end{bmatrix}_k, \qquad \boldsymbol{N}_k = \begin{bmatrix} \mu m(v) & 0 \\ 0 & -\mu n(v) \end{bmatrix}_k,$$

where

$$m(v) = \left(1-\alpha_s^2\right) - \frac{2\left(\alpha_l^2-\alpha_s^2\right)}{1-\alpha_l^2}, \qquad n(v) = 1-\alpha_s^2 .$$

Also, define complex vectors,

$$\begin{aligned}\boldsymbol{f}_k(z;t) &= \left(F_{2k}(z;t),\ G_{2k}(z;t) \right)^{\mathsf{T}}, \\ \hat{\boldsymbol{f}}_k(z;t) &= \left(\hat{F}_k(z;t),\ \hat{G}_k(z;t) \right)^{\mathsf{T}}, \\ \tilde{\boldsymbol{f}}_k(z;t) &= \left(\tilde{F}_k(z;t),\ \tilde{G}_k(z;t) \right)^{\mathsf{T}}.\end{aligned}$$

Then, by using the above definitions, the traction free condition on the crack faces will

be

$$\left.\begin{aligned}
&\boldsymbol{P}_1\left[\boldsymbol{f}_1^{\prime\prime+}(\eta_1;t)-\eta_1\hat{\boldsymbol{f}}_1^{\prime\prime+}(\eta_1;t)-\eta_1^2\tilde{\boldsymbol{f}}_1^{\prime\prime+}(\eta_1;t)\right]\\
&+\boldsymbol{Q}_1\left[\overline{\boldsymbol{f}}_1^{\prime\prime-}(\eta_1;t)-\eta_1\overline{\hat{\boldsymbol{f}}}_1^{\prime\prime-}(\eta_1;t)-\eta_1^2\overline{\tilde{\boldsymbol{f}}}_1^{\prime\prime-}(\eta_1;t)\right]\\
&-2\boldsymbol{M}_1\left[\hat{\boldsymbol{f}}_1^{\prime+}(\eta_1;t)+2\eta_1\tilde{\boldsymbol{f}}_1^{\prime+}(\eta_1;t)\right]-2\boldsymbol{N}_1\left[\overline{\hat{\boldsymbol{f}}}_1^{\prime-}(\eta_1;t)+2\eta_1\overline{\tilde{\boldsymbol{f}}}_1^{\prime-}(\eta_1;t)\right]\\
&-2\,\dot{\boldsymbol{P}}_1\,\tilde{\boldsymbol{f}}_1^{+}(\eta_1;t)-2\,\dot{\boldsymbol{Q}}_1\,\overline{\tilde{\boldsymbol{f}}}_1^{-}(\eta_1;t)=\mathbf{o}\\
&\boldsymbol{P}_2\left[\boldsymbol{f}_2^{\prime\prime-}(\eta_1;t)-\eta_1\hat{\boldsymbol{f}}_2^{\prime\prime-}(\eta_1;t)-\eta_1^2\tilde{\boldsymbol{f}}_2^{\prime\prime-}(\eta_1;t)\right]\\
&+\boldsymbol{Q}_2\left[\overline{\boldsymbol{f}}_2^{\prime\prime+}(\eta_1;t)-\eta_1\overline{\hat{\boldsymbol{f}}}_2^{\prime\prime+}(\eta_1;t)-\eta_1^2\overline{\tilde{\boldsymbol{f}}}_2^{\prime\prime+}(\eta_1;t)\right]\\
&-2\boldsymbol{M}_2\left[\hat{\boldsymbol{f}}_2^{\prime-}(\eta_1;t)+2\eta_1\tilde{\boldsymbol{f}}_2^{\prime-}(\eta_1;t)\right]-2\boldsymbol{N}_2\left[\overline{\hat{\boldsymbol{f}}}_2^{\prime+}(\eta_1;t)+2\eta_1\overline{\tilde{\boldsymbol{f}}}_2^{\prime+}(\eta_1;t)\right]\\
&-2\,\dot{\boldsymbol{P}}_2\,\tilde{\boldsymbol{f}}_2^{-}(\eta_1;t)-2\,\dot{\boldsymbol{Q}}_2\,\overline{\tilde{\boldsymbol{f}}}_2^{+}(\eta_1;t)=\mathbf{o}
\end{aligned}\right\},\ \forall\eta_1<0. \tag{3.45}$$

The continuity of traction along the interface will reduce to

$$\left.\begin{aligned}
&\Big\{\boldsymbol{P}_1\left[\boldsymbol{f}_1^{\prime\prime+}(\eta_1;t)-\eta_1\hat{\boldsymbol{f}}_1^{\prime\prime+}(\eta_1;t)-\eta_1^2\tilde{\boldsymbol{f}}_1^{\prime\prime+}(\eta_1;t)\right]\\
&+\boldsymbol{Q}_1\left[\overline{\boldsymbol{f}}_1^{\prime\prime-}(\eta_1;t)-\eta_1\overline{\hat{\boldsymbol{f}}}_1^{\prime\prime-}(\eta_1;t)-\eta_1^2\overline{\tilde{\boldsymbol{f}}}_1^{\prime\prime-}(\eta_1;t)\right]\\
&-2\boldsymbol{M}_1\left[\hat{\boldsymbol{f}}_1^{\prime+}(\eta_1;t)+2\eta_1\tilde{\boldsymbol{f}}_1^{\prime+}(\eta_1;t)\right]-2\boldsymbol{N}_1\left[\overline{\hat{\boldsymbol{f}}}_1^{\prime-}(\eta_1;t)+2\eta_1\overline{\tilde{\boldsymbol{f}}}_1^{\prime-}(\eta_1;t)\right]\\
&-2\,\dot{\boldsymbol{P}}_1\,\tilde{\boldsymbol{f}}_1^{+}(\eta_1;t)-2\,\dot{\boldsymbol{Q}}_1\,\overline{\tilde{\boldsymbol{f}}}_1^{-}(\eta_1;t)\Big\}\\
&-\Big\{\boldsymbol{P}_2\left[\boldsymbol{f}_2^{\prime\prime-}(\eta_1;t)-\eta_1\hat{\boldsymbol{f}}_2^{\prime\prime-}(\eta_1;t)-\eta_1^2\tilde{\boldsymbol{f}}_2^{\prime\prime-}(\eta_1;t)\right]\\
&+\boldsymbol{Q}_2\left[\overline{\boldsymbol{f}}_2^{\prime\prime+}(\eta_1;t)-\eta_1\overline{\hat{\boldsymbol{f}}}_2^{\prime\prime+}(\eta_1;t)-\eta_1^2\overline{\tilde{\boldsymbol{f}}}_2^{\prime\prime+}(\eta_1;t)\right]\\
&-2\boldsymbol{M}_2\left[\hat{\boldsymbol{f}}_2^{\prime-}(\eta_1;t)+2\eta_1\tilde{\boldsymbol{f}}_2^{\prime-}(\eta_1;t)\right]-2\boldsymbol{N}_2\left[\overline{\hat{\boldsymbol{f}}}_2^{\prime+}(\eta_1;t)+2\eta_1\overline{\tilde{\boldsymbol{f}}}_2^{\prime+}(\eta_1;t)\right]\\
&-2\,\dot{\boldsymbol{P}}_2\,\tilde{\boldsymbol{f}}_2^{-}(\eta_1;t)-2\,\dot{\boldsymbol{Q}}_2\,\overline{\tilde{\boldsymbol{f}}}_2^{+}(\eta_1;t)\Big\}=\mathbf{o}
\end{aligned}\right\},\forall\ \eta_1>0, \tag{3.46}$$

and the continuity of the displacement along the interface will be

$$\left.\begin{aligned}
&\Big\{\boldsymbol{U}_1\Big[\boldsymbol{f}_1'^{+}(\eta_1;t)-\eta_1\tilde{\boldsymbol{f}}_1'^{+}(\eta_1;t)-\eta_1^2\tilde{\boldsymbol{f}}_1'^{+}(\eta_1;t)\Big]\\
&+\boldsymbol{V}_1\Big[\overline{\boldsymbol{f}}_1'^{-}(\eta_1;t)-\eta_1\overline{\tilde{\boldsymbol{f}}}_1'^{-}(\eta_1;t)-\eta_1^2\overline{\tilde{\boldsymbol{f}}}_1'^{-}(\eta_1;t)\Big]\\
&-\dot{\boldsymbol{U}}_1\Big[\tilde{\boldsymbol{f}}_1^{+}(\eta_1;t)+2\eta_1\tilde{\boldsymbol{f}}_1^{+}(\eta_1;t)\Big]-\dot{\boldsymbol{V}}_1\Big[\overline{\tilde{\boldsymbol{f}}}_1^{-}(\eta_1;t)+2\eta_1\overline{\tilde{\boldsymbol{f}}}_1^{-}(\eta_1;t)\Big]\Big\}\\
&-\Big\{\boldsymbol{U}_2\Big[\boldsymbol{f}_2'^{-}(\eta_1;t)-\eta_1\tilde{\boldsymbol{f}}_2'^{-}(\eta_1;t)-\eta_1^2\tilde{\boldsymbol{f}}_2'^{-}(\eta_1;t)\Big]\\
&+\boldsymbol{V}_2\Big[\overline{\boldsymbol{f}}_2'^{+}(\eta_1;t)-\eta_1\overline{\tilde{\boldsymbol{f}}}_2'^{+}(\eta_1;t)-\eta_1^2\overline{\tilde{\boldsymbol{f}}}_2'^{+}(\eta_1;t)\Big]\\
&-\dot{\boldsymbol{U}}_2\Big[\tilde{\boldsymbol{f}}_2^{-}(\eta_1;t)+2\eta_1\tilde{\boldsymbol{f}}_2^{-}(\eta_1;t)\Big]-\dot{\boldsymbol{V}}_2\Big[\overline{\tilde{\boldsymbol{f}}}_2^{+}(\eta_1;t)+2\eta_1\overline{\tilde{\boldsymbol{f}}}_2^{+}(\eta_1;t)\Big]\Big\}=\mathbf{o}
\end{aligned}\right\},\ \forall\eta_1>0. \tag{3.47}$$

Similar to the procedure in the previous section, by rearranging the bonding condition (3.46) and (3.47), we may introduce two new functions $\boldsymbol{\kappa}(z;t)$ and $\boldsymbol{\theta}(z;t)$, which are analytic in the cut-plane $S^+\cup S^-$. In order to keep our notation short, we define some new quantities,

$$\left.\begin{aligned}
\boldsymbol{g}_k(z;t) &= \boldsymbol{f}_k''(z;t)-z\tilde{\boldsymbol{f}}_k''(z;t)-z^2\tilde{\boldsymbol{f}}_k''(z;t)\\
&-\ 2\boldsymbol{P}_k^{-1}\boldsymbol{M}_k\Big[\tilde{\boldsymbol{f}}_k'(z;t)+2z\tilde{\boldsymbol{f}}_k'(z;t)\Big]\ -\ 2\boldsymbol{P}_k^{-1}\dot{\boldsymbol{P}}_k\,\tilde{\boldsymbol{f}}_k(z;t)
\end{aligned}\right\},\quad k\in\{1,2\}.$$

Therefore, we can write that

$$\left.\begin{aligned}
\boldsymbol{\kappa}(z;t)&=\boldsymbol{P}_1\boldsymbol{g}_1(z;t)-\boldsymbol{Q}_2\overline{\boldsymbol{g}}_2(z;t)\\
\boldsymbol{\theta}'(z;t)&=\boldsymbol{U}_1\boldsymbol{g}_1(z;t)-\boldsymbol{V}_2\overline{\boldsymbol{g}}_2(z;t)+\boldsymbol{q}_1(z;t)-\dot{\overline{\boldsymbol{q}}}_2(z;t)
\end{aligned}\right\},\quad z\in S^+, \tag{3.48}$$

and

$$\left.\begin{aligned}
\boldsymbol{\kappa}(z;t)&=\boldsymbol{P}_2\boldsymbol{g}_2(z;t)-\boldsymbol{Q}_1\overline{\boldsymbol{g}}_1(z;t)\\
\boldsymbol{\theta}'(z;t)&=\boldsymbol{U}_2\boldsymbol{g}_2(z;t)-\boldsymbol{V}_1\overline{\boldsymbol{g}}_1(z;t)+\boldsymbol{q}_2(z;t)-\dot{\overline{\boldsymbol{q}}}_1(z;t)
\end{aligned}\right\},\quad z\in S^-, \tag{3.49}$$

where

$$\left.\begin{aligned}
\boldsymbol{q}_k(z;t)&=2\left(\boldsymbol{L}_k\boldsymbol{M}_k-\boldsymbol{I}\right)\Big[\tilde{\boldsymbol{f}}_k'(z;t)+2z\tilde{\boldsymbol{f}}_k'(z;t)\Big]+2\left(\boldsymbol{L}_k\dot{\boldsymbol{P}}_k-\dot{\boldsymbol{U}}_k\right)\tilde{\boldsymbol{f}}_k(z;t)\\
\dot{\boldsymbol{q}}_k(z;t)&=2\left(\dot{\boldsymbol{L}}_k\boldsymbol{N}_k-\boldsymbol{J}\right)\Big[\tilde{\boldsymbol{f}}_k'(z;t)+2z\tilde{\boldsymbol{f}}_k'(z;t)\Big]+2\left(\dot{\boldsymbol{L}}_k\dot{\boldsymbol{Q}}_k-\dot{\boldsymbol{V}}_k\right)\tilde{\boldsymbol{f}}_k(z;t)
\end{aligned}\right\}, \tag{3.50}$$

and

$$\boldsymbol{I} = \begin{bmatrix} 1 & 0 \\ 0 & 1 \end{bmatrix}, \qquad \boldsymbol{J} = \begin{bmatrix} 1 & 0 \\ 0 & -1 \end{bmatrix}.$$

Vector $\overset{*}{\boldsymbol{q}}_k(z;t)$ is related to vector $\boldsymbol{q}_k(z;t)$ by

$$\overset{*}{\boldsymbol{q}}_k(z;t) = \left(q_k^{(1)}(z;t),\ -q_k^{(2)}(z;t) \right)^{\mathsf{T}}, \quad \boldsymbol{q}_k(z;t) = \left(q_k^{(1)}(z;t),\ q_k^{(2)}(z;t) \right)^{\mathsf{T}}.$$

This notation will be used throughout the paper to signify this operation. In calculating $\overset{*}{\boldsymbol{q}}_k(z;t)$ and $\boldsymbol{q}_k(z;t)$ in equation (3.50), we have used the fact that

$$\boldsymbol{P}_k^{-1}\boldsymbol{M}_k = \boldsymbol{Q}_k^{-1}\boldsymbol{N}_k, \qquad \boldsymbol{P}_k^{-1}\overset{*}{\boldsymbol{P}}_k = \boldsymbol{Q}_k^{-1}\overset{*}{\boldsymbol{Q}}_k, \qquad k \in \{1,2\}.$$

By solving equations (3.48) and (3.49) for $\boldsymbol{g}_k(z;t)$ and $\overline{\boldsymbol{g}}_k(z;t)$, we obtain

$$\left.\begin{aligned} \boldsymbol{g}_1(z;t) &= \boldsymbol{P}_1^{-1}\boldsymbol{H}^{-1}\left\{\boldsymbol{\theta}'(z;t) - \overset{*}{\boldsymbol{L}}_2\,\boldsymbol{\kappa}(z;t) - \left[\boldsymbol{q}_1(z;t) - \overline{\overset{*}{\boldsymbol{q}}}_2(z;t)\right]\right\} \\ \overline{\boldsymbol{g}}_2(z;t) &= \boldsymbol{Q}_2^{-1}\boldsymbol{H}^{-1}\left\{\boldsymbol{\theta}'(z;t) - \boldsymbol{L}_1\boldsymbol{\kappa}(z;t) - \left[\boldsymbol{q}_1(z;t) - \overline{\overset{*}{\boldsymbol{q}}}_2(z;t)\right]\right\} \end{aligned}\right\}, \ z \in S^+, \quad (3.51)$$

and

$$\left.\begin{aligned} \boldsymbol{g}_2(z;t) &= -\boldsymbol{P}_2^{-1}\overset{*}{\boldsymbol{H}}^{-1}\left\{\boldsymbol{\theta}'(z;t) - \overset{*}{\boldsymbol{L}}_1\,\boldsymbol{\kappa}(z;t) - \left[\boldsymbol{q}_2(z;t) - \overline{\overset{*}{\boldsymbol{q}}}_1(z;t)\right]\right\} \\ \overline{\boldsymbol{g}}_1(z;t) &= -\boldsymbol{Q}_1^{-1}\overset{*}{\boldsymbol{H}}^{-1}\left\{\boldsymbol{\theta}'(z;t) - \boldsymbol{L}_2\boldsymbol{\kappa}(z;t) - \left[\boldsymbol{q}_2(z;t) - \overline{\overset{*}{\boldsymbol{q}}}_1(z;t)\right]\right\} \end{aligned}\right\}, z \in S^-. \quad (3.52)$$

It can be seen that the above equations are very similar to equations (3.14) and (3.15) with the exception of terms $\boldsymbol{q}_1(z;t) - \overline{\overset{*}{\boldsymbol{q}}}_2(z;t)$ and $\boldsymbol{q}_2(z;t) - \overline{\overset{*}{\boldsymbol{q}}}_1(z;t)$, which are totally determined by the solution for $m = 0$.

By substituting equations (3.51) and (3.52) into the boundary condition (3.45), one can show that $\boldsymbol{\kappa}(z;t)$ is an entire function. As a result, the boundary condition (3.45) will reduce to

$$\overset{*}{\boldsymbol{H}}\,\boldsymbol{\theta}'^{+}(\eta_1;t) - \boldsymbol{H}\boldsymbol{\theta}'^{-}(\eta_1;t) = \boldsymbol{R}\boldsymbol{\kappa}(\eta_1;t) + \hat{\boldsymbol{\kappa}}(\eta_1;t), \qquad \forall\ \eta_1 < 0, \quad (3.53)$$

where

$$\hat{\boldsymbol{\kappa}}(\eta_1;t) = \overset{*}{\boldsymbol{H}}\left[\boldsymbol{q}_1^{+}(\eta_1;t) - \overline{\overset{*}{\boldsymbol{q}}}_2^{+}(\eta_1;t)\right] - \boldsymbol{H}\left[\boldsymbol{q}_2^{-}(\eta_1;t) - \overline{\overset{*}{\boldsymbol{q}}}_1^{-}(\eta_1;t)\right].$$

Equation (3.53) also represents a Riemann-Hilbert problem for $\boldsymbol{\theta}'(z;t)$. It requires that $\boldsymbol{\theta}'(z;t)$ is analytic in the cut-plane $S^+ \cup S^-$, and along the cut satisfies the above equation. By using the properties of our asymptotic expansion, equations (2.9) - (2.11), it can be shown that $\boldsymbol{\theta}'(z;t)$ should vary as,

$$| \boldsymbol{\theta}'(z;t) | = O (|z|^{\alpha}) , \qquad \text{as} \quad |z| \to 0 , \tag{3.54}$$

for some $\alpha > 0$. The complete solution of (3.53) is generated by splitting the problem to the following two parts.

To obtain the first part, let $\overset{\circ}{\boldsymbol{\theta}}{}'(z;t)$ be an analytic function in the cut-plane $S^+ \cup S^-$, such that

$$\boldsymbol{H}\,\overset{\circ}{\boldsymbol{\theta}}{}'^{+}(\eta_1;t) - \boldsymbol{H}\,\overset{\circ}{\boldsymbol{\theta}}{}'^{-}(\eta_1;t) = \boldsymbol{R}\boldsymbol{\kappa}(\eta_1;t) , \qquad \forall\, \eta_1 < 0 . \tag{3.55}$$

This is exactly the same as equation (3.18). One basic difference, however, is that unlike the previous case, here $\overset{\circ}{\boldsymbol{\theta}}{}'(z;t)$ has to satisfy (3.54) (recall that before, $\alpha > -1$). As a result of this observation, in the material above the interface, the solution for $\overset{\circ}{\boldsymbol{g}}_1(z;t)$ is given by

$$\left.\begin{aligned}
&\overset{\circ}{g}{}_1^{(1)}(z;t) = -\frac{[(1+\alpha_s^2) - 2\eta\alpha_s]\, e^{\epsilon\pi}}{\mu D(v)\cosh\epsilon\pi} z^{\frac{1}{2}+i\epsilon}\, \overset{\circ}{A}_2(z;t) \\
&-\frac{[(1+\alpha_s^2) + 2\eta\alpha_s]\, e^{-\epsilon\pi}}{\mu D(v)\cosh\epsilon\pi} z^{\frac{1}{2}-i\epsilon}\, \overline{\overset{\circ}{A}}_2(z;t) \\
&-\frac{1}{\mu D(v)} \left\{ \left(\frac{1+\alpha_s^2}{1+\omega_l} - \frac{2\alpha_s}{1+\omega_s} \right) \overset{\circ}{B}_2(z;t) - \left(\frac{1+\alpha_s^2}{1+\omega_l} + \frac{2\alpha_s}{1+\omega_s} \right) \overline{\overset{\circ}{B}}_2(z;t) \right\} z
\end{aligned}\right\} , \tag{3.56}$$

and

$$\left.\begin{aligned}
&\overset{\circ}{g}{}_1^{(2)}(z;t) = \frac{[2\alpha_l - \eta(1+\alpha_s^2)]\, e^{\epsilon\pi}}{\mu D(v)\cosh\epsilon\pi} z^{\frac{1}{2}+i\epsilon}\, \overset{\circ}{A}_2(z;t) \\
&+\frac{[2\alpha_l + \eta(1+\alpha_s^2)]\, e^{-\epsilon\pi}}{\mu D(v)\cosh\epsilon\pi} z^{\frac{1}{2}-i\epsilon}\, \overline{\overset{\circ}{A}}_2(z;t) \\
&+\frac{1}{\mu D(v)} \left\{ \left(\frac{2\alpha_l}{1+\omega_l} - \frac{1+\alpha_s^2}{1+\omega_s} \right) \overset{\circ}{B}_2(z;t) - \left(\frac{2\alpha_l}{1+\omega_l} + \frac{1+\alpha_s^2}{1+\omega_s} \right) \overline{\overset{\circ}{B}}_2(z;t) \right\} z
\end{aligned}\right\} , \tag{3.57}$$

where

$$\overset{\circ}{\boldsymbol{g}}_1(z;t) = \left(\overset{\circ(1)}{g}_1(z;t),\ \overset{\circ(2)}{g}_1(z;t) \right)^{\top} ,$$

and the entire functions $\overset{\circ}{A}_2(z;t)$ and $\overset{\circ}{B}_2(z;t)$ can only be determined by the far field conditions. Similarly, the solution for $\overset{\circ}{\boldsymbol{g}}_2(z;t)$, in the material below the interface, can be obtained by changing the corresponding parameters in equations (3.56) and (3.57).

The second part of the solution is obtained by letting

$$\left.\begin{aligned} \hat{\boldsymbol{\theta}}'(z;t) &= \boldsymbol{\theta}'(z;t) - \overset{\circ}{\boldsymbol{\theta}}'(z;t) \\ \hat{\boldsymbol{g}}_k(z;t) &= \boldsymbol{g}_k(z;t) - \overset{\circ}{\boldsymbol{g}}_k(z;t) \end{aligned}\right\} .$$

Then, $\hat{\boldsymbol{\theta}}'(z;t)$ will be analytic in the cut-plane $S^+ \cup S^-$, and satisfy

$$\overset{*}{\boldsymbol{H}}\, \hat{\boldsymbol{\theta}}'^{+}(\eta_1;t) - \boldsymbol{H}\hat{\boldsymbol{\theta}}'^{-}(\eta_1;t) = \hat{\boldsymbol{\kappa}}(\eta_1;t) , \qquad \forall\ \eta_1 < 0 . \tag{3.58}$$

Because the right hand side of equation (3.58), $\hat{\boldsymbol{\kappa}}(\eta_1;t)$ is totally determined by the solutions $\phi_0(\eta_1,\eta_2,t)$ and $\psi_0(\eta_1,\eta_2,t)$, $\hat{\boldsymbol{\theta}}'(z;t)$, and therefore, $\hat{\boldsymbol{g}}_k(z;t)$ are also completely determined.

By using the results in Appendix II, we can write

$$\hat{\boldsymbol{\theta}}'(z;t) = \frac{1}{4\pi i}\int_{-\infty}^{0} \left\{ \frac{1}{\lambda_2}\frac{L(z)}{L^+(\eta_1)}\boldsymbol{\Gamma}\hat{\boldsymbol{\kappa}}(\eta_1;t) + \frac{1}{\lambda_1}\frac{\overline{L}(z)}{\overline{L}^+(\eta_1)}\,\overset{*}{\boldsymbol{\Gamma}}\,\hat{\boldsymbol{\kappa}}(\eta_1;t) \right\} \frac{\mathrm{d}\eta_1}{\eta_1 - z} , \tag{3.59}$$

where

$$L(z) = z^{\frac{1}{2}+i\epsilon} .$$

The explicit dependence of $\boldsymbol{q}_k(z;t)$ on z can be obtained from equation (3.50),

$$\left.\begin{aligned} \boldsymbol{q}_k(z;t) &= \boldsymbol{t}_k\{a_0(t),c_0(t)\}z^{\frac{1}{2}+i\epsilon} + \overline{\boldsymbol{t}}_k\{b_0(t),d_0(t)\}z^{\frac{1}{2}-i\epsilon} \\ &+ \dot{\epsilon}\,(3+2i\epsilon)(\boldsymbol{L}_k\boldsymbol{M}_k - \boldsymbol{I})\boldsymbol{k}_k\{a_0(t),c_0(t)\}z^{\frac{1}{2}+i\epsilon}\ln z \\ &+ \dot{\epsilon}\,(3-2i\epsilon)(\boldsymbol{L}_k\boldsymbol{M}_k - \boldsymbol{I})\overline{\boldsymbol{k}}_k\{b_0(t),d_0(t)\}z^{\frac{1}{2}-i\epsilon}\ln z \end{aligned}\right\} , \tag{3.60}$$

where operators like $\boldsymbol{t}_k\{a_0(t), c_0(t)\}$ and $\boldsymbol{k}_k\{a_0(t), c_0(t)\}$, etc., are given in Appendix I. From the definitions for $\overset{*}{\boldsymbol{q}}_k(z;t)$ and the above, one can get

$$\left.\begin{aligned} \boldsymbol{q}_1(z;t) - \overline{\overset{*}{\boldsymbol{q}}}_2(z;t) &= \boldsymbol{\beta} z^{\frac{1}{2}+i\epsilon} - \overline{\overset{*}{\boldsymbol{\gamma}}} z^{\frac{1}{2}-i\epsilon} + \dot{\epsilon}\,\boldsymbol{\xi} z^{\frac{1}{2}+i\epsilon}\ln z - \dot{\epsilon}\,\overline{\overset{*}{\boldsymbol{\varsigma}}} z^{\frac{1}{2}-i\epsilon}\ln z \\ \boldsymbol{q}_2(z;t) - \overline{\overset{*}{\boldsymbol{q}}}_1(z;t) &= \boldsymbol{\gamma} z^{\frac{1}{2}+i\epsilon} - \overline{\overset{*}{\boldsymbol{\beta}}} z^{\frac{1}{2}-i\epsilon} + \dot{\epsilon}\,\boldsymbol{\varsigma} z^{\frac{1}{2}+i\epsilon}\ln z - \dot{\epsilon}\,\overline{\overset{*}{\boldsymbol{\xi}}} z^{\frac{1}{2}-i\epsilon}\ln z \end{aligned}\right\}, \qquad (3.61)$$

where quantities of $\boldsymbol{\beta}$, $\boldsymbol{\gamma}$, $\boldsymbol{\xi}$, and $\boldsymbol{\varsigma}$ are also given in Appendix I. It should be noted here that $\boldsymbol{\beta}$ and $\boldsymbol{\gamma}$ depend on the crack-tip speed and the complex parameter $A_0(t)$, as well as their time derivatives. However, $\boldsymbol{\xi}$ and $\boldsymbol{\varsigma}$ depend only on the crack-tip speed and the complex parameter $A_0(t)$. The right hand side of equation (3.58), $\hat{\boldsymbol{\kappa}}(\eta_1;t)$, becomes

$$\left.\begin{aligned} \hat{\boldsymbol{\kappa}}(\eta_1;t) &= \dot{\epsilon}\,\boldsymbol{\omega}_d(-\eta_1)^{\frac{1}{2}+i\epsilon}\ln(-\eta_1) + \dot{\epsilon}\,\overline{\overset{*}{\boldsymbol{\omega}}}_d(-\eta_1)^{\frac{1}{2}-i\epsilon}\ln(-\eta_1) \\ &+ \boldsymbol{\omega}_t(-\eta_1)^{\frac{1}{2}+i\epsilon} + \overline{\overset{*}{\boldsymbol{\omega}}}_t(-\eta_1)^{\frac{1}{2}-i\epsilon} \end{aligned}\right\}, \quad \forall\ \eta_1 < 0\,, \qquad (3.62)$$

where

$$\left.\begin{aligned} \boldsymbol{\omega}_d &= i\left\{e^{-\epsilon\pi}\,\overset{*}{\boldsymbol{H}}\,\boldsymbol{\xi} + e^{\epsilon\pi}\boldsymbol{H}\boldsymbol{\varsigma}\right\} \\ \boldsymbol{\omega}_t &= i\left\{e^{-\epsilon\pi}\,\overset{*}{\boldsymbol{H}}\,\boldsymbol{\beta} + e^{\epsilon\pi}\boldsymbol{H}\boldsymbol{\gamma}\right\} - \pi\dot{\epsilon}\left\{e^{-\epsilon\pi}\,\overset{*}{\boldsymbol{H}}\,\boldsymbol{\xi} - e^{\epsilon\pi}\boldsymbol{H}\boldsymbol{\varsigma}\right\} \end{aligned}\right\}.$$

Once again, it can be seen that $\boldsymbol{\omega}_d$ does not depend on the time derivatives of the complex parameter $A_0(t)$ and the crack-tip speed, while $\boldsymbol{\omega}_t$ depends on these quantities. The functions inside the integrand of equation (3.59) can be rewritten as

$$\left.\begin{aligned} \frac{\hat{\boldsymbol{\kappa}}(\eta_1;t)}{L^+(\eta_1)} &= -ie^{\pi\epsilon}\left\{\dot{\epsilon}\,\boldsymbol{\omega}_d\ln(-\eta_1) + \dot{\epsilon}\,\overline{\overset{*}{\boldsymbol{\omega}}}_d(-\eta_1)^{-2i\epsilon}\ln(-\eta_1)\right. \\ &\qquad \left. +\boldsymbol{\omega}_t + \overline{\overset{*}{\boldsymbol{\omega}}}_t(-\eta_1)^{-2i\epsilon}\right\} \\ \frac{\hat{\boldsymbol{\kappa}}(\eta_1;t)}{\overline{L}^+(\eta_1)} &= -ie^{-\pi\epsilon}\left\{\dot{\epsilon}\,\boldsymbol{\omega}_d(-\eta_1)^{2i\epsilon}\ln(-\eta_1) + \dot{\epsilon}\,\overline{\overset{*}{\boldsymbol{\omega}}}_d\ln(-\eta_1)\right. \\ &\qquad \left. +\boldsymbol{\omega}_t(-\eta_1)^{2i\epsilon} + \overline{\overset{*}{\boldsymbol{\omega}}}_t\right\} \end{aligned}\right\}. \qquad (3.63)$$

In order to obtain the solution for $\hat{\boldsymbol{\theta}}'(z;t)$, we recast equation (3.59) into the form of a Stieltjes transform by using (3.63). However, one can see that for our case, a closed form evaluation of the Stieltjes transform integral is very difficult. At the beginning of this

section, it has been mentioned that only the most singular terms in the solution of $F_0(z;t)$ and $G_0(z;t)$ are considered. This implies that we are only interested in the region where $|z| \to 0$, i.e. very close to the interfacial crack-tip. As a result, instead of evaluating the entire Stieltjes transform, we only need to study the asymptotic behavior of that transform as $|z| \to 0$. The details of this asymptotic analysis are given in Appendix III. If only the leading terms in the Stieltjes transform are retained, by using the results provided in Appendix III, the solution for $\hat{\boldsymbol{\theta}}'(z;t)$ can be obtained as

$$\left.\begin{aligned} \hat{\boldsymbol{\theta}}'(z;t) &= \dot{\epsilon}\left[\boldsymbol{\zeta}_d z^{\frac{1}{2}+i\epsilon} - \bar{\boldsymbol{\zeta}}_d z^{\frac{1}{2}-i\epsilon}\right](\ln z)^2 + \left[\boldsymbol{\zeta}_t z^{\frac{1}{2}+i\epsilon} - \bar{\boldsymbol{\zeta}}_t z^{\frac{1}{2}-i\epsilon}\right]\ln z \\ &+ \left[\boldsymbol{\zeta}_{tt} z^{\frac{1}{2}+i\epsilon} - \bar{\boldsymbol{\zeta}}_{tt} z^{\frac{1}{2}-i\epsilon}\right] + O\left(|z|\right) \end{aligned}\right\}, \tag{3.64}$$

where in developing the above equation, the relation

$$\frac{e^{\pi\epsilon}}{\lambda_2} = -\frac{e^{-\pi\epsilon}}{\lambda_1},$$

has been used, and the following notations have been defined:

$$\left.\begin{aligned} \boldsymbol{\zeta}_d &= \frac{e^{-\pi\epsilon}}{8\pi\lambda_1}\boldsymbol{\Gamma}\boldsymbol{\omega}_d \\ \boldsymbol{\zeta}_t &= \frac{e^{-\pi\epsilon}}{4\pi\lambda_1}\left\{\boldsymbol{\Gamma}\boldsymbol{\omega}_t - \frac{i\pi\dot{\epsilon}}{\sinh(2\pi\epsilon)}\dot{\bar{\boldsymbol{\Gamma}}}\,\boldsymbol{\omega}_d\right\} \\ \boldsymbol{\zeta}_{tt} &= \frac{e^{-\pi\epsilon}}{4\pi\lambda_1}\left\{\left[\frac{\pi\dot{\epsilon}}{6}\boldsymbol{\Gamma}\boldsymbol{\omega}_d - \frac{\dot{\epsilon}}{4\epsilon^2}\boldsymbol{\Gamma}\bar{\boldsymbol{\omega}}_d - \frac{i}{2\epsilon}\boldsymbol{\Gamma}\dot{\bar{\boldsymbol{\omega}}}_t\right]\right. \\ &+ \left.\left[\frac{\pi^2\dot{\epsilon}\cosh(2\pi\epsilon)}{\sinh^2(2\pi\epsilon)}\dot{\bar{\boldsymbol{\Gamma}}}\,\boldsymbol{\omega}_d + \frac{i\pi}{\sinh(2\pi\epsilon)}\dot{\bar{\boldsymbol{\Gamma}}}\,\boldsymbol{\omega}_t\right]\right\} \end{aligned}\right\}.$$

In constructing the entire solution for $\boldsymbol{g}_1(z;t)$ and $\boldsymbol{g}_2(z;t)$, the leading terms in (3.56) and (3.57), are considered. This is consistent with the fact that (3.64) contains only

leading terms of the same order. The final solutions for $\boldsymbol{g}_1(z;t)$ and $\boldsymbol{g}_2(z;t)$, are therefore

$$\left.\begin{aligned}
\boldsymbol{g}_1(z;t) = \dot{\epsilon}\Big[&\boldsymbol{P}_1^{-1}\boldsymbol{H}^{-1}\boldsymbol{\zeta}_d z^{\frac{1}{2}+i\epsilon} - \boldsymbol{Q}_1^{-1}\overset{*}{\boldsymbol{H}}^{-1}\overline{\boldsymbol{\zeta}}_d z^{\frac{1}{2}-i\epsilon}\Big](\ln z)^2 \\
+\Big[&\boldsymbol{P}_1^{-1}\boldsymbol{H}^{-1}(\boldsymbol{\zeta}_t - \dot{\epsilon}\,\boldsymbol{\xi})z^{\frac{1}{2}+i\epsilon} - \boldsymbol{Q}_1^{-1}\overset{*}{\boldsymbol{H}}^{-1}\left(\overline{\boldsymbol{\zeta}}_t - \dot{\epsilon}\,\overline{\boldsymbol{\varsigma}}\right)z^{\frac{1}{2}-i\epsilon}\Big]\ln z \\
+\Big[&\boldsymbol{P}_1^{-1}\boldsymbol{H}^{-1}(\boldsymbol{\zeta}_{tt} - \boldsymbol{\beta})z^{\frac{1}{2}+i\epsilon} - \boldsymbol{Q}_1^{-1}\overset{*}{\boldsymbol{H}}^{-1}\left(\overline{\boldsymbol{\zeta}}_{tt} - \overline{\boldsymbol{\gamma}}\right)z^{\frac{1}{2}-i\epsilon}\Big] \\
+&\frac{e^{\epsilon\pi}\boldsymbol{P}_1^{-1}\boldsymbol{\zeta}}{\cosh\epsilon\pi}z^{\frac{1}{2}+i\epsilon}\,\overset{\circ}{\boldsymbol{A}}_2(t) + \frac{e^{-\epsilon\pi}\boldsymbol{Q}_1^{-1}\boldsymbol{\zeta}}{\cosh\epsilon\pi}z^{\frac{1}{2}-i\epsilon}\overline{\overset{\circ}{\boldsymbol{A}}}_2(t) + O\left(|z|\right)
\end{aligned}\right\},\quad z\in S^+, \tag{3.65}$$

and

$$\left.\begin{aligned}
\boldsymbol{g}_2(z;t) = -\dot{\epsilon}\Big[&\boldsymbol{P}_2^{-1}\overset{*}{\boldsymbol{H}}^{-1}\boldsymbol{\zeta}_d z^{\frac{1}{2}+i\epsilon} - \boldsymbol{Q}_2^{-1}\boldsymbol{H}^{-1}\overline{\boldsymbol{\zeta}}_d z^{\frac{1}{2}-i\epsilon}\Big](\ln z)^2 \\
-\Big[&\boldsymbol{P}_2^{-1}\overset{*}{\boldsymbol{H}}^{-1}(\boldsymbol{\zeta}_t - \dot{\epsilon}\,\boldsymbol{\varsigma})z^{\frac{1}{2}+i\epsilon} - \boldsymbol{Q}_2^{-1}\boldsymbol{H}^{-1}\left(\overline{\boldsymbol{\zeta}}_t - \dot{\epsilon}\,\overline{\boldsymbol{\xi}}\right)z^{\frac{1}{2}-i\epsilon}\Big]\ln z \\
-\Big[&\boldsymbol{P}_2^{-1}\overset{*}{\boldsymbol{H}}^{-1}(\boldsymbol{\zeta}_{tt} - \boldsymbol{\gamma})z^{\frac{1}{2}+i\epsilon} - \boldsymbol{Q}_2^{-1}\boldsymbol{H}^{-1}\left(\overline{\boldsymbol{\zeta}}_{tt} - \overline{\boldsymbol{\beta}}\right)z^{\frac{1}{2}-i\epsilon}\Big] \\
+&\frac{e^{-\epsilon\pi}\boldsymbol{P}_2^{-1}\boldsymbol{\zeta}}{\cosh\epsilon\pi}z^{\frac{1}{2}+i\epsilon}\,\overset{\circ}{\boldsymbol{A}}_2(t) + \frac{e^{\epsilon\pi}\boldsymbol{Q}_2^{-1}\boldsymbol{\zeta}}{\cosh\epsilon\pi}z^{\frac{1}{2}-i\epsilon}\overline{\overset{\circ}{\boldsymbol{A}}}_2(t) + O\left(|z|\right)
\end{aligned}\right\},\quad z\in S^-, \tag{3.66}$$

where $\overset{\circ}{\boldsymbol{A}}_2(t) = \overset{\circ}{\boldsymbol{A}}_2(0;t)$.

Our final target is to find the complex potentials $\boldsymbol{f}_k(z;t) = \left(F_{2k}(z;t), G_{2k}(z;t)\right)^{\mathsf{T}}$. After some manipulations, $\boldsymbol{f}_1''(z;t)$ and $\boldsymbol{f}_2''(z;t)$ can be expressed as

$$\left.\begin{aligned}
\boldsymbol{f}_1''(z;t) = \dot{\epsilon}\Big\{&\boldsymbol{P}_1^{-1}\boldsymbol{H}^{-1}\boldsymbol{\zeta}_d z^{\frac{1}{2}+i\epsilon} - \boldsymbol{Q}_1^{-1}\overset{*}{\boldsymbol{H}}^{-1}\overline{\boldsymbol{\zeta}}_d z^{\frac{1}{2}-i\epsilon}\Big\}(\ln z)^2 \\
+\Big\{&\left[\boldsymbol{P}_1^{-1}\boldsymbol{H}^{-1}(\boldsymbol{\zeta}_t - \dot{\epsilon}\,\boldsymbol{\xi}) + \dot{\epsilon}\,\boldsymbol{w}_{d1}\{a_0(t), c_0(t)\}\right]z^{\frac{1}{2}+i\epsilon} \\
-&\left[\boldsymbol{Q}_1^{-1}\overset{*}{\boldsymbol{H}}^{-1}\left(\overline{\boldsymbol{\zeta}}_t - \dot{\epsilon}\,\overline{\boldsymbol{\varsigma}}\right) - \dot{\epsilon}\,\overline{\boldsymbol{w}}_{d1}\{b_0(t), d_0(t)\}\right]z^{\frac{1}{2}-i\epsilon}\Big\}\ln z \\
+\Big\{&\left[\boldsymbol{P}_1^{-1}\boldsymbol{H}^{-1}(\boldsymbol{\zeta}_{tt} - \boldsymbol{\beta}) + \boldsymbol{w}_{t1}\{a_0(t), c_0(t)\}\right]z^{\frac{1}{2}+i\epsilon} \\
-&\left[\boldsymbol{Q}_1^{-1}\overset{*}{\boldsymbol{H}}^{-1}\left(\overline{\boldsymbol{\zeta}}_{tt} - \overline{\boldsymbol{\gamma}}\right) - \overline{\boldsymbol{w}}_{t1}\{b_0(t), d_0(t)\}\right]z^{\frac{1}{2}-i\epsilon}\Big\} \\
+&\frac{e^{\epsilon\pi}\boldsymbol{P}_1^{-1}\boldsymbol{\zeta}}{\cosh\epsilon\pi}z^{\frac{1}{2}+i\epsilon}\,\overset{\circ}{\boldsymbol{A}}_2(t) + \frac{e^{-\epsilon\pi}\boldsymbol{Q}_1^{-1}\boldsymbol{\zeta}}{\cosh\epsilon\pi}z^{\frac{1}{2}-i\epsilon}\overline{\overset{\circ}{\boldsymbol{A}}}_2(t) + O\left(|z|\right)
\end{aligned}\right\},\quad z\in S^+, \tag{3.67}$$

and

$$
\left.
\begin{aligned}
\boldsymbol{f}_2''(z;t) = &-\dot{\epsilon}\left\{\boldsymbol{P}_2^{-1}\,\overset{*}{\boldsymbol{H}}^{-1}\,\boldsymbol{\zeta}_d z^{\frac{1}{2}+i\epsilon} - \boldsymbol{Q}_2^{-1}\boldsymbol{H}^{-1}\overline{\boldsymbol{\zeta}}_d z^{\frac{1}{2}-i\epsilon}\right\}(\ln z)^2 \\
&-\left\{\left[\boldsymbol{P}_2^{-1}\,\overset{*}{\boldsymbol{H}}^{-1}\,(\boldsymbol{\zeta}_t - \dot{\epsilon}\,\boldsymbol{\varsigma}) - \dot{\epsilon}\,\boldsymbol{w}_{d2}\{a_0(t), c_0(t)\}\right] z^{\frac{1}{2}+i\epsilon}\right. \\
&\left.-\left[\boldsymbol{Q}_2^{-1}\boldsymbol{H}^{-1}\left(\overline{\boldsymbol{\zeta}}_t - \dot{\epsilon}\,\overline{\boldsymbol{\xi}}\right) + \dot{\epsilon}\,\overline{\boldsymbol{w}}_{d2}\{b_0(t), d_0(t)\}\right] z^{\frac{1}{2}-i\epsilon}\right\}\ln z \\
&-\left\{\left[\boldsymbol{P}_2^{-1}\,\overset{*}{\boldsymbol{H}}^{-1}\,(\boldsymbol{\zeta}_{tt} - \boldsymbol{\gamma}) - \boldsymbol{w}_{t2}\{a_0(t), c_0(t)\}\right] z^{\frac{1}{2}+i\epsilon}\right. \\
&\left.-\left[\boldsymbol{Q}_2^{-1}\boldsymbol{H}^{-1}\left(\overline{\boldsymbol{\zeta}}_{tt} - \overline{\boldsymbol{\beta}}\right) + \overline{\boldsymbol{w}}_{t2}\{b_0(t), d_0(t)\}\right] z^{\frac{1}{2}-i\epsilon}\right] \\
&+\frac{e^{-\epsilon\pi}\boldsymbol{P}_2^{-1}\boldsymbol{\zeta}}{\cosh\epsilon\pi} z^{\frac{1}{2}+i\epsilon}\,\overset{\circ}{A}_2(t) + \frac{e^{\epsilon\pi}\boldsymbol{Q}_2^{-1}\boldsymbol{\zeta}}{\cosh\epsilon\pi} z^{\frac{1}{2}-i\epsilon}\,\overline{\overset{\circ}{A}}_2(t) + O\left(|z|\right)
\end{aligned}
\right\},\quad z\in S^-, \qquad (3.68)
$$

where the operators $\boldsymbol{w}_{dk}(\cdot,\cdot)$ and $\boldsymbol{w}_{tk}(\cdot,\cdot)$ are given in Appendix I. By integrating the above two expressions with respect to the complex argument z, we can finally obtain the complex potential $\boldsymbol{f}_k(z;t) = \left(\, F_{2k}(z;t), G_{2k}(z;t)\,\right)^{\mathsf{T}}$ for both materials.

Since equations (3.67) and (3.68) are directly related to the stress components around the interfacial crack-tip, some of the noteworthy features of the asymptotic field can be studied through them. The most interesting feature is that there exist two terms in the above equations, which are totally different in nature from the terms found in the solution of a crack propagating transiently in a homogeneous material. The first of these terms is that associated with $z^{1/2}(\ln z)^2$. This term is clearly associated with the interfacial nature of crack growth since it is proportional to the quantity $\dot{\epsilon}$. This quantity is also related to the transient nature (existence of non-zero accelerations) of the problem. By observing that

$$\dot{\epsilon} = \frac{\mathrm{d}\epsilon}{\mathrm{d}v}\frac{\mathrm{d}v}{\mathrm{d}t}\,,$$

One can easily see that $\dot{\epsilon}$ and thus the $z^{1/2}(\ln z)^2$ term vanish either when the crack-tip speed is constant and/or when the material mismatch parameter ϵ vanishes.

The second term is that associated with $z^{1/2}\ln z$. The coefficient of this term is related

to the complex parameter $A_0(t)$ and also depends on the crack-tip speed, as well as on their time derivatives. So it depends on both $\dot{v}(t)$ and $K^d(t)$. It can be seen that for constant speed transient crack growth ($\dot{v} = 0$, $\dot{K}_d \neq 0$), this term will still be present. Indeed the $r^{1/2} \ln r$ term has been observed by WILLIS (1973), who studied a particular constant velocity, transient interfacial crack growth problem. Both of these two terms which include logarithms will vanish at the same time only if the situation is strictly *steady state.* Otherwise one or both will be present. These logarithmic sigularities are the consequences of the existence of both the interface and the transient nature of the propagating crack. For the case of crack growth in a homogeneous material ($\epsilon = 0$), $\boldsymbol{\beta} = \boldsymbol{\gamma}$ and $\boldsymbol{\xi} = \boldsymbol{\varsigma}$, see Appendix I. This is true even if crack propagation is transient. As a result, it can be shown that $\boldsymbol{\omega}_d = \boldsymbol{\omega}_t = \mathbf{0}$, and consequently, $\boldsymbol{\zeta}_d$, $\boldsymbol{\zeta}_t$, and $\boldsymbol{\zeta}_{tt}$ will vanish. The logarithmic terms also disappear. In this case, the transient field reduces to the one obtained by LIU and ROSAKIS (1992) which does not feature any logarithms. It should be stated at this point that transient higher order terms involving logarithmic singularities have also been observed in the solution of dislocation lines propagating transiently in elastic solids (CALLIAS *et al.*, 1990, and MARKENSCOFF and NI, 1990). These terms were shown to vanish when the dislocations propagated with constant speed.

In this section, we have provided a procedure which allows us to investigate higher order transient effects systematically. By imposing the boundary and bonding conditions on the complex potentials, the problem was recasted into the Riemann-Hilbert problem. By solving the Riemann-Hilbert equations, and by evaluating the Stieltjes transforms, the higher order terms were obtained. This procedure can be repeated to any order, and we may therefore claim that it is constructive.

4 The asymptotic elastodynamic field around a non-uniformly propagating interfacial crack-tip

For planar deformation of a homogeneous, isotropic, linearly elastic material, the ordered array $[u_\alpha, \varepsilon_{\alpha\beta}, \sigma_{\alpha\beta}]$, $\alpha,\ \beta \in \{1,2\}$, is said to be an elastodynamic state in the absence of body force density, if the following conditions are satisfied

$$\left.\begin{aligned} \varepsilon_{\alpha\beta} &= \frac{1}{2}\left(u_{\alpha,\beta} + u_{\beta,\alpha}\right) \\ \sigma_{\alpha\beta} &= 2\mu\varepsilon_{\alpha\beta} + \lambda\varepsilon_{\gamma\gamma}\delta_{\alpha\beta} \\ \sigma_{\alpha\beta,\beta} &= \rho\ddot{u}_\alpha \end{aligned}\right\}, \qquad \alpha,\ \beta \in \{1,2\}\ , \tag{4.1}$$

where ρ is the mass density and λ, μ are Lamé constants of the material. In addition, the field quantities u_α, $\varepsilon_{\alpha\beta}$, and $\sigma_{\alpha\beta}$ must satisfy the smoothness requirements outlined in WHEELER and STERNBERG (1968).

In the Cartesian coordinate system (ξ_1, ξ_2), let $\phi_m(\xi_1, \xi_2, t)$ and $\psi_m(\xi_1, \xi_2, t)$ be solutions of equations (2.12), $m = 0, 1, 2, \cdots$, such that

$$\left.\begin{aligned} \frac{\phi_{m+n}(\xi_1,\xi_2,t)}{\phi_m(\xi_1,\xi_2,t)} &\to 0 \\ \frac{\psi_{m+n}(\xi_1,\xi_2,t)}{\psi_m(\xi_1,\xi_2,t)} &\to 0 \end{aligned}\right\}, \quad \text{as } r = \sqrt{\xi_1^2 + \xi_2^2} \to 0\ , \quad m = 0,1,2,\cdots, \tag{4.2}$$

for any positive integer n. Thus, $\phi_m(\xi_1, \xi_2, t)$ and $\psi_m(\xi_1, \xi_2, t)$ will be two asymptotic sequences as $r = (\xi_1^2 + \xi_2^2)^{1/2} \to 0$. Define $\phi(\xi_1, \xi_2, t)$ and $\psi(\xi_1, \xi_2, t)$ by

$$\left.\begin{aligned} \phi(\xi_1,\xi_2,t) &= \sum_{m=0}^{\infty} \phi_m(\xi_1,\xi_2,t) \\ \psi(\xi_1,\xi_2,t) &= \sum_{m=0}^{\infty} \psi_m(\xi_1,\xi_2,t) \end{aligned}\right\}. \tag{4.3}$$

Then, the array $[u_\alpha, \varepsilon_{\alpha\beta}, \sigma_{\alpha\beta}]$, $\alpha,\ \beta \in \{1,2\}$, will constitute an *asymptotic* elastodynamic

state as $r = (\xi_1^2 + \xi_2^2)^{1/2} \to 0$, if it satisfies

$$\left.\begin{aligned} v_\alpha &= \phi_{,\alpha} + e_{\alpha\beta}\psi_{,\beta} \\ \varepsilon_{\alpha\beta} &= \frac{1}{2}\left(u_{\alpha,\beta} + u_{\beta,\alpha}\right) \\ \sigma_{\alpha\beta} &= 2\mu\varepsilon_{\alpha\beta} + \lambda\varepsilon_{\gamma\gamma}\delta_{\alpha\beta} \end{aligned}\right\}, \qquad \alpha,\ \beta \in \{1,2\}\ . \tag{4.4}$$

Now, consider a planar body composed of two homogeneous, isotropic, and linearly elastic materials bonded along a straight interface. Let the two displacement potentials for each material be given by (4.3), where each term of the asymptotic series is the solution which has been discussed in the previous section. The asymptotic elastodynamic state near the non-uniformly propagating interfacial crack-tip can then be obtained from relations (4.4).

For its importance in the experimental investigation described in section 7, we only provide the asymptotic expression of the first stress invariant around the interfacial crack-tip. However, in order to shorten our expression, some notation needs to be defined first. In the expressions below, the superscript (1) or (2) denotes the components of the vectors defined in Appendix I and in previous sections. For the material above the interface, we may define the following quantities,

$$\Omega_d(t) = -\frac{1}{\mu D(v)\lambda_1\lambda_2}\left\{\left[(1+\alpha_s^2)h_{11} + 2\alpha_s h_{21}\right]\zeta_d^{(1)} - \left[(1+\alpha_s^2)h_{12} + 2\alpha_s h_{11}\right]\zeta_d^{(2)}\right\}\ ,$$

$$\mathring{\Omega}_d(t) = -\frac{1}{\mu D(v)\lambda_1\lambda_2}\left\{\left[(1+\alpha_s^2)h_{11} + 2\alpha_s h_{21}\right]\overline{\zeta}_d^{(1)} + \left[(1+\alpha_s^2)h_{12} + 2\alpha_s h_{11}\right]\overline{\zeta}_d^{(2)}\right\}\ ,$$

$$\begin{aligned}\Omega_t(t) = -\frac{1}{\mu D(v)\lambda_1\lambda_2}\Big\{&\left[(1+\alpha_s^2)h_{11} + 2\alpha_s h_{21}\right]\left(\zeta_t^{(1)} - \dot{\epsilon}\,\xi^{(1)}\right) \\ &- \left[(1+\alpha_s^2)h_{12} + 2\alpha_s h_{11}\right]\left(\zeta_t^{(2)} - \dot{\epsilon}\,\xi^{(2)}\right)\Big\} + \dot{\epsilon}\, w_d^{(1)}\{a_0(t), c_0(t)\}\ ,\end{aligned}$$

$$\begin{aligned}\mathring{\Omega}_t(t) = -\frac{1}{\mu D(v)\lambda_1\lambda_2}\Big\{&\left[(1+\alpha_s^2)h_{11} + 2\alpha_s h_{21}\right]\left(\overline{\zeta}_t^{(1)} - \dot{\epsilon}\,\overline{\xi}^{(1)}\right) \\ &+ \left[(1+\alpha_s^2)h_{12} + 2\alpha_s h_{11}\right]\left(\overline{\zeta}_t^{(2)} - \dot{\epsilon}\,\overline{\xi}^{(2)}\right)\Big\} - \dot{\epsilon}\,\overline{w}_d^{(1)}\{b_0(t), d_0(t)\}\ ,\end{aligned}$$

$$\Omega_{tt}(t) = -\frac{1}{\mu D(v)\lambda_1\lambda_2}\left\{\left[(1+\alpha_s^2)h_{11}+2\alpha_s h_{21}\right]\left(\zeta_{tt}^{(1)}-\beta^{(1)}\right)\right.$$
$$\left.-\left[(1+\alpha_s^2)h_{12}+2\alpha_s h_{11}\right]\left(\zeta_{tt}^{(2)}-\beta^{(2)}\right)\right\}+w_t^{(1)}\{a_0(t),c_0(t)\}\ ,$$

$$\overset{*}{\Omega}_{tt}(t) = -\frac{1}{\mu D(v)\lambda_1\lambda_2}\left\{\left[(1+\alpha_s^2)h_{11}+2\alpha_s h_{21}\right]\left(\overline{\zeta}_{tt}^{(1)}-\overline{\gamma}^{(1)}\right)\right.$$
$$\left.+\left[(1+\alpha_s^2)h_{12}+2\alpha_s h_{11}\right]\left(\overline{\zeta}_{tt}^{(2)}-\overline{\gamma}^{(2)}\right)\right\}-\overline{w}_t^{(1)}\{b_0(t),d_0(t)\}\ .$$

Now, one can show that by using equations (3.32) and (3.67), the first stress invariant in the material above the interface will be given by

$$\left.\begin{aligned}\frac{\sigma_{11}+\sigma_{22}}{2\mu(\alpha_l^2-\alpha_s^2)} &= \mathrm{Re}\left\{\overset{\circ}{A}_0(t)a_0(t)z_l^{-\frac{1}{2}+i\epsilon}+\overline{\overset{\circ}{A}}_0(t)b_0(t)z_l^{-\frac{1}{2}-i\epsilon}\right.\\
&+\frac{2\alpha_s}{\mu D(v)(1+\omega_s)}\left(\overset{\circ}{A}_1(t)+\overline{\overset{\circ}{A}}_1(t)\right)+\overset{\circ}{A}_2(t)a_0(t)z_l^{\frac{1}{2}+i\epsilon}+\overline{\overset{\circ}{A}}_2(t)b_0(t)z_l^{\frac{1}{2}-i\epsilon}\\
&+\left[A_{tt}(t)z_l^{\frac{1}{2}+i\epsilon}+B_{tt}(t)\overline{z}_l z_l^{-\frac{1}{2}+i\epsilon}+C_{tt}(t)\overline{z}_l^2 z_l^{-\frac{3}{2}+i\epsilon}\right.\\
&\left.-\overset{*}{A}_{tt}(t)z_l^{\frac{1}{2}-i\epsilon}-\overset{*}{B}_{tt}(t)\overline{z}_l z_l^{-\frac{1}{2}-i\epsilon}-\overset{*}{C}_{tt}(t)\overline{z}_l^2 z_l^{-\frac{3}{2}-i\epsilon}\right]\\
&+\left[A_t(t)z_l^{\frac{1}{2}+i\epsilon}+B_t(t)\overline{z}_l z_l^{-\frac{1}{2}+i\epsilon}-\overset{*}{A}_t(t)z_l^{\frac{1}{2}-i\epsilon}-\overset{*}{B}_t(t)\overline{z}_l z_l^{-\frac{1}{2}-i\epsilon}\right]\ln z_l\\
&\left.+\dot{\epsilon}\left[\Omega_d(t)z_l^{\frac{1}{2}+i\epsilon}-\overset{*}{\Omega}_d(t)z_l^{\frac{1}{2}-i\epsilon}\right](\ln z_l)^2\right\}+O\left(|z_l|\right)\end{aligned}\right\}\ , \qquad (4.5)$$

where

$$A_{tt}(t) = \Omega_{tt}(t)-\frac{2(1+\alpha_l^2)}{1-\alpha_l^2}\left\{\left(\frac{3}{2}+i\epsilon\right)D_l\{a_0(t)\}+\dot{\epsilon}\,K_l(t)a_0(t)\right\}-2B_l(t)a_0(t)\ ,$$

$$\overset{*}{A}_{tt}(t) = \overset{*}{\Omega}_{tt}(t)+\frac{2(1+\alpha_l^2)}{1-\alpha_l^2}\left\{\left(\frac{3}{2}-i\epsilon\right)\overline{D}_l\{b_0(t)\}+\dot{\epsilon}\,\overline{K}_l(t)b_0(t)\right\}+2\overline{B}_l(t)b_0(t)\ ,$$

$$B_{tt}(t) = -\left(\frac{3}{2}+i\epsilon\right)\left(\frac{1}{2}+i\epsilon\right)D_l\{a_0(t)\}-2\dot{\epsilon}(1+i\epsilon)K_l(t)a_0(t)$$
$$-\frac{2(1+\alpha_l^2)}{1-\alpha_l^2}\left(\frac{1}{2}+i\epsilon\right)B_l(t)a_0(t)\ ,$$

$$\overset{*}{B}_{tt}(t) = \left(\frac{3}{2}-i\epsilon\right)\left(\frac{1}{2}-i\epsilon\right)\overline{D}_l\{b_0(t)\}+2\dot{\epsilon}(1-i\epsilon)\overline{K}_l(t)b_0(t)$$

$$+\frac{2(1+\alpha_l^2)}{1-\alpha_l^2}\left(\frac{1}{2}-i\epsilon\right)\overline{B}_l(t)b_0(t)\ ,$$

$$C_{tt}(t) = \left(\frac{1}{4}+\epsilon^2\right)B_l(t)a_0(t)\ , \quad \overset{\bullet}{C}_{tt}(t) = -\left(\frac{1}{4}+\epsilon^2\right)\overline{B}_l(t)b_0(t)\ ,$$

$$A_t(t) = \Omega_t(t) - \frac{2(1+\alpha_l^2)\dot{\epsilon}}{1-\alpha_l^2}\left(\frac{3}{2}+i\epsilon\right)K_l(t)a_0(t)\ ,$$

$$\overset{\bullet}{A}_t(t) = \overset{\bullet}{\Omega}_t(t) + \frac{2(1+\alpha_l^2)\dot{\epsilon}}{1-\alpha_l^2}\left(\frac{3}{2}-i\epsilon\right)\overline{K}_l(t)b_0(t)\ ,$$

$$B_t(t) = -\dot{\epsilon}\left(\frac{3}{2}+i\epsilon\right)\left(\frac{1}{2}+i\epsilon\right)K_l(t)a_0(t)\ ,$$

$$\overset{\bullet}{B}_t(t) = \dot{\epsilon}\left(\frac{3}{2}-i\epsilon\right)\left(\frac{1}{2}-i\epsilon\right)\overline{K}_l(t)b_0(t)\ ,$$

$$K_l(t) = -i\frac{v}{4\sqrt{2\pi}\alpha_l^2 c_l^2}\frac{K(t)}{\left(\frac{3}{2}+i\epsilon\right)\left(\frac{1}{2}+i\epsilon\right)}\ .$$

In expression (4.5), functions of time $\overset{\circ}{A}_0(t)$, $\overset{\circ}{A}_1(t)$, and $\overset{\circ}{A}_2(t)$ are undetermined by the asymptotic analysis. On the other hand, functions $A_{tt}(t)$, $B_{tt}(t)$, $C_{tt}(t)$, $\overset{\bullet}{A}_{tt}(t)$, $\cdots$, are known in terms of $\overset{\circ}{A}_0(t)$, the crack-tip acceleration $\dot{v}(t)$, and the time derivative of $\overset{\circ}{A}_0(t)$. As a result, these functions are also undetermined by the asymptotic analysis. However, their dependence on time derivatives of $v(t)$ and $\overset{\circ}{A}_0(t)$ constitutes the mathematical demonstration of transient effects.

It is often convenient to express the first stress invariant in terms of real quantities. For any complex function of time $W(t)$, let its magnitude be denoted by $|W|$, and its phase be denoted by $\Phi(W)$. Meanwhile, a scaled polar coordinate system (r_l, θ_l) centered at the moving crack-tip is defined by

$$r_l = \left\{\xi_1^2 + \alpha_l^2\xi_2^2\right\}^{1/2}\ , \qquad \theta_l = \tan^{-1}\frac{\alpha_l\xi_2}{\xi_1}\ .$$

The first stress invariant in the material above the interface can therefore be expressed

as

$$\left.\begin{aligned}
\frac{\sigma_{11}+\sigma_{22}}{2\mu\,(\alpha_l^2-\alpha_s^2)} &= |\,\mathring{A}_0\,(t)|\left\{\Sigma_0(\theta_l)\cos(\epsilon\ln r_l)+\mathring{\Sigma}_0\,(\theta_l)\sin(\epsilon\ln r_l)\right\}r_l^{-1/2}\\
&+ \frac{4\alpha_s}{\mu D(v)(1+\omega_s)}|\,\mathring{A}_1\,(t)|\cos\Phi(\mathring{A}_1)\\
&+ \dot{\epsilon}\left\{\Sigma_d(\theta_l)\cos(\epsilon\ln r_l)+\mathring{\Sigma}_d\,(\theta_l)\sin(\epsilon\ln r_l)\right\}r_l^{1/2}(\ln r_l)^2\\
&+ \left\{\Sigma_t(\theta_l)\cos(\epsilon\ln r_l)+\mathring{\Sigma}_t\,(\theta_l)\sin(\epsilon\ln r_l)\right\}r_l^{1/2}\ln r_l\\
&+ \left\{\Sigma_{tt}(\theta_l)\cos(\epsilon\ln r_l)+\mathring{\Sigma}_{tt}\,(\theta_l)\sin(\epsilon\ln r_l)\right\}r_l^{1/2}\\
&+ |\,\mathring{A}_2\,(t)|\left\{\Sigma_2(\theta_l)\cos(\epsilon\ln r_l)+\mathring{\Sigma}_2\,(\theta_l)\sin(\epsilon\ln r_l)\right\}r_l^{1/2}\\
&+ O(r_l)
\end{aligned}\right\}, \qquad (4.6)$$

where

$$\begin{aligned}
\Sigma_0(\theta_l) &= a_0(t)e^{-\epsilon\theta_l}\cos\left(\frac{\theta_l}{2}-\Phi(\mathring{A}_0)\right)+b_0(t)e^{\epsilon\theta_l}\cos\left(\frac{\theta_l}{2}+\Phi(\mathring{A}_0)\right),\\
\mathring{\Sigma}_0\,(\theta_l) &= a_0(t)e^{-\epsilon\theta_l}\sin\left(\frac{\theta_l}{2}-\Phi(\mathring{A}_0)\right)-b_0(t)e^{\epsilon\theta_l}\sin\left(\frac{\theta_l}{2}+\Phi(\mathring{A}_0)\right),\\
\Sigma_2(\theta_l) &= a_0(t)e^{-\epsilon\theta_l}\cos\left(\frac{\theta_l}{2}+\Phi(\mathring{A}_2)\right)+b_0(t)e^{\epsilon\theta_l}\cos\left(\frac{\theta_l}{2}-\Phi(\mathring{A}_2)\right),\\
\mathring{\Sigma}_2\,(\theta_l) &= -\left\{a_0(t)e^{-\epsilon\theta_l}\sin\left(\frac{\theta_l}{2}+\Phi(\mathring{A}_2)\right)-b_0(t)e^{\epsilon\theta_l}\sin\left(\frac{\theta_l}{2}-\Phi(\mathring{A}_0)\right)\right\},\\
\Sigma_d(\theta_l) &= |\Omega_d(t)|e^{-\epsilon\theta_l}\cos\left(\frac{\theta_l}{2}+\Phi(\Omega_d)\right)-|\,\mathring{\Omega}_d\,(t)|e^{\epsilon\theta_l}\cos\left(\frac{\theta_l}{2}+\Phi(\mathring{\Omega}_d)\right),\\
\mathring{\Sigma}_d\,(\theta_l) &= -\left\{|\Omega_d(t)|e^{-\epsilon\theta_l}\sin\left(\frac{\theta_l}{2}+\Phi(\Omega_d)\right)+|\,\mathring{\Omega}_d\,(t)|e^{\epsilon\theta_l}\sin\left(\frac{\theta_l}{2}+\Phi(\mathring{\Omega}_d)\right)\right\},\\
\Sigma_t(\theta_l) &= |A_t(t)|e^{-\epsilon\theta_l}\cos\left(\frac{\theta_l}{2}+\Phi(A_t)\right)-|\,\mathring{A}_t\,(t)|e^{\epsilon\theta_l}\cos\left(\frac{\theta_l}{2}+\Phi(\mathring{A}_t)\right)\\
&+ |B_t(t)|e^{-\epsilon\theta_l}\cos\left(\frac{3\theta_l}{2}-\Phi(B_t)\right)-|\,\mathring{B}_t\,(t)|e^{\epsilon\theta_l}\cos\left(\frac{3\theta_l}{2}-\Phi(\mathring{B}_t)\right)\\
&- 2\dot{\epsilon}\left\{|\Omega_d(t)|e^{-\epsilon\theta_l}\sin\left(\frac{\theta_l}{2}+\Phi(\Omega_d)\right)-|\,\mathring{\Omega}_d\,(t)|e^{\epsilon\theta_l}\sin\left(\frac{\theta_l}{2}+\Phi(\mathring{\Omega}_d)\right)\right\}\theta_l,
\end{aligned}$$

$$
\begin{aligned}
\dot{\Sigma}_t\,(\theta_l) &= -\left\{|A_t(t)|e^{-\epsilon\theta_l}\sin\left(\frac{\theta_l}{2}+\Phi(A_t)\right)+|\dot{A}_t\,(t)|e^{\epsilon\theta_l}\sin\left(\frac{\theta_l}{2}+\Phi(\dot{A}_t)\right)\right\}\\
&+ |B_t(t)|e^{-\epsilon\theta_l}\sin\left(\frac{3\theta_l}{2}-\Phi(B_t)\right)+|\dot{B}_t\,(t)|e^{\epsilon\theta_l}\sin\left(\frac{3\theta_l}{2}-\Phi(\dot{B}_t)\right)\\
&- 2\dot{\epsilon}\left\{|\Omega_d(t)|e^{-\epsilon\theta_l}\cos\left(\frac{\theta_l}{2}+\Phi(\Omega_d)\right)+|\dot{\Omega}_d\,(t)|e^{\epsilon\theta_l}\cos\left(\frac{\theta_l}{2}+\Phi(\dot{\Omega}_d)\right)\right\}\theta_l,\\
\Sigma_{tt}(\theta_l) &= |A_{tt}(t)|e^{-\epsilon\theta_l}\cos\left(\frac{\theta_l}{2}+\Phi(A_{tt})\right)-|\dot{A}_{tt}\,(t)|e^{\epsilon\theta_l}\cos\left(\frac{\theta_l}{2}+\Phi(\dot{A}_{tt})\right)\\
&+ |B_{tt}(t)|e^{-\epsilon\theta_l}\cos\left(\frac{3\theta_l}{2}-\Phi(B_{tt})\right)-|\dot{B}_{tt}\,(t)|e^{\epsilon\theta_l}\cos\left(\frac{3\theta_l}{2}-\Phi(\dot{B}_{tt})\right)\\
&+ |C_{tt}(t)|e^{-\epsilon\theta_l}\cos\left(\frac{7\theta_l}{2}-\Phi(C_{tt})\right)-|\dot{C}_{tt}\,(t)|e^{\epsilon\theta_l}\cos\left(\frac{7\theta_l}{2}-\Phi(\dot{C}_{tt})\right)\\
&- \left\{|A_t(t)|e^{-\epsilon\theta_l}\sin\left(\frac{\theta_l}{2}+\Phi(A_t)\right)-|\dot{A}_t\,(t)|e^{\epsilon\theta_l}\sin\left(\frac{\theta_l}{2}+\Phi(\dot{A}_t)\right)\right\}\theta_l\\
&+ \left\{|B_t(t)|e^{-\epsilon\theta_l}\sin\left(\frac{3\theta_l}{2}-\Phi(B_t)\right)-|\dot{B}_t\,(t)|e^{\epsilon\theta_l}\sin\left(\frac{3\theta_l}{2}-\Phi(\dot{B}_t)\right)\right\}\theta_l\\
&- \dot{\epsilon}\left\{|\Omega_d(t)|e^{-\epsilon\theta_l}\cos\left(\frac{\theta_l}{2}+\Phi(\Omega_d)\right)-|\dot{\Omega}_d\,(t)|e^{\epsilon\theta_l}\cos\left(\frac{\theta_l}{2}+\Phi(\dot{\Omega}_d)\right)\right\}\theta_l^2,\\
\dot{\Sigma}_{tt}\,(\theta_l) &= -\left\{|A_{tt}(t)|e^{-\epsilon\theta_l}\sin\left(\frac{\theta_l}{2}+\Phi(A_{tt})\right)+|\dot{A}_{tt}\,(t)|e^{\epsilon\theta_l}\sin\left(\frac{\theta_l}{2}+\Phi(\dot{A}_{tt})\right)\right\}\\
&+ |B_{tt}(t)|e^{-\epsilon\theta_l}\sin\left(\frac{3\theta_l}{2}-\Phi(B_{tt})\right)+|\dot{B}_{tt}\,(t)|e^{\epsilon\theta_l}\sin\left(\frac{3\theta_l}{2}-\Phi(\dot{B}_{tt})\right)\\
&+ |C_{tt}(t)|e^{-\epsilon\theta_l}\sin\left(\frac{7\theta_l}{2}-\Phi(C_{tt})\right)+|\dot{C}_{tt}\,(t)|e^{\epsilon\theta_l}\sin\left(\frac{7\theta_l}{2}-\Phi(\dot{C}_{tt})\right)\\
&- \left\{|A_t(t)|e^{-\epsilon\theta_l}\cos\left(\frac{\theta_l}{2}+\Phi(A_t)\right)+|\dot{A}_t\,(t)|e^{\epsilon\theta_l}\cos\left(\frac{\theta_l}{2}+\Phi(\dot{A}_t)\right)\right\}\theta_l\\
&- \left\{|B_t(t)|e^{-\epsilon\theta_l}\cos\left(\frac{3\theta_l}{2}-\Phi(B_t)\right)+|\dot{B}_t\,(t)|e^{\epsilon\theta_l}\cos\left(\frac{3\theta_l}{2}-\Phi(\dot{B}_t)\right)\right\}\theta_l\\
&+ \dot{\epsilon}\left\{|\Omega_d(t)|e^{-\epsilon\theta_l}\sin\left(\frac{\theta_l}{2}+\Phi(\Omega_d)\right)+|\dot{\Omega}_d\,(t)|e^{\epsilon\theta_l}\sin\left(\frac{\theta_l}{2}+\Phi(\dot{\Omega}_d)\right)\right\}\theta_l^2.
\end{aligned}
$$

The first term in equation (4.6) has a square root singuarity and oscillatory nature.

It is associated with the complex dynamic stress intensity factor $K^d(t)$ (defined by YANG *et al.*, 1991) which is related to the complex coefficient $\overset{\circ}{A}_0(t)$ by

$$K^d(t) = -2\sqrt{2\pi}\ \overset{\circ}{A}_0(t)\ .$$

The second term is the so-called T-stress term, and is independent of position. The first two terms have the same spatial form as those obtained under steady state conditions by DENG (1992). However, the remaining four terms, proportional to the square root of the radial distance from the crack-tip, are more complicated and have some unusual features. The part associated with $|\overset{\circ}{A}_2(t)|$ has the same form as that predicted by the steady state solution and is of order $r^{1/2}$. The term of order $r^{1/2}(\ln r)^2$ has a coefficient proportional to $\dot{\epsilon} = \epsilon'(v)\dot{v}(t)$. This term vanishes either when $\dot{v} = 0$ and/or $\epsilon = 0$. The remaining two terms contain the functions $\Sigma_t(\theta_l)$, $\overset{*}{\Sigma}_t(\theta_l)$, $\Sigma_{tt}(\theta_l)$, and $\overset{*}{\Sigma}_{tt}(\theta_l)$ which depend on the time derivatives of the complex dynamic stress intensity factor and the crack-tip speed, i.e. they depend on transient effects. These parts also vanish for steady state crack growth. The term of order $r^{1/2}\ln r$ was first observed by WILLIS (1973) who analyzed the stresses in the case of constant speed, transient interfacial crack growth. In this case, $\dot{v} = 0$, $\dot{K}^d \neq 0$, and the only surviving terms will be of order $r^{1/2}\ln r$ and $r^{1/2}$. If the two elastic materials that constitute the bimaterial system become identical, the terms associated with $r^{1/2}(\ln r)^2$ and $r^{1/2}\ln r$ will disappear. However, in this case, the functions $\Sigma_{tt}(\theta_l)$ and $\overset{*}{\Sigma}_{tt}(\theta_l)$ do not vanish and reduce to the ordinary transient term given by LIU and ROSAKIS (1992) in studying the transient growth of a crack in homogeneous materials. It is significant to note at this point that transient effects may noticeably change the r and θ structure of the field from that predicted by the steady state approximation (e.g. existence of logarithmic $r^{1/2}\ln r$ and $r^{1/2}(\ln r)^2$ terms).

5 Properties of the mismatch parameters in dynamic interfacial fracture

In the analysis of an interfacial crack dynamically propagating along the interface, there are two mismatch parameters which depend not only on the properties of the materials that constitute the bimaterial system, but also on the crack-tip velocity. The properties of these parameters are very important since we have seen that the asymptotic representation of the crack-tip field is drastically changed due to their presence. One of these parameters is defined by

$$\epsilon = \frac{1}{2\pi} \ln \frac{1-\beta}{1+\beta} , \qquad \beta = \frac{h_{11}}{\sqrt{h_{12} h_{21}}} , \tag{5.1}$$

while the other one by

$$\eta = \sqrt{\frac{h_{21}}{h_{12}}} . \tag{5.2}$$

In the above two definitions,

$$\left.\begin{aligned} h_{11} &= \left\{ \frac{2\alpha_l \alpha_s - (1+\alpha_s^2)}{\mu D(v)} \right\}_1 - \left\{ \frac{2\alpha_l \alpha_s - (1+\alpha_s^2)}{\mu D(v)} \right\}_2 \\ h_{12} &= \left\{ \frac{\alpha_s (1-\alpha_s^2)}{\mu D(v)} \right\}_1 + \left\{ \frac{\alpha_s (1-\alpha_s^2)}{\mu D(v)} \right\}_2 \\ h_{21} &= \left\{ \frac{\alpha_l (1-\alpha_s^2)}{\mu D(v)} \right\}_1 + \left\{ \frac{\alpha_l (1-\alpha_s^2)}{\mu D(v)} \right\}_2 \end{aligned}\right\} , \tag{5.3}$$

where

$$\alpha_l = \left(1 - \frac{v^2}{c_l^2}\right)^{1/2} , \qquad \alpha_s = \left(1 - \frac{v^2}{c_s^2}\right)^{1/2} , \qquad D(v) = 4\alpha_l \alpha_s - \left(1+\alpha_s^2\right)^2 .$$

To illustrate the properties of the mismatch parameters, we choose a bimaterial system composed of PMMA and AISI 4340 steel. We denote PMMA as material-1, and AISI 4340 steel as material-2. The mechanical properties for these two materials are listed in the table below.

Table: Properties of selected materials[1]

Parameter	$\mu(GPa)$	ν	$c_l(m/s)^*$	$c_l(m/s)^{**}$	$c_s(m/s)$	$c_R(m/s)$	$\rho(kg/m^3)$
PMMA	1.20	0.35	2081.7	1761.5	1004.0	937.8	1190.0
AISI 4340	80.0	0.30	5978.8	5401.9	3195.8	2959.8	7823.0

*plane-strain **plane-stress

For both plane strain and plane stress, Figure 2 presents the variation of the parameter η with respect to the crack-tip speed. We can see that η varies smoothly from 1.0 for the stationary interfacial crack, to ∞ as the crack-tip speed approaches the shear wave speed of PMMA ($c_s^{(1)}$). However, the situation is different for the parameter β. In Figure 3, we can observe that if the crack-tip velocity is less than the Rayleigh wave speed of PMMA ($c_R^{(1)}$), β varies smoothly and tends to -1 when the crack-tip speed is very close to $c_R^{(1)}$. Since $D_1(v)$ will change sign as the crack-tip speed crosses $c_R^{(1)}$, β jumps from -1 to 1, and then tends to ∞ as the crack-tip speed tends to $c_s^{(1)}$. Figure 4 shows the variation of β when the crack-tip speed is bigger than $c_R^{(1)}$. Figure 5 presents the behavior of the parameter ϵ when the crack-tip speed is below the Rayleigh wave speed of PMMA. It shows that ϵ tends to ∞ as the crack-tip speed is very close to $c_R^{(1)}$. However, as the crack-tip speed crosses the speed $c_R^{(1)}$, since β is larger than 1, ϵ will become complex, and thus ϵ can be written as

$$\epsilon = \overset{*}{\epsilon} + \frac{1}{2}i\,, \quad \overset{*}{\epsilon} = \frac{1}{2\pi}\ln\frac{\beta-1}{\beta+1}\,. \tag{5.4}$$

Figure 6 gives the variation of the real part of ϵ (i.e. $\overset{*}{\epsilon}$) with repect to the crack-tip speed when the interfacial crack is running at speeds between $c_R^{(1)}$ and $c_s^{(1)}$. We can see that the real part of ϵ changes from $-\infty$ to 0 when the crack-tip speed is in the range of $c_R^{(1)} < v < c_s^{(1)}$.

[1]the parameters for PMMA are from CYRO Industries, Woodcliff Lake, NJ 06675; the parameters for AISI 4340 steel are from *Aerospace Structural Metals Handbook*, Battelle Columbus Laboratories, Columbus, Ohio

6 The asymptotic field of an interfacial crack propagating at a speed between the lower Rayleigh and shear wave speeds

In recent experimental investigations, described in section 7, bimaterial specimens composed of PMMA and AISI 4340 steel have been tested dynamically. This bimaterial combination exhibits a remarkable stiffness mismatch. It was observed that under impact loading conditions, interfacial cracks may propagate at speeds exceeding $c_R^{(1)}$, see section 7. This experimental observation motivates our attempt to investigate dynamic crack growth in interfaces at speeds exceeding the lower Rayleigh wave speed. In homogeneous materials, an infinite amount of energy has to be transmitted to the crack-tip to maintain extension at the Rayleigh wave speed if the dynamic stress intensity factor is non-zero (FREUND, 1990). This makes it impossible for a crack in a homogeneous solid to exceed the Rayleigh wave speed of that material. However, for a crack growing along a bimaterial interface, it has been shown that as the crack-tip speed approaches the lower Rayleigh wave speed, say $c_R^{(1)}$, only a finite amount of energy has to be transmitted to the crack-tip if the dynamic stress intensity factor is non-zero (see YANG *et al.*, 1991). Accordingly, there is no energetic restriction for an interfacial crack to exceed the lower Rayleigh wave speed. Indeed, the experimentally obtained velocity histories reported in section 7, see Figure 14, are seen to largely exceed the Rayleigh wave speed of PMMA.

In the analysis of previous sections, the governing equations hold for crack-tip speeds in the range $0 < v < c_s^{(1)}$, if material–1 is more compliant than material–2. Also, the development of the asymptotic stress field around the tip of a non-uniformly propagating interfacial crack is dependent on the complete solution of the Riemann-Hilbert problem. However, from the procedure provided in Appendix II, we can see that there are no restrictions imposed on crack-tip speed from this procedure. The only consequence of the restriction that the crack-tip speed is in the range of $0 < v < c_R^{(1)}$, is that all parameters

appearing in the solution are real. Nevertheless, the mathematical approach is not limited by this restriction, even if some of the parameters become complex. Therefore, we can directly extend our solution to the case where the crack-tip speed exceeds the lower Rayleigh wave speed.

Suppose the properties of the materials constituting the interface are such that $c_s^{(1)} < c_R^{(2)}$, and $c_R^{(1)} < v < c_s^{(1)}$. As we have shown in the previous section, the parameter η remains real, but ϵ becomes complex and is given by equation (5.4). If only the leading term is considered, under the requirement of bounded displacement, or integrable mechanical energy density (FREUND, 1990), the two complex displacement potentials in equation (3.32) for the material above the interface, become

$$\left.\begin{aligned} F_0(z_l;t) &= -\frac{[(1+\alpha_s^2)-2\eta\alpha_s]\,e^{\dot{\epsilon}\pi}}{(2+i\,\dot{\epsilon})(1+i\,\dot{\epsilon})\mu D(v)\sinh\dot{\epsilon}\,\pi} z_l^{2+i\dot{\epsilon}} A_0(t) \\ &\quad + \frac{[(1+\alpha_s^2)+2\eta\alpha_s]\,e^{-\dot{\epsilon}\pi}}{(2-i\,\dot{\epsilon})(1-i\,\dot{\epsilon})\mu D(v)\sinh\dot{\epsilon}\,\pi} z_l^{2-i\dot{\epsilon}} \overline{A}_0(t) \\ G_0(z_s;t) &= \frac{[2\alpha_l-\eta(1+\alpha_s^2)]\,e^{\dot{\epsilon}\pi}}{(2+i\,\dot{\epsilon})(1+i\,\dot{\epsilon})\mu D(v)\sinh\dot{\epsilon}\,\pi} z_s^{2+i\dot{\epsilon}} A_0(t) \\ &\quad - \frac{[2\alpha_l+\eta(1+\alpha_s^2)]\,e^{-\dot{\epsilon}\pi}}{(2-i\,\dot{\epsilon})(1-i\,\dot{\epsilon})\mu D(v)\sinh\dot{\epsilon}\,\pi} z_s^{2-i\dot{\epsilon}} \overline{A}_0(t) \end{aligned}\right\}, \tag{6.1}$$

for an arbitrary complex function $A_0(t)$. To obtain this result, the definition of ϵ in the speed range $c_R^{(1)} < v < c_s^{(1)}$, equation (5.4), has been used. For the material below the interface, we need to change $\dot{\epsilon}\,\pi$ to $-\dot{\epsilon}\,\pi$ in the above expressions. By setting

$$A_0(t) = A(t)e^{i\Phi(t)}\,,$$

the first invariant of stress for the material above the interface becomes

$$\left.\begin{aligned} \sigma_{11}+\sigma_{22} &= \frac{4\,(\alpha_l^2-\alpha_s^2)\,A(t)}{D(v)\sinh\dot{\epsilon}\,\pi}\Big\{2\eta\alpha_s\cosh\left[\dot{\epsilon}\,(\pi-\theta_l)\right] \\ &\quad - (1+\alpha_s^2)\sinh\left[\dot{\epsilon}\,(\pi-\theta_l)\right]\Big\}\cos\left(\dot{\epsilon}\ln r_l+\Phi(t)\right) \end{aligned}\right\}. \tag{6.2}$$

It can be observed that oscillations still exist along the radial direction. However, there is no singularity at the propagating crack-tip.

At a position, r, ahead of the interfacial crack-tip, the traction on the interface can be expressed as

$$\eta\sigma_{22}(r;t) + i\sigma_{12}(r;t) = -2\eta r^{i\overset{*}{\epsilon}} A_0(t) \ . \tag{6.3}$$

At a position, r, behind the interfacial crack-tip, the crack face displacement difference is found to be

$$\delta_1(r;t) - i\frac{\delta_2(r;t)}{\eta} = \frac{2\eta h_{12}}{\sinh \overset{*}{\epsilon}} \frac{r^{1+i\overset{*}{\epsilon}}}{1+i\overset{*}{\epsilon}} A_0(t) \ . \tag{6.4}$$

If the interfacial crack extended an amount δ, then the energy released by this extension, $\Delta W(\delta)$ can be calculated by

$$\Delta W(\delta) = \frac{1}{2}\int_0^\delta \{\sigma_{22}(\xi_1;t)\delta_2(\delta-\xi_1;t) + \sigma_{12}(\xi_1;t)\delta_1(\delta-\xi_1;t)\}\,\mathrm{d}\xi_1 \ . \tag{6.5}$$

By using (6.3) and (6.4), we can express the above equation as

$$\Delta W(\delta) = \frac{2\eta^2 h_{12}|A_0(t)|^2}{\sinh \overset{*}{\epsilon}} \mathrm{Im}\left\{\int_0^\delta \frac{(\delta-\xi_1)^{1+i\overset{*}{\epsilon}}\xi_1^{-i\overset{*}{\epsilon}}}{1+i\overset{*}{\epsilon}}\mathrm{d}\xi_1\right\} \ . \tag{6.6}$$

Further, it can be shown that

$$\int_0^\delta \frac{(\delta-\xi_1)^{1+i\overset{*}{\epsilon}}\xi_1^{-i\overset{*}{\epsilon}}}{1+i\overset{*}{\epsilon}}\mathrm{d}\xi_1 = \int_0^\delta \frac{(\delta-\xi_1)^{1-i\overset{*}{\epsilon}}\xi_1^{i\overset{*}{\epsilon}}}{1-i\overset{*}{\epsilon}}\mathrm{d}\xi_1 \ .$$

Therefore, the energy release rate at the tip of an interfacial crack moving at speeds in the range $c_R^{(1)} < v < c_s^{(1)}$, $\mathcal{G}$, will be

$$\mathcal{G} \ = \ \lim_{\delta\to 0}\frac{\Delta W(\delta)}{\delta} = 0 \ . \tag{6.7}$$

This result may be anticipated since in this range of speeds, both stress and strain are bounded. Equation (6.7) states that if the speed of the interfacial crack is in the range $c_R^{(1)} < v < c_s^{(1)}$, no energy is needed to create new surfaces.

7 Experimental evidence for the importance of transient effects in the dynamic fracture of bimaterials

To investigate the validity of the analysis presented in this work, a sequence of dynamic impact experiments of bimaterial specimens has been performed. Stress waves generated by impact, load an interfacial pre-crack, which subsequently propagates dynamically along the bimaterial interface. High speed interferograms of the near-tip region of the propagating crack are recorded. The optical method used is the newly developed method of Coherent Gradient Sensing (CGS) (TIPPUR *et al.*, 1991; ROSAKIS, 1993) described below.

7.1 Experimental technique (transmission CGS)

Consider a planar wavefront normally incident on an optically and mechanically isotropic, transparent plate of initial uniform thickness h and refractive index n. As shown in Figure 7, the specimen occupies the (x_1, x_2) plane in the undeformed configuration. When the specimen undergoes any kind of deformation (static or dynamic), the transmitted wavefront can be expressed as $S(x_1, x_2, x_3) = x_3 + \Delta S(x_1, x_2) = \text{constant}$, where ΔS is the optical path change acquired during refraction. As discussed in detail by ROSAKIS (1993), ΔS is related to the deformation state by the relation,

$$\Delta S(x_1, x_2) = 2h(n-1)\int_0^{1/2} \epsilon_{33} \mathrm{d}(x_3/h) + 2h\int_0^{1/2} \Delta n \mathrm{d}(x_3/h)\ . \qquad (7.1)$$

The first term of equation (7.1) represents the net optical path difference due to the plate thickness change caused by the strain component ϵ_{33}. The second term is due to the stress induced change of refractive index of the material. This change in refrative

index Δn is given by the Maxwell relation,

$$\Delta n = D_1 \left(\sigma_{11} + \sigma_{22} + \sigma_{33}\right) \ , \tag{7.2}$$

where D_1 is the stress optic coefficient and σ_{ij} are Cartesian components of the nominal stress tensor. The above relation is strictly true for isotropic, linearly elastic solids. For such solids, the strain component ϵ_{33} can also be related to the stresses, and equation (7.1) then becomes:

$$\Delta S(x_1, x_2) = 2hc_\sigma \int_0^{1/2} \left\{ (\sigma_{11} + \sigma_{22}) \left[1 - D_2 \left(\frac{\sigma_{33}}{\nu(\sigma_{11} + \sigma_{22})} \right) \right] \right\} (x_3/h) \ , \tag{7.3}$$

where

$$c_\sigma = D_1 - \frac{\nu(n-1)}{E} \ , \qquad D_2 = -\frac{\nu D_1 + \dfrac{\nu(n-1)}{E}}{\dfrac{\nu(n-1)}{E} D_1} \ ,$$

and E, ν, and c_σ are the Young's modulus, Poisson's ratio and stress optical coefficient of the material, respectively.

A schematic of the experimental apparatus is also shown in Figure 7. When the transmitted wavefront emerges from the specimen after being distorted, it passes through two high density gratings, G_1 and G_2 of pitch p, separated by a distance Δ. The gratings have their rulings parallel to either the x_1 or x_2 directions. The action of the gratings is to displace (shear) the diffracted beam and recombined it with itself, thus creating an interferogram after G_2. The filtering lens L processes the light emerging from G_2 and its frequency content (diffraction spots) is displayed on the back focal plane of L. By physically blocking all diffraction orders except for either the ± 1 orders, information regarding the gradient components of $\Delta S(x_1, x_2)$ along either the x_1 or x_2-axis is obtained on the image plane. The camera is kept focused on the specimen plane. For grating rulings perpendicular to the x_α-axis, the resulting fringe pattern is proportional to $\partial(\Delta S)/\partial x_\alpha$, $\alpha \in \{1, 2\}$.

A first order analysis described by TIPPUR *et al.* (1991), or a higher order Fourier

optics analysis by LEE *et al.* (1993), have shown that the resulting fringes can be related to gradients of $\Delta S(x_1, x_2)$ as follows:

$$\frac{\partial(\Delta S)}{\partial x_\alpha} = \frac{k_\alpha p}{\Delta} , \qquad \alpha \in \{1,2\} , \tag{7.4}$$

where

$$k_\alpha = \begin{cases} m & \text{for} \quad \alpha = 1, \ m = 0, \pm 1, \pm 2, \cdots \\ n & \text{for} \quad \alpha = 2, \ n = 0, \pm 1, \pm 2, \cdots \end{cases}$$

and m and n are the fringe orders for the x_1, x_2 gradient contours respectively.

Invariably a near-tip three-dimensional region will exist in any real specimen geometry. However, outside this three-dimensional zone, a plane stress approximation will be valid. A numerical study of each particular specimen configuration is needed to identify the extent and exact location of such a plane stress region. Such a calculation has been performed by LEE and ROSAKIS (1992) for a three point bend bimaterial specimen. A rather large two-dimensional plane stress region was seen over a significant portion of the specimen. In this region, $\sigma_{33}/\nu(\sigma_{11} + \sigma_{22})$ (a measure of three-dimensionality) tends to zero. For points ouside the three-dimensional region ($\sigma_{33}/\nu(\sigma_{11} + \sigma_{22}) \to 0$), the optical path difference in equation (7.3) will simplify to

$$\Delta S(x_1, x_2) \simeq c_\sigma h \left\{ \hat{\sigma}_{11}(x_1, x_2) + \hat{\sigma}_{22}(x_1, x_2) \right\} , \tag{7.5}$$

where $\hat{\sigma}_{11}$ and $\hat{\sigma}_{22}$ are *thickness averages* of the stress components in the plate.

As a result, for points outside the near-tip three-dimensional region, the CGS patterns assume a simple interpretation in terms of two-dimensional stress field approximations. In particular, equations (7.4) and (7.5) now indicate that fringes obtained from regions surrounding the three-dimensional zone can be related to the in-plane gradients of $\hat{\sigma}_{11}+\hat{\sigma}_{22}$ as follows:

$$c_\sigma h \frac{\partial(\hat{\sigma}_{11} + \hat{\sigma}_{22})}{\partial x_1} = \frac{mp}{\Delta} , \quad c_\sigma h \frac{\partial(\hat{\sigma}_{11} + \hat{\sigma}_{22})}{\partial x_2} = \frac{np}{\Delta} , \quad m, n = 0, \pm 1, \pm 2, \cdots \tag{7.6}$$

where in the case of transmission c_σ is the stress optical coefficient of the material (e.g. PMMA).

7.2 Experimental set-up and procedure

Bimaterial specimens used in the dynamic experiments are of the three point or one point bend configuration and are made from 9mm thickness sheets of commercially available poly-methylmethacrylate (PMMA) (material-1) and AISI 4340 steel (material-2). The bonding procedure is outlined in TIPPUR and ROSAKIS (1990). A bond strength calibration experiment was also performed in that study, demonstrating that the bond toughness was at least as much as that of a homogeneous PMMA specimen. This fact testifies to the strength of the bond and becomes important in the discussion of the dynamic experiments presented bellow.

The bimaterial specimens have either a pre-cut edge notch, or a sharp pre-crack of length 25mm along the interface. The specimens are either impact loaded in a drop weight tower (Dynatup-8100A) or a high speed gas gun. After the impact event, the crack propagates dynamically along the interface. The transmission CGS technique in conjunction with high speed photography is used to record dynamic fields around the crack-tip (only on the PMMA side, of course). A rotating mirror high speed camera (Cordin model 330A) is used. A Spectra-Physics Argon-ion pulse laser (model 166) is used as the light source. By using short pulses of 30nsec duration, we are able to freeze even the fastest of running cracks and thus produce a sharp interference pattern during crack growth. The interframe time (controlled by the interval between pulses) is typically set at 1μsec for a total recording time of 80μsec. The laser pulsing is triggered by a strain gauge on the specimen that senses the impact.

True symmetric one or three point bend loading cannot be achieved since it is extremely difficult to apply the impact load exactly on the interface, which is very thin. In addition since the wave speeds of PMMA and steel are vastly different, the loading history at the crack-tip would be completely different if the specimen were impacted on

the PMMA or the steel side. Thus it was chosen to impact the specimen a small distance (7mm) into the steel side of the bond.

A sequence of high speed interferograms from a PMMA/steel test is shown in Figure 8. This is a three point bend test conducted in a drop weight tower. The impact speed was 4m/sec. When the crack initiates (t = 0μsec), intense stress waves emanate from the crack-tip. These waves are visible in Figure 8 as discrete kinks in otherwise smooth fringes and as circular lines centered at points along the crack line (see frames at $t = 16.5\mu$sec and $t = 23\mu$sec). This observation is a reliable sign of a highly dynamic event, as will be discussed later.

7.3 Analysis of experimental data

In subsequent sections we shall present an analysis of CGS interferograms of dynamic bimaterial specimens first using a K^d-dominant assumption and then using the higher order transient field described in section 4.

7.3.1 Singular field (K^d-dominance)

The governing relations for CGS (7.6) can be used to estimate fracture parameters from points outside the three-dimensional zone of a given interferogram. One could expect that the plane stress region surrounding the near-tip three-dimensional region would be well described by the most singular term in the asymptotic expansion for stress, i.e. that a K^d-dominant region would exist somewhere around the crack-tip. This is something to be verified though and should not be taken for granted, especially in regions relatively far from the crack-tip or in experiments showing transient effects (e.g. rapidly changing crack-tip speed). In such cases the deformation field around the crack-tip may be better described by a higher order analysis.

As was stated earlier (see section 4), for cracks propagating dynamically under *steady state* conditions in bimaterial specimens, YANG *et al.* (1991) and the first part of the present analysis observed that near the crack-tip the stress field assumes the form,

$$\sigma_{\alpha\beta} = \mathrm{Re}\left\{\frac{K^d r^{i\epsilon}}{\sqrt{2\pi r}}\right\}\tilde{\sigma}^{(I)}_{\alpha\beta}(\theta, v) + \mathrm{Im}\left\{\frac{K^d r^{i\epsilon}}{\sqrt{2\pi r}}\right\}\tilde{\sigma}^{(II)}_{\alpha\beta}(\theta, v)\ , \tag{7.7}$$

where (r, θ) are polar coordinates of a coordinate system translating with the crack-tip at speed v, and K^d is the complex dynamic stress intensity factor. The material mismatch parameter $\epsilon = \epsilon(v)$ is now a function of crack-tip speed and of the elastic moduli of the materials of the bimaterial system. Analytical expressions for $\tilde{\sigma}^{(I)}_{\alpha\beta}$ and $\tilde{\sigma}^{(II)}_{\alpha\beta}$ are given by YANG *et al.* (1991).

By using equation (7.7) and after some algebraic manipulations, $\hat{\sigma}_{11} + \hat{\sigma}_{22}$ can be written as

$$\left.\begin{aligned}\hat{\sigma}_{11} + \hat{\sigma}_{22} \;=\; & \frac{A(t)}{\sqrt{2\pi r_l}}\left\{\left(1 + \alpha_s^2 - 2\eta\alpha_s\right) e^{\epsilon(\pi-\theta_l)} \cos\left(\frac{\theta_l}{2} - \Phi(t) - \epsilon \ln r_l\right)\right. \\ & \left. + \left(1 + \alpha_s^2 + 2\eta\alpha_s\right) e^{-\epsilon(\pi-\theta_l)} \cos\left(\frac{\theta_l}{2} + \Phi(t) + \epsilon \ln r_l\right)\right\}\end{aligned}\right\}\ , \tag{7.8}$$

where

$$A(t) = \frac{(\alpha_l^2 - \alpha_s^2)\left|K^d(t)\right|}{D(v)\cosh(\epsilon\pi)}\ , \quad K^d(t) = K_1^d(t) + iK_2^d(t)\ , \quad \Phi(t) = \tan^{-1}\frac{K_2^d(t)}{K_1^d(t)}\ ,$$

and $\alpha_{l,s}$, $r_{l,s}$, and $\theta_{l,s}$ have been defined in previous sections. The mismatch parameters η and ϵ are functions of crack-tip speed and of material properties. These functions are given in section 5 and appear in Figures 2 and 5, respectively. Note that equation (7.8) is the first part of equation (4.6) in section 4. The field quantity of interest in analyzing the CGS patterns for material-1 is $c_\sigma h \partial(\hat{\sigma}_{11} + \hat{\sigma}_{22})/\partial x_1$. By differentiating equation (7.8)

with respect to x_1, we have

$$\left.\begin{aligned} c_\sigma h \frac{\partial(\hat{\sigma}_{11}+\hat{\sigma}_{22})}{\partial x_1} &= \frac{c_\sigma h r_l^{-3/2} e^{-\epsilon(\pi-\theta_l)} A(t)}{2\sqrt{2\pi}} \\ &\times \left\{ -\left(1+\alpha_s^2-2\eta\alpha_s\right) e^{2\epsilon(\pi-\theta_l)} \cos\left(\frac{3\theta_l}{2}-\Phi(t)-\epsilon\ln r_l\right)\right. \\ &-\left(1+\alpha_s^2+2\eta\alpha_s\right)\cos\left(\frac{3\theta_l}{2}+\Phi(t)+\epsilon\ln r_l\right) \\ &+2\epsilon\left(1+\alpha_s^2-2\eta\alpha_s\right) e^{2\epsilon(\pi-\theta_l)} \sin\left(\frac{3\theta_l}{2}-\Phi(t)-\epsilon\ln r_l\right) \\ &\left.-2\epsilon\left(1+\alpha_s^2+2\eta\alpha_s\right)\sin\left(\frac{3\theta_l}{2}+\Phi(t)+\epsilon\ln r_l\right)\right\} \end{aligned}\right\}, \qquad (7.9)$$

where $A(t)$ is as defined in equation (7.8) and $0 \le \theta_l \le \pi$.

From the above discussion it becomes obvious that extraction of parameters like K^d is now possible *provided* that experimental data are gathered from a region near the moving crack-tip characterized by the structure presented in equations (7.8) and (7.9). In a laboratory specimen of finite size where transient effects may be important, the field may not be K^d-dominant and the use of a higher order analysis may be necessary. The necessity of a higher order analysis in the interpetation of optical data from crack growth in homogeneous specimens was demonstrated by FREUND and ROSAKIS (1992) and KRISHNASWAMY and ROSAKIS (1991). An equivalent analysis for a transiently propagating interfacial crack has been provided in previous sections and its effect on data interpretation is discussed in the next section.

7.3.2 Higher order transient analysis

In section 4, a higher order expansion for the trace of the stress tensor in plane stress is shown in equation (4.6). By differentiating with respect to the x_1 coordinate, we obtain a relation for the x_1-gradient of $\hat{\sigma}_{11}+\hat{\sigma}_{22}$, which is relevant to the analysis of CGS

interferograms,

$$\left.\begin{aligned}
\frac{(\sigma_{11}+\sigma_{22})_{,1}}{2\mu\,(\alpha_l^2-\alpha_s^2)} &= |\mathcal{A}_0(t)|\left\{\Pi_0(\theta_l)\cos(\epsilon\ln r_l)+\overset{*}{\Pi}_0(\theta_l)\sin(\epsilon\ln r_l)\right\}r_l^{-3/2}\\
&+ \dot{\epsilon}\left\{\Pi_d(\theta_l)\cos(\epsilon\ln r_l)+\overset{*}{\Pi}_d(\theta_l)\sin(\epsilon\ln r_l)\right\}r_l^{-1/2}(\ln r_l)^2\\
&+ \left\{\Pi_t(\theta_l)\cos(\epsilon\ln r_l)+\overset{*}{\Pi}_t(\theta_l)\sin(\epsilon\ln r_l)\right\}r_l^{-1/2}\ln r_l\\
&+ \left\{\Pi_{tt}(\theta_l)\cos(\epsilon\ln r_l)+\overset{*}{\Pi}_{tt}(\theta_l)\sin(\epsilon\ln r_l)\right\}r_l^{-1/2}\\
&+ |\mathcal{A}_2(t)|\left\{\Pi_2(\theta_l)\cos(\epsilon\ln r_l)+\overset{*}{\Pi}_2(\theta_l)\sin(\epsilon\ln r_l)\right\}r_l^{-1/2}\\
&+ O(r_l)
\end{aligned}\right\}, \quad (7.10)$$

where

$$\begin{aligned}
\Pi_0(\theta_l) &= a_0(t)e^{-\epsilon\theta_l}\cos\left(\frac{3\theta_l}{2}-\Phi(\mathcal{A}_0)\right)+b_0(t)e^{\epsilon\theta_l}\cos\left(\frac{3\theta_l}{2}+\Phi(\mathcal{A}_0)\right),\\
\overset{*}{\Pi}_0(\theta_l) &= a_0(t)e^{-\epsilon\theta_l}\sin\left(\frac{3\theta_l}{2}-\Phi(\mathcal{A}_0)\right)-b_0(t)e^{\epsilon\theta_l}\sin\left(\frac{3\theta_l}{2}+\Phi(\mathcal{A}_0)\right),\\
\Pi_2(\theta_l) &= a_0(t)e^{-\epsilon\theta_l}\cos\left(\frac{\theta_l}{2}-\Phi(\mathcal{A}_2)\right)+b_0(t)e^{\epsilon\theta_l}\cos\left(\frac{\theta_l}{2}+\Phi(\mathcal{A}_2)\right),\\
\overset{*}{\Pi}_2(\theta_l) &= a_0(t)e^{-\epsilon\theta_l}\sin\left(\frac{\theta_l}{2}-\Phi(\mathcal{A}_2)\right)-b_0(t)e^{\epsilon\theta_l}\sin\left(\frac{\theta_l}{2}+\Phi(\mathcal{A}_2)\right),\\
\Pi_d(\theta_l) &= |\mathcal{Q}_d(t)|e^{-\epsilon\theta_l}\cos\left(\frac{\theta_l}{2}-\Phi(\mathcal{Q}_d)\right)-|\overset{*}{\mathcal{Q}}_d(t)|e^{\epsilon\theta_l}\cos\left(\frac{\theta_l}{2}+\Phi(\overset{*}{\mathcal{Q}}_d)\right),\\
\overset{*}{\Pi}_d(\theta_l) &= |\mathcal{Q}_d(t)|e^{-\epsilon\theta_l}\sin\left(\frac{\theta_l}{2}-\Phi(\mathcal{Q}_d)\right)+|\overset{*}{\mathcal{Q}}_d(t)|e^{\epsilon\theta_l}\sin\left(\frac{\theta_l}{2}+\Phi(\overset{*}{\mathcal{Q}}_d)\right),\\
\Pi_t(\theta_l) &= |\mathcal{A}_t(t)|e^{-\epsilon\theta_l}\cos\left(\frac{\theta_l}{2}-\Phi(\mathcal{A}_t)\right)-|\overset{*}{\mathcal{A}}_t(t)|e^{\epsilon\theta_l}\cos\left(\frac{\theta_l}{2}-\Phi(\overset{*}{\mathcal{A}}_t)\right)\\
&+ |\mathcal{B}_t(t)|e^{-\epsilon\theta_l}\cos\left(\frac{5\theta_l}{2}-\Phi(\mathcal{B}_t)\right)-|\overset{*}{\mathcal{B}}_t(t)|e^{\epsilon\theta_l}\cos\left(\frac{5\theta_l}{2}-\Phi(\overset{*}{\mathcal{B}}_t)\right)\\
&+ 2\dot{\epsilon}\left\{|\mathcal{Q}_d(t)|e^{-\epsilon\theta_l}\sin\left(\frac{\theta_l}{2}-\Phi(\mathcal{Q}_d)\right)-|\overset{*}{\mathcal{Q}}_d(t)|e^{\epsilon\theta_l}\sin\left(\frac{\theta_l}{2}-\Phi(\overset{*}{\mathcal{Q}}_d)\right)\right\}\theta_l,
\end{aligned}$$

$$
\begin{aligned}
\overset{*}{\Pi}_t(\theta_l) &= |\mathcal{A}_t(t)|e^{-\epsilon\theta_l}\sin\left(\frac{\theta_l}{2}-\Phi(\mathcal{A}_t)\right)+|\overset{*}{\mathcal{A}}_t(t)|e^{\epsilon\theta_l}\sin\left(\frac{\theta_l}{2}-\Phi(\overset{*}{\mathcal{A}}_t)\right)\\
&+ |\mathcal{B}_t(t)|e^{-\epsilon\theta_l}\sin\left(\frac{5\theta_l}{2}-\Phi(\mathcal{B}_t)\right)+|\overset{*}{\mathcal{B}}_t(t)|e^{\epsilon\theta_l}\sin\left(\frac{5\theta_l}{2}-\Phi(\overset{*}{\mathcal{B}}_t)\right)\\
&- 2\dot{\epsilon}\left\{|\mathcal{Q}_d(t)|e^{-\epsilon\theta_l}\cos\left(\frac{\theta_l}{2}-\Phi(\mathcal{Q}_d)\right)+|\overset{*}{\mathcal{Q}}_d(t)|e^{\epsilon\theta_l}\cos\left(\frac{\theta_l}{2}-\Phi(\overset{*}{\mathcal{Q}}_d)\right)\right\}\theta_l,\\
\Pi_{tt}(\theta_l) &= |\mathcal{A}_{tt}(t)|e^{-\epsilon\theta_l}\cos\left(\frac{\theta_l}{2}-\Phi(\mathcal{A}_{tt})\right)-|\overset{*}{\mathcal{A}}_{tt}(t)|e^{\epsilon\theta_l}\cos\left(\frac{\theta_l}{2}-\Phi(\overset{*}{\mathcal{A}}_{tt})\right)\\
&+ |\mathcal{B}_{tt}(t)|e^{-\epsilon\theta_l}\cos\left(\frac{5\theta_l}{2}-\Phi(\mathcal{B}_{tt})\right)-|\overset{*}{\mathcal{B}}_{tt}(t)|e^{\epsilon\theta_l}\cos\left(\frac{5\theta_l}{2}-\Phi(\overset{*}{\mathcal{B}}_{tt})\right)\\
&+ |\mathcal{C}_{tt}(t)|e^{-\epsilon\theta_l}\cos\left(\frac{9\theta_l}{2}-\Phi(\mathcal{C}_{tt})\right)-|\overset{*}{\mathcal{C}}_{tt}(t)|e^{\epsilon\theta_l}\cos\left(\frac{9\theta_l}{2}-\Phi(\overset{*}{\mathcal{C}}_{tt})\right)\\
&+ \left\{|\mathcal{A}_t(t)|e^{-\epsilon\theta_l}\sin\left(\frac{\theta_l}{2}-\Phi(\mathcal{A}_t)\right)-|\overset{*}{\mathcal{A}}_t(t)|e^{\epsilon\theta_l}\sin\left(\frac{\theta_l}{2}-\Phi(\overset{*}{\mathcal{A}}_t)\right)\right\}\theta_l\\
&+ \left\{|\mathcal{B}_t(t)|e^{-\epsilon\theta_l}\sin\left(\frac{5\theta_l}{2}-\Phi(\mathcal{B}_t)\right)-|\overset{*}{\mathcal{B}}_t(t)|e^{\epsilon\theta_l}\sin\left(\frac{5\theta_l}{2}-\Phi(\overset{*}{\mathcal{B}}_t)\right)\right\}\theta_l\\
&- \dot{\epsilon}\left\{|\mathcal{Q}_d(t)|e^{-\epsilon\theta_l}\cos\left(\frac{\theta_l}{2}-\Phi(\mathcal{Q}_d)\right)-|\overset{*}{\mathcal{Q}}_d(t)|e^{\epsilon\theta_l}\cos\left(\frac{\theta_l}{2}-\Phi(\overset{*}{\mathcal{Q}}_d)\right)\right\}\theta_l^2,\\
\overset{*}{\Pi}_{tt}(\theta_l) &= |\mathcal{A}_{tt}(t)|e^{-\epsilon\theta_l}\sin\left(\frac{\theta_l}{2}-\Phi(\mathcal{A}_{tt})\right)+|\overset{*}{\mathcal{A}}_{tt}(t)|e^{\epsilon\theta_l}\sin\left(\frac{\theta_l}{2}-\Phi(\overset{*}{\mathcal{A}}_{tt})\right)\\
&+ |\mathcal{B}_{tt}(t)|e^{-\epsilon\theta_l}\sin\left(\frac{5\theta_l}{2}-\Phi(\mathcal{B}_{tt})\right)+|\overset{*}{\mathcal{B}}_{tt}(t)|e^{\epsilon\theta_l}\sin\left(\frac{5\theta_l}{2}-\Phi(\overset{*}{\mathcal{B}}_{tt})\right)\\
&+ |\mathcal{C}_{tt}(t)|e^{-\epsilon\theta_l}\sin\left(\frac{9\theta_l}{2}-\Phi(\mathcal{C}_{tt})\right)+|\overset{*}{\mathcal{C}}_{tt}(t)|e^{\epsilon\theta_l}\sin\left(\frac{9\theta_l}{2}-\Phi(\overset{*}{\mathcal{C}}_{tt})\right)\\
&- \left\{|\mathcal{A}_t(t)|e^{-\epsilon\theta_l}\cos\left(\frac{\theta_l}{2}-\Phi(\mathcal{A}_t)\right)+|\overset{*}{\mathcal{A}}_t(t)|e^{\epsilon\theta_l}\cos\left(\frac{\theta_l}{2}+\Phi(\overset{*}{\mathcal{A}}_t)\right)\right\}\theta_l\\
&- \left\{|\mathcal{B}_t(t)|e^{-\epsilon\theta_l}\cos\left(\frac{5\theta_l}{2}-\Phi(\mathcal{B}_t)\right)+|\overset{*}{\mathcal{B}}_t(t)|e^{\epsilon\theta_l}\cos\left(\frac{5\theta_l}{2}-\Phi(\overset{*}{\mathcal{B}}_t)\right)\right\}\theta_l\\
&- \dot{\epsilon}\left\{|\mathcal{Q}_d(t)|e^{-\epsilon\theta_l}\sin\left(\frac{\theta_l}{2}-\Phi(\mathcal{Q}_d)\right)+|\overset{*}{\mathcal{Q}}_d(t)|e^{\epsilon\theta_l}\sin\left(\frac{\theta_l}{2}-\Phi(\overset{*}{\mathcal{Q}}_d)\right)\right\}\theta_l^2,
\end{aligned}
$$

The functions of time $\mathcal{A}_0(t)$, $\mathcal{A}_2(t)$, $\mathcal{A}_{tt}(t)$, $\cdots$, that appear in the above expressions, are related to functions $A_0(t)$, $A_2(t)$, $A_{tt}(t)$, $\cdots$, in equation (4.5) by

$$\mathcal{A}_0(t) = \left(-\frac{1}{2}+i\epsilon\right)\mathring{A}_0(t)\,, \qquad \mathcal{A}_2(t) = \left(\frac{1}{2}+i\epsilon\right)\mathring{A}_2(t)\,,$$

$$\mathcal{A}_{tt}(t) = \left(\frac{1}{2}+i\epsilon\right)A_{tt}(t) + A_t(t) + B_{tt}(t)\,,$$

$$\mathring{\mathcal{A}}_{tt}(t) = \left(\frac{1}{2}-i\epsilon\right)\mathring{A}_{tt}(t) + \mathring{A}_t(t) + \mathring{B}_{tt}(t)\,,$$

$$\mathcal{B}_{tt}(t) = \left(-\frac{1}{2}+i\epsilon\right)B_{tt}(t) + B_t(t) + 2C_{tt}(t)\,,$$

$$\mathring{\mathcal{B}}_{tt}(t) = \left(-\frac{1}{2}-i\epsilon\right)\mathring{B}_{tt}(t) + \mathring{B}_t(t) + 2\,\mathring{C}_{tt}(t)\,,$$

$$\mathcal{C}_{tt}(t) = \left(-\frac{3}{2}+i\epsilon\right)C_{tt}(t)\,, \qquad \mathring{\mathcal{C}}_{tt}(t) = \left(-\frac{3}{2}-i\epsilon\right)\mathring{C}_{tt}(t)\,,$$

$$\mathcal{A}_t(t) = \left(\frac{1}{2}+i\epsilon\right)A_{tt}(t) + 2\dot{\epsilon}\Omega_d(t) + B_t(t)\,,$$

$$\mathring{\mathcal{A}}_t(t) = \left(\frac{1}{2}-i\epsilon\right)\mathring{A}_{tt}(t) + 2\dot{\epsilon}\,\mathring{\Omega}_d(t) + \mathring{B}_t(t)\,,$$

$$\mathcal{B}_t(t) = \left(-\frac{1}{2}+i\epsilon\right)B_t(t)\,, \qquad \mathring{\mathcal{B}}_t(t) = \left(-\frac{1}{2}-i\epsilon\right)\mathring{B}_t(t)\,,$$

$$\mathcal{Q}_d(t) = \left(\frac{1}{2}+i\epsilon\right)\Omega_d(t)\,, \qquad \mathring{\mathcal{Q}}_d(t) = \left(\frac{1}{2}-i\epsilon\right)\mathring{\Omega}_d(t)\,.$$

This gradient contains 4 orders in r_l. They are $r_l^{-3/2}$, $r_l^{-1/2}(\ln r_l)^2$, $r_l^{-1/2}\ln r_l$, and $r_l^{-1/2}$. It also contains 28 undetermined constants. The first two constants $|\mathcal{A}_0|$ and $\Phi(\mathcal{A}_0)$ are related to $|K^d|$ and Φ (or K_1^d, K_2^d) of the expression of YANG *et al.* (1991) (see equation (7.9)). In fact the most singular term of equation (7.10) reduces to equation (7.9). Under steady state conditions, equation (7.10) reduces to an expression with 4 terms which are identical to the first 4 terms of the higher order steady state expression derived by DENG (1992). The transient contributions to the expression for the gradient (7.9) are those that exbihit an $r_l^{-1/2}(\ln r_l)^2$ and $r_l^{-1/2}\ln r_l$ radial dependence: It is worth noting that most of these transient terms are multiplied by the quantity $\dot{\epsilon}$, the rate of change of the ocsillatory index with time ($\dot{\epsilon} = \epsilon'(v)\dot{v}$). Thus, to a certain extent, $\dot{\epsilon}$ is a measure of

transience of the propagating crack. If $\dot{\epsilon} = 0$, most, but not all transient terms disappear. Those that remain are those related to the rate of change of the complex stress intensity factor. Note that it is possible for $\dot{\epsilon}$ to be small even if a large acceleration exists, but $\epsilon'(v)$ is small. Conversely it is possible to have a large $\dot{\epsilon}$ corresponding to small $\dot{v}$ but large $\epsilon'(v)$. It should be noted that $\epsilon'(v)$ tends to infinity as v tends to $c_R^{(1)}$, see Figure 5. Whether or not $\dot{\epsilon}$ can be used as a reliable measure of transience will be investigated in the subsequent section.

It is clear at this point that analysis of the fringe patterns obtained from a dynamic experiment can be made using either equation (7.9) or equaton (7.10). The choice of one or the other depends on whether a region of K^d-dominance has been estalished somewhere outside the near-tip three-dimensional zone. Use of either equation allows estimation of the time variation of the relevant parameters. This is done by performing a least squares fitting procedure to data points digitized from the CGS interferograms obtained during an experiment. Of course the crack-tip speed $v(t)$ is measured independently. There are 2 undetermined parameters in equation (7.9) and 28 undetermined constants in equation (7.10).

7.4 Results and discussion

The velocity and acceleration histories corresponding to the sequence of photographs in Figure 8 are shown in Figures 9(a) and 9(b). This is a test performed in a drop weight tower under the relatively small impact speed of 4m/sec. Indeed the terminal speed in this test seem to be about 90% of the Rayleigh wave speed of PMMA, $c_R^{(1)}$, see Figure 9(a). In contrast, previous experience with dynamic crack growth in *homogeneous* PMMA specimens of the same configuration show a maximum speed of about $0.35c_R^{(1)}$. Note also that in this particular bimaterial case there is a very large crack-tip acceleration (approximately $10^7\mathbf{g}$, where $\mathbf{g}$ is the acceleration of gravity) immediately after the crack

initiates, see Figure 9(b). This would suggest that transient effects would be present close to initiation ($t = 0\mu$sec). As was mentioned earlier the rate of change of the oscillatory index with time ($\dot{\epsilon}$) may be considered a partial measure of transience. For the same test as Figure 8, we have plotted ϵ and $\dot{\epsilon}$ versus time in Figures 10(a) and 10(b). In Figure 10(b), $\dot{\epsilon}$ exhibits a local maximum at about $t = 10\mu$sec after initiation. It then starts increasing again after 25μsec. At short times after initiation, $\epsilon'(v)$ is close to zero although $\dot{v}$ is large (10^7**g**). This accounts for the initially low values of $\dot{\epsilon}$. In this regime transient effects are demonstrated through large changes in the complex dynamic stress intensity factor. As time increases the combinaton of $\epsilon'(v)$ and $\dot{v}$ results in a local maximum in $\dot{\epsilon}$. At later times ($t > 25\mu$sec) and as the crack-tip velocity approaches the Rayleigh wave speed of PMMA, $\dot{\epsilon}$ increases again.

To demonstrate the need of a transient analysis in interpreting experimental data, let us now attempt to analyze the frame of Figure 8 at $t = 9.5\mu$sec. This corresponds to a local maximum value of $\dot{\epsilon}$ in this particular test. By following the fitting procedure described in section 7.3.2, we can obtain the coefficients of either equation (7.9) or equation (7.10). The result of such a fit for the K^d-dominant field (equation (7.9)) is shown in Figure 11(a). The diamonds are digitized data points from the interferogram at $t = 9.5\mu$sec. The solid line is the contour of the quantity $\partial(\hat{\sigma}_{11} + \hat{\sigma}_{22})/\partial x_1$ calculated numerically by using the results for K^d from the fit generated by the same data points. As can be clearly seen, equation (7.9) cannot represent the data to any reasonable extent. The deformation field of this particular picture therefore is nowhere near K^d-dominant. In fact the main feature which is that the fringes vertically approach the interface cannot be captured at all by equation (7.9). The result of the fit of the transient higher order field (equation (7.10)) derived earlier is shown in Figure 11(b). The data points are exactly the same as before and the solid line is the result of the fit. Clearly the fit is very good over a large area of the specimen. All features of the field are successfully captured by equation (7.10). This shows that the K^d-dominant analysis cannot be used for cases

where $\dot{\epsilon}$ is high.

To further investigate the effect of $\dot{\epsilon}$ on the interpretation of optical data, we chose to analyze an interferogram corresponding to the minimum value of $\dot{\epsilon}$ within the duration of the test. This occurs at $t = 23\mu$sec. Figure 12(a) shows the result of the K^d-dominant fit to the experimental data. As the crack-tip is approached, equation (7.9) seems to adequately describe the experimental measurement. However, as the distance from the crack-tip is increased, K^d-dominance is lost. Nevertheless, the lack of K^d-dominance in Figure 12(a) ($\dot{\epsilon} \sim 1.0 \times 10^2 \text{sec}^{-1}$) is not as dramatic as in Figure 11(a) ($\dot{\epsilon} \sim 1.2 \times 10^4 \text{sec}^{-1}$). Figure 12(b) shows the result of the fit of the transient higher order field to the same experimental data as Figure 12(a). The fit is now much better over the whole range of radii. The above observations show that in general a transient analysis of data is necessary if fracture parameters such as K^d are to be obtained with confidence.

7.5 Transonic terminal speeds

The next cycle of experimentation involved bimaterial specimens loaded at higher loading rates than in a drop weight tower. This was achieved by using a high speed gas gun. A one point bend impact geometry was used. Again the issues of crack-tip loading history, as dependent upon PMMA or steel side impact, arise. It was chosen to impact the specimens on the steel side, to remain consistent with the drop weight tower tests. The gas gun projectile was 50mm in diameter and the impact velocity was 20m/sec, thus resulting in considerably larger near-tip loading rates than in the drop weight device. A sequence of interferograms from such a test is shown in Figure 13. Its corresponding $v(t)$, $\dot{v}(t)$, $\epsilon(t)$ and $\dot{\epsilon}(t)$ plots are shown in Figures 14(a), (b), and 15(a), (b). In general terms the results are similar to those obtained from the drop weight tower experiments. A main difference is that the speed and acceleration are much higher. In fact the crack-tip speed seems to exceed the Rayleigh wave speed of PMMA after a relatively short time. In some

cases (as in Figure 14) the velocity even exceeds the shear wave speed and approaches the longitudinal wave speed of PMMA, thus entering the transonic speed range for the PMMA side.

For a crack speed less than the Rayleigh wave speed, we can repeat a fitting procedure exactly as before. For the frame at $t = 8\mu$sec in Figure 13, the result of such fit is shown in Figure 16. Here the white lines, obtained from plotting the field of equation (7.10) using the values of the fitted parameters, are superposed on the actual picture (instead of the digitized points as in Figures 11 and 12). The illustration is the same though, i.e. that a transient field is necessary to describe a picture such as this which corresponds to a high $\dot{\epsilon}$ and acceleration.

Unfortunately given the existing theoretical analyses, we do not have the tools to fit any field to interferograms having a speed in the transonic range for PMMA ($c_s^{(1)} < v < c_l^{(1)}$). These large speeds were observed in a number of tests involving one point bend interfacial specimens containing *sharp* pre-cracks lying along the interface. When a specimen containing a blunt starter notch was impacted, recorded crack-tip terminal speeds were even higher; at some cases approaching the longitudinal wave speed of PMMA. Such a velocity history is given in Figure 17. Here the maximum crack-tip speed is estimated to be $0.9c_l^{(1)}$. These observations are very interesting because to our knowledge no evidence of transonic or supersonic crack propagation has ever been seen in homogeneous materials even though a large number of the theoretical studies exist on the subject (FREUND, 1990). It is believed that transonic crack growth is possible in a bimaterial situation because of an energy transfer mechanism from the stiffer to the softer material. It can be seen in Figure 13 that the nature of the fringes changes, approximately around the time at which the crack-tip speed exceeds the Rayleigh wave speed. A sequence corresponding to the same test whose velocity is shown in Figure 17 (blunt starter notch) is presented in Figure 18. In these pictures, we see an even more drastic change in the nature of the

fringe patterns as the crack-tip speed exceeds both Rayleigh and shear wave speeds. To see this effect clearly, compare the second frame in Figure 18 to the sixth frame. Finally, additional visual proof of the existence of large transient effects is shown in Figure 19. We are now in the process of developing an analysis for the propagation of an interfacial crack at speeds exceeding $c_s^{(1)}$. It is hoped to be able to predict fringe patterns as those observed in Figures 13, 18, and 19.

8 Conclusions

Experimental observations of high speed (transonic terminal speeds) and high acceleration (10^8m/sec^2) crack growth in PMMA/steel interfaces are reported for the first time. Motivated by these observations, a fully transient higher order asymptotic analysis of dynamic interfacial crack growth is performed. This analysis is valid for crack-tip speed in the range $0 < v < c_s^{(1)}$ ($c_s^{(1)}$ is the shear wave speed of PMMA). Explicit expressions for stresses are provided. In addition to the classical $r^{-1/2}$, r^0, and $r^{1/2}$, $\cdots$, terms of steady state expansion for the stresses, new transient contributions of order $r^{1/2}\ln r$ and $r^{1/2}(\ln r)^2$ appear. The structure of the near-tip field obtained by the analysis is found to describe well the experimentally obtained stress fields. For subsonic crack growth, the experiments demonstrate the necessity of employing the fully transient expression in the analysis of optical experimental data. Terminal speeds of up to 90% of the plane stress dilatational wave speeds of PMMA are observed.

Acknowledgements

The support of ONR Grant N00014-90-J-1340 and NSF Grant MSS-9024838 is gratefully appreciated.

References

Atkinson, C., (1977), "Dynamic Crack Problems in Dissimilar Media," in *Mechanics of Fracture*, **4**, edited by Sih, G.C., Leyden: Noordhoff, pp.213–248.

Brock, L. M. and Achenbach, J. D., (1973), "Extension of an Interface Flaw under the Influence of Transient Waves," *International Journal of Solids and Structures*, **9**, pp.53–67.

Callias, C, Markenscoff, X., and Ni, L., (1990), "A Singular Asymptotic Expansion for the Field Near a Moving Dislocation Loop," *Quarterly of Applied Mathematics*, **48**(1), pp.113–132.

Deng, X., (1992), "Complete Complex Series Expansions of Near-Tip Fields for Steadily Growing Interface Cracks in Dissimilar Isotropic Materials," *Engineering Fracture Mechanics*, **42**(2), pp.237–242.

England, A. H., (1965), "A Crack Between Dissimilar Media," *Journal of Applied Mechanics*, **32**, pp.400–402.

Erdogan, F., (1965), "Stress Distribution in Bonded Dissimilar Materials with Cracks," *Journal of Applied Mechanics*, **32**(2), pp.403–410.

Freund, L. B., (1990), *Dynamic Fracture Mechanics*, Cambridge University Press.

Freund, L. B. and Rosakis, A. J., (1992), " The Structure of the Near Tip Field during Transient Elastodynamic Crack Growth", *Journal of the Mechanics and Physics of Solids*, **40**(3), pp.699–719.

Gol'dstein, R. V., (1967), "On Surface Waves in Jointed Elastic Materials and Their Relation to Crack Propagation Along the Junction," *Applied Mathematics and Mechanics*, **31**, pp.496–502.

Hutchinson, J. W. and Suo, Z., (1992), "Mixed Mode Cracking in Layered Materials," in *Advances in Applied Mechanics*, **29**, edited by J. W. Hutchinson and T. Y. Wu, New York: Academic Press, pp.163–191.

Krishnaswamy, S. and Rosakis, A. J., (1991), "On the Extent of Dominace of Asymptotic Elastodynamic Crack-Tip Fields: Part I - An Experimental Study Using Bifocal Caustics," *Journal of Applied Mechanics*, **58**(1), pp.87-94.

Lee, Y.J., Lambros, J., and Rosakis, A. J., (1993), "Analysis of Coherent Gradient Sensing (CGS) by Fourier Optics," submitted to the *Journal of Applied Optics.*

Lee, Y. J. and Rosakis, A. J., (1992), "Interfacial Cracks in Plates: A Three-Dimensional Numerical Investigation," submitted to the *International Journal of Solids and Structures.*

Liu, C. and Rosakis, A. J., (1992), "On the Higher Order Asymptotic Analysis of a Non-Uniformly Propagating Dynamic Crack Along an Arbitrary Path." SM Report 92–45, Graduate Aeronautical Laboratories, California Institute of Technology. Submitted to the *Journal of Elasticity.*

Lo, C. Y., Nakamura, T., and Kushner, A., (1992), "Computational Analysis of Dynamic Crack Propagation Along Bimaterial Interface," in preparation.

Malyshev, B. M. and Salganik, R. L., (1965), "The Strength of Adhesive Joints Using the Theory of Crack," *International Journal of Fracture Mechanics*, **1**, pp.114–128.

Markenscoff, X. and Ni, L., (1990), "The Singular Nature of the Stress Field Near an Arbitrarily Moving Dislocation Loop," Journal of the Mechanics and Physics of Solids, **38**(4), pp.481–490.

Rice, J. R., (1988), "Elastic Fracture Mechanics Concept for Interfacial Cracks," *Journal of Applied Mechanics*, **55**(1), pp.98–103.

Rice, J. R. and Sih, G. C., (1965), "Plane Problems of Cracks in Dissimilar Media," *Journal of Applied Mechanics*, **32**(2), pp.418–423.

Rosakis, A. J., (1993), "Two Optical Techniques Sensitive to Gradients of Optical Path Difference: The Method of Caustics and the Coherent Gradient Sensor (CGS)," to appear in *Experimental Techniques in Fracture*, **3**, edited by J. Epstein, Chapter 10, pp.327–425.

Rosakis, A. J., Lee, Y. J., and Lambros, J., (1991), "Dynamic Crack Growth in Bimaterial Interfaces," in *Experiments in Micromechanics of Failure Resistant Materials*, AMD-Vol 130, AMSE 1991, edited by K. -S. Kim, pp.17–23.

Rosakis, A. J., Liu, C., and Freund, L. B., (1991), "A Note on the Asymptotic Stress Field of a Non-Uniformly Propagating Dynamic Crack", *International Journal of Fracture*, **50**, R39-R45.

Shih, C. F., (1991), "Cracks on Bimaterial Interfaces: Elasticity and Plasticity Aspects," *Material Science and Engineering*, **A143**, pp.77–90.

Sih, G. C. and Rice, J. R., (1964), "Bending of Plates of Dissimilar Materials with Cracks," *Journal of Applied Mechanics*, **31**, pp.477–482.

Tippur, H. V., Krishnaswamy, S., and Rosakis, A. J., (1991), "A Coherent Gradient Sensor for Crack Tip Measurements: Analysis and Experimental Results," *International Journal of Fracture*, **48**, pp.193–204.

Tippur, H. V. and Rosakis, A. J., (1991), "Quasi-Static and Dynamic Crack Growth Along Bimaterial Interfaces: A Note on Crack-Tip Field Measurements Using Coherent Gradient Sensing," *Experimental Mechanics*, **31**(3), pp.243–251.

Wheeler, L. T. and Sternberg, E., (1968), "Some Theorems in Classical Elastodynamics," *Achive for Rational Mechanics and Analysis*, **31**(1), pp.51-90.

Williams, M. L., (1959), "The Stresses Around a Fault or Crack in Dissimilar Media," *Bulletin of the Seismological Society of America*, **49**(2), pp.199–203.

Willis, J. R., (1971), "Fracture Mechanics of Interfacial Cracks," *Journal of the Mechanics and Physics of Solids*, **19**, pp.353–368.

Willis, J. R., (1973), "Self-Similar Problems in Elastodynamics," *Philosophical Transactions of the Royal Society* (London), **274**, pp.435–491.

Willis, J. R., (1992), "The Stress Field Near the Tip of an Accelerating Crack," *Journal of the Mechanics and Physics of Solids*, **40**(7), pp.1671–1681.

Wu, K. C., (1991), "Explicit Crack-Tip Fields of an Extending Interface Crack in an Anisotropic Bimaterial," *International Journal of Solids and Structures*, **27**(4), pp.455–466.

Yang, W., Suo, Z., and Shih, C. F., (1991), "Mechanics of Dynamic Debonding," *Proceedings of the Royal Society of London* **A**, **433**, pp.679–697.

Appendix

I: Definitions and properties of matrices used in section 3

Let $\boldsymbol{P}_k$, $\boldsymbol{Q}_k$, $\boldsymbol{U}_k$, and $\boldsymbol{V}_k$ be defined as in page 12, section 3, and $\boldsymbol{L}_k$ and $\dot{\boldsymbol{L}}_k$ be given by

$$\boldsymbol{L}_k = \boldsymbol{U}_k \boldsymbol{P}_k^{-1} , \qquad \dot{\boldsymbol{L}}_k = \boldsymbol{V}_k \boldsymbol{Q}_k^{-1} .$$

Matrices $\boldsymbol{H}$ and $\dot{\boldsymbol{H}}$ are defined as,

$$\boldsymbol{H} = \boldsymbol{L}_1 - \dot{\boldsymbol{L}}_2 , \qquad \dot{\boldsymbol{H}} = \dot{\boldsymbol{L}}_1 - \boldsymbol{L}_2 .$$

By algebraic calculations, it can be shown that for $k \in \{1, 2\}$,

$$\boldsymbol{L}_k = \begin{bmatrix} (l_{11})_k & (l_{12})_k \\ (l_{21})_k & (l_{11})_k \end{bmatrix} , \qquad \dot{\boldsymbol{L}}_k = \begin{bmatrix} (l_{11})_k & -(l_{12})_k \\ -(l_{21})_k & (l_{11})_k \end{bmatrix} ,$$

where

$$(l_{11})_k = \left\{ \frac{2\alpha_l \alpha_s - (1+\alpha_s^2)}{\mu D(v)} \right\}_k , \quad (l_{12})_k = \left\{ \frac{\alpha_s (1-\alpha_s^2)}{\mu D(v)} \right\}_k , \quad (l_{21})_k = \left\{ \frac{\alpha_l (1-\alpha_s^2)}{\mu D(v)} \right\}_k ,$$

and

$$D(v) = 4\alpha_l \alpha_s - (1+\alpha_s^2)^2 .$$

Therefore,

$$\boldsymbol{H} = \begin{bmatrix} h_{11} & h_{12} \\ h_{21} & h_{11} \end{bmatrix} , \qquad \dot{\boldsymbol{H}} = \begin{bmatrix} h_{11} & -h_{12} \\ -h_{21} & h_{11} \end{bmatrix} ,$$

where

$$h_{11} = (l_{11})_1 - (l_{11})_2 , \qquad h_{12} = (l_{12})_1 + (l_{12})_2 , \qquad h_{21} = (l_{21})_1 + (l_{21})_2 .$$

Notice that

$$\boldsymbol{H}\,\dot{\boldsymbol{H}} = \dot{\boldsymbol{H}}\,\boldsymbol{H} = (h_{11}^2 - h_{12}h_{21})\boldsymbol{I} ,$$

where $\boldsymbol{I}$ is the 2×2 identity matrix. Thus,

$$\boldsymbol{H}^{-1} = \frac{1}{h_{11}^2 - h_{12}h_{21}}\,\dot{\boldsymbol{H}} , \qquad \dot{\boldsymbol{H}}^{-1} = \frac{1}{h_{11}^2 - h_{12}h_{21}}\boldsymbol{H} .$$

Also, it can be shown that

$$\boldsymbol{L}_k \overset{*}{\boldsymbol{L}}_k = \overset{*}{\boldsymbol{L}}_k \boldsymbol{L}_k \ , \qquad k \in \{1,2\}.$$

A sequence of operator definitions follows. These are related to the analysis in section 3.2. Let $p(t)$ and $q(t)$ be two real functions of time t and define the vector operators

$$\begin{aligned}
\boldsymbol{d}_k\{p(t),q(t)\} &= \{\ D_l\{p(t)\},\ D_s\{q(t)\}\ \}_k^{\mathsf{T}} \ , \\
\boldsymbol{k}_k\{p(t),q(t)\} &= \{\ K_l(t)p(t),\ K_s(t)q(t)\ \}_k^{\mathsf{T}} \ , \\
\boldsymbol{b}_k\{p(t),q(t)\} &= \{\ B_l(t)p(t),\ B_s(t)q(t)\ \}_k^{\mathsf{T}} \ ,
\end{aligned}$$

where operators $D_{l,s}\{\cdot\}$ and functions $K_{l,s}(t)$ and $B_{l,s}(t)$ have been defined in section 3.2. With the above definitions,

$$\begin{aligned}
\boldsymbol{t}_k\{p(t),q(t)\} &= (3+2i\epsilon)\,(\boldsymbol{L}_k\boldsymbol{M}_k - \boldsymbol{I})\,\boldsymbol{d}_k\{p(t),q(t)\} + 2\dot{\epsilon}\,(\boldsymbol{L}_k\boldsymbol{M}_k - \boldsymbol{I})\,\boldsymbol{k}_k\{p(t),q(t)\} \\
&+ 2\left[(1+2i\epsilon)\,(\boldsymbol{L}_k\boldsymbol{M}_k - \boldsymbol{I}) + \boldsymbol{L}_k\,\overset{*}{\boldsymbol{P}}_k - \overset{*}{\boldsymbol{U}}_k\right]\boldsymbol{b}_k\{p(t),q(t)\} \ ,
\end{aligned}$$

where $\boldsymbol{M}_k$, $\overset{*}{\boldsymbol{P}}_k$, and $\overset{*}{\boldsymbol{U}}_k$ have also been defined in section 3.2. In addition, for any given operator

$$\boldsymbol{m}_k\{p(t),q(t)\} = \left\{\ m_k^{(1)}\{p(t),q(t)\},\ m_k^{(2)}\{p(t),q(t)\}\ \right\}^{\mathsf{T}} \ ,$$

the associated operato. $\overset{*}{\boldsymbol{m}}_k\ \{p(t),q(t)\}$ is defined as

$$\overset{*}{\boldsymbol{m}}_k\ \{p(t),q(t)\} = \left\{\ m_k^{(1)}\{p(t),q(t)\},\ -m_k^{(2)}\{p(t),q(t)\}\ \right\}^{\mathsf{T}} \ .$$

Also vectors $\boldsymbol{\beta}$, $\boldsymbol{\gamma}$, $\boldsymbol{\xi}$, and $\boldsymbol{\varsigma}$, are defined as

$$\left.\begin{aligned}
\boldsymbol{\beta} &= \boldsymbol{t}_1\{a_0(t),c_0(t)\} - \overset{*}{\boldsymbol{t}}_2\ \{b_0(t),d_0(t)\} \\
\boldsymbol{\gamma} &= \boldsymbol{t}_2\{a_0(t),c_0(t)\} - \overset{*}{\boldsymbol{t}}_1\ \{b_0(t),d_0(t)\} \\
\boldsymbol{\xi} &= (3+2i\epsilon)\left[(\boldsymbol{L}_1\boldsymbol{M}_1 - \boldsymbol{I})\,\boldsymbol{k}_1\{a_0(t),c_0(t)\} - \left(\overset{*}{\boldsymbol{L}}_2\,\boldsymbol{M}_2 - \boldsymbol{I}\right)\overset{*}{\boldsymbol{k}}_2\ \{b_0(t),d_0(t)\}\right] \\
\boldsymbol{\varsigma} &= (3+2i\epsilon)\left[(\boldsymbol{L}_2\boldsymbol{M}_2 - \boldsymbol{I})\,\boldsymbol{k}_2\{a_0(t),c_0(t)\} - \left(\overset{*}{\boldsymbol{L}}_1\,\boldsymbol{M}_1 - \boldsymbol{I}\right)\overset{*}{\boldsymbol{k}}_1\ \{b_0(t),d_0(t)\}\right]
\end{aligned}\right\} \ ,$$

and operators $\boldsymbol{w}_{dk}\{p(t),q(t)\}$ and $\boldsymbol{w}_{tk}\{p(t),q(t)\}$ as

$$\left.\begin{aligned}
\boldsymbol{w}_{dk}\{p(t),q(t)\} &= \left(\frac{3}{2}+i\epsilon\right)\left[2\boldsymbol{P}_k^{-1}\boldsymbol{M}_k+\left(\frac{1}{2}+i\epsilon\right)\boldsymbol{I}\right]\boldsymbol{k}_k\{p(t),q(t)\} \\
\boldsymbol{w}_{tk}\{p(t),q(t)\} &= \left(\frac{3}{2}+i\epsilon\right)\left[2\boldsymbol{P}_k^{-1}\boldsymbol{M}_k+\left(\frac{1}{2}+i\epsilon\right)\boldsymbol{I}\right]\boldsymbol{d}_k\{p(t),q(t)\} \\
&+ 2\dot{\epsilon}\left[\boldsymbol{P}_k^{-1}\boldsymbol{M}_k+(1+i\epsilon)\boldsymbol{I}\right]\boldsymbol{k}_k\{p(t),q(t)\} \\
&+ \left[2\boldsymbol{P}_k^{-1}\,\dot{\boldsymbol{P}}_k+2(1+2i\epsilon)\boldsymbol{P}_k^{-1}\boldsymbol{M}_k-\left(\frac{1}{4}+\epsilon^2\right)\boldsymbol{I}\right]\boldsymbol{b}_k\{p(t),q(t)\}
\end{aligned}\right\}.$$

II: Solution of the Riemann-Hilbert problem

Consider the problem formulated as following: Find a function

$$\boldsymbol{\theta}(z)=(\ \theta_1(z),\ \theta_2(z)\ )^{\mathsf{T}}\ ,$$

$z=\eta_1+i\eta_2$, which is analytic in the whole z-plane except along the branch cut $-\infty<\eta_1\leq 0$, $\eta_2=0$, and satisfies the equation,

$$\dot{\boldsymbol{H}}\,\boldsymbol{\theta}^{+}(\eta_1)-\boldsymbol{H}\boldsymbol{\theta}^{-}(\eta_1)=\boldsymbol{\kappa}(\eta_1)\ ,\qquad \forall\ \eta_1<0\ , \tag{1}$$

where $\dot{\boldsymbol{H}}$ and $\boldsymbol{H}$ are 2×2 matrices, defined in Appendix I, and

$$\boldsymbol{\kappa}(\eta_1)=(\ \kappa_1(\eta_1),\ \kappa_2(\eta_1)\ )^{\mathsf{T}}\ ,$$

with κ_1 and κ_2 are known functions of η_1. Near the origin, function $\boldsymbol{\theta}(z)$ should satisfy the requirement that

$$|\ \boldsymbol{\theta}(z)\ |=O\ (\ |z|^{\alpha}\ )\ ,\qquad \text{as } |z|\to 0\ , \tag{2}$$

for some real number α, and generally, $\alpha>-1$.

In order to obtain the solution to the above Riemann-Hilbert problem, the eigen-values and eigen-vectors of $\boldsymbol{H}$, and $\dot{\boldsymbol{H}}$ need to be studied first. By solving the equation

$$\det\{\boldsymbol{H}-\lambda\boldsymbol{I}\}=0\ , \tag{3}$$

where $\boldsymbol{I}$ is the identity matrix, the eigen-values for $\boldsymbol{H}$ are found to be

$$\lambda_{1,2} = h_{11} \pm \sqrt{h_{12} h_{21}} \ . \tag{4}$$

The expressions of functions h_{11}, h_{12}, and h_{21} in our problem are dependent upon the mechanical properties of the constituents of the bimaterial system and the speed of propagation of the interfacial crack. h_{11}, h_{12}, and h_{21} ensure that the eigen-values, λ_1 and λ_2, are real, provided that the crack-tip speed is less than the lower Rayleigh wave speed of the bimaterial. The corresponding eigen-vectors are

$$\boldsymbol{w}^{(1,2)} = (\ 1, \ \pm\eta \ )^{\mathsf{T}} \ , \tag{5}$$

where the parameter η is defined by

$$\eta = \sqrt{\frac{h_{21}}{h_{12}}} \ .$$

It can be shown that the eigen-values for $\overset{*}{\boldsymbol{H}}$ are the same as those for $\boldsymbol{H}$, which are given in (4), while the corresponding eigen-vectors are

$$\overset{*}{\boldsymbol{w}}^{(1,2)} = (\ 1, \ \mp\eta \ )^{\mathsf{T}} \ . \tag{6}$$

Define the matrix $\boldsymbol{B}$, by

$$\boldsymbol{B} = \begin{bmatrix} 1 & 1 \\ \eta & -\eta \end{bmatrix} \ ,$$

and set

$$\overset{*}{\boldsymbol{H}}' = \boldsymbol{B}^{-1} \overset{*}{\boldsymbol{H}} \boldsymbol{B} \ , \qquad \boldsymbol{H}' = \boldsymbol{B}^{-1} \boldsymbol{H} \boldsymbol{B} \ ,$$

and

$$\overset{\diamond}{\boldsymbol{\theta}} (z) = \boldsymbol{B}^{-1} \boldsymbol{\theta}(z) \ , \qquad \overset{\diamond}{\boldsymbol{\kappa}} (\eta_1) = \boldsymbol{B}^{-1} \boldsymbol{\kappa}(\eta_1) \ .$$

Then, equation (1) becomes

$$\overset{*}{\boldsymbol{H}}' \overset{\diamond}{\boldsymbol{\theta}}^{+} (\eta_1) - \boldsymbol{H}' \overset{\diamond}{\boldsymbol{\theta}}^{-} (\eta_1) = \overset{\diamond}{\boldsymbol{\kappa}} (\eta_1) \ , \qquad \forall \ \eta_1 < 0 \ , \tag{7}$$

or, in component form,

$$\left.\begin{aligned} \lambda_2 \overset{\circ}{\theta}_1^{+}(\eta_1) - \lambda_1 \overset{\circ}{\theta}_1^{-}(\eta_1) &= \overset{\circ}{\kappa}_1(\eta_1) \\ \lambda_1 \overset{\circ}{\theta}_2^{+}(\eta_1) - \lambda_2 \overset{\circ}{\theta}_2^{-}(\eta_1) &= \overset{\circ}{\kappa}_2(\eta_1) \end{aligned}\right\}, \qquad \forall\, \eta_1 < 0\,. \tag{8}$$

It can be seen from above analysis that $\boldsymbol{H}$ and $\dot{\boldsymbol{H}}$ can be diagonalized simultaneously by the same transformation. Therefore, the originally coupled equations (1) can be reduced to the uncoupled equations (8).

If we express the ratio λ_1/λ_2 as having the following dependence on β:

$$-\frac{\lambda_1}{\lambda_2} = \frac{1+\beta}{1-\beta}\,,$$

then the parameter β must be expressed as,

$$\beta = \frac{h_{11}}{\sqrt{h_{12}h_{21}}}\,.$$

As a result, the solution for the first equation in (8) can be obtained as

$$\frac{\overset{\circ}{\theta}_1(z)}{L(z)} = \frac{1}{2\pi i}\int_C \frac{\overset{\circ}{\kappa}_1(\tau)\mathrm{d}\tau}{\lambda_2 L^{+}(\tau)(\tau - z)} + \overset{\circ}{A}(z)\,, \tag{9}$$

where $\overset{\circ}{A}(z)$ is an arbitrary entire function. C is a contour along the entire branch cut, and extends from negative infinity to the interfacial crack-tip. The function $L(z)$ is given by

$$L(z) = z^{-\frac{1}{2}+k_1+i\epsilon}\,, \tag{10}$$

where

$$\epsilon = \frac{1}{2\pi}\ln\frac{1-\beta}{1+\beta}\,,$$

and k_1 is an real integer. Integer k_1 is chosen so that

$$|\,L(z)\,| = O\,(\,|z|^{\alpha}\,)\,, \qquad \text{as } |z| \to 0\,,$$

which complies with the restriction of equation (2).

Similarly, we can obtain that

$$\frac{\mathring{\theta}_2(z)}{\overline{L}(z)} = \frac{1}{2\pi i}\int_C \frac{\mathring{\kappa}_2(\tau)\mathrm{d}\tau}{\lambda_1 \overline{L}^+(\tau)(\tau - z)} + \mathring{B}(z)\,, \tag{11}$$

where $\mathring{B}(z)$ is also an arbitrary entire function. $\overline{L}$ stands for the complex conjugate of L.

Returning to the original function $\boldsymbol{\theta}(z)$,

$$\left.\begin{aligned} \boldsymbol{\theta}(z) &= \frac{1}{4\pi i}\int_C \left\{ \frac{1}{\lambda_2}\frac{L(z)}{L^+(\tau)}\boldsymbol{\Gamma}\boldsymbol{\kappa}(\tau) + \frac{1}{\lambda_1}\frac{\overline{L}(z)}{\overline{L}^+(\tau)}\,\overset{*}{\boldsymbol{\Gamma}}\,\boldsymbol{\kappa}(\tau)\right\}\frac{\mathrm{d}\tau}{\tau - z} \\ &+ L(z)\,\mathring{\boldsymbol{A}}(z)\boldsymbol{\zeta} + \overline{L}(z)\,\mathring{\boldsymbol{B}}(z)\,\overset{*}{\boldsymbol{\zeta}} \end{aligned}\right\}\,, \tag{12}$$

where

$$\boldsymbol{\Gamma} = \begin{bmatrix} 1 & \frac{1}{\eta} \\ \eta & 1 \end{bmatrix}\,, \qquad \overset{*}{\boldsymbol{\Gamma}} = \begin{bmatrix} 1 & -\frac{1}{\eta} \\ -\eta & 1 \end{bmatrix}\,,$$

and

$$\boldsymbol{\zeta} = (\,1,\ \eta\,)^{\mathsf{T}}\,, \qquad \overset{*}{\boldsymbol{\zeta}} = (\,1,\ -\eta\,)^{\mathsf{T}}\,.$$

III: Some asymptotic results of the Stieltjes transform

In solving the Riemann-Hilbert problem, we need to evaluate the integral

$$I(z) = \int_{-\infty}^{0} \frac{f(-\eta_1)}{\eta_1 - z}\mathrm{d}\eta_1\,. \tag{13}$$

Setting $t = -\eta_1$, we get

$$I(z) = -\int_0^{\infty} \frac{f(t)}{t + z}\mathrm{d}t\,. \tag{14}$$

As we can see from equation (14), $-I(z)$ is the Stieltjes transform of function $f(t)$. Here we want to study the asymptotic behavior of the Stieltjes transform as $z \to 0$. Alternatively, we may set $\lambda = 1/z$ to get

$$I(z) = -\lambda H[f;\lambda]\,, \tag{15}$$

where

$$H[f;\lambda] = \int_0^\infty \frac{f(t)}{1+\lambda t} dt \ . \tag{16}$$

Studying the asymptotic behavior of (14) as $z \to 0$ is equivalent to studying the asymptotic behavior of (16) as $\lambda \to \infty$.

Suppose that $f(t)$ is locally integrable in $(0,\infty)$. Recall that the Mellin transform of $f(t)$ is defined by

$$M[f;s] = \int_0^\infty t^{s-1} f(t) dt \ , \tag{17}$$

and set

$$h(t) = \frac{1}{1+t} \ .$$

Then, by using the Parseval formula, we can obtain that

$$H[f;\lambda] = \frac{1}{2\pi i} \int_{r-i\infty}^{r+i\infty} \lambda^{-s} M[h;s] M[f;1-s] ds \ , \tag{18}$$

where the constant r is such that $\mathrm{Re}(s) = r$ lies in the common strip of analyticity of the Mellin transforms $M[h;s]$ and $M[f;1-s]$.

After some manipulations, it can be shown that

$$M[h;s] = \frac{\pi}{\sin \pi s} \ , \tag{19}$$

where $M[h;s]$ is analytic in the strip $0 < \mathrm{Re}(s) < 1$. In analogy to the particular problem of interfacial fracture that we are interested in, we will define the function $f(t)$ as,

$$f(t) = t^{i\alpha} (\ln t)^\beta \ , \tag{20}$$

where $\alpha = \pm 2\epsilon$, or 0, and $\beta = 0$, or 1. For this function, the Mellin transform $M[f;s]$ only exits in the generalized sense. Let

$$f_1(t) = \begin{cases} f(t), & t \in (0,1] \\ 0, & t \in [1,\infty) \end{cases} \ ; \qquad f_2(t) = \begin{cases} 0, & t \in (0,1] \\ f(t), & t \in [1,\infty) \end{cases} \ .$$

Then, we may write

$$H[f_j;\lambda] = L_j(\lambda) = \int_0^\infty \frac{f_j(t)}{1+\lambda t}\mathrm{d}t\ , \qquad j = 1,\ 2\ , \tag{21}$$

and

$$H[f;\lambda] = L_1(\lambda) + L_2(\lambda)\ . \tag{22}$$

Also let

$$G_j(s) = M[h;s]M[f_j;1-s]\ , \qquad j = 1,\ 2\ . \tag{23}$$

Then,

$$G(s) = M[h;s]M[f;1-s] = G_1(s) + G_2(s)\ .$$

In addition, from the Parseval formula,

$$L_j(\lambda) = \frac{1}{2\pi i}\int_{r_j-i\infty}^{r_j+i\infty} \lambda^{-s}G_j(s)\mathrm{d}s\ , \qquad j = 1,\ 2\ , \tag{24}$$

and

$$H[f;\lambda] = \frac{1}{2\pi i}\sum_{j=1}^{2}\int_{r_j-i\infty}^{r_j+i\infty} \lambda^{-s}G_j(s)\mathrm{d}s\ . \tag{25}$$

Using the specific function $f(t)$ chosen in (20), it can be shown that

$$G_1(s) = -\frac{1}{[s-(1+i\alpha)]^{\beta+1}}\frac{\pi}{\sin\pi s}\ . \tag{26}$$

In the above we can see that $G_1(s)$ is analytic in the strip $0 < \mathrm{Re}(s) < 1$. Since $M[f_2;1-s]$ is analytic in the half plane $\mathrm{Re}(s) > 1$, and $M[h;s]$ can be analytically continued into the entire s–plane as a meromorphic function, $G_2(s)$ is a meromorphic function in the half plane $\mathrm{Re}(s) > 1$ with simple poles at $s = 2, 3, \cdots$. Then in equation (24), we can always choose that $0 < r_1 < 1$ and $r_2 > r_1$. Observe that if $s = s_1 + is_2$, $G_1(s)$ has the property

$$\lim_{|s_2|\to\infty} G_1(s_1+is_2) = 0\ , \qquad r_1 < s_1 < r_2\ . \tag{27}$$

Therefore, we can apply Cauchy's integral theorem to equation (25), which results in

$$H[f;\lambda] = \sum_{r_1<\mathrm{Re}(s)<r_2} \mathrm{res}\left\{-\lambda^{-s}G_1(s)\right\} + \frac{1}{2\pi i}\int_{r_2-i\infty}^{r_2+i\infty} \lambda^{-s}G(s)\mathrm{d}s\ . \tag{28}$$

For our case, it is easy to show that $G(s) = 0$. So finally, we get

$$H[f;\lambda] = \sum_{r_1<\mathrm{Re}(s)<r_2} \mathrm{res}\left\{\frac{\lambda^{-s}}{[s-(1+i\alpha)]^{\beta+1}}\frac{\pi}{\sin \pi s}\right\} . \tag{29}$$

Letting $r_2 \to +\infty$, we get an infinite asymptotic series for $H[f;\lambda]$ as $\lambda \to \infty$.

By applying the above analysis to our particular problem, for $\alpha \neq 0$, we will obtain following asymptotic results:

$$\left.\begin{aligned}
\int_{-\infty}^{0} \frac{(-\eta_1)^{i\alpha}\ln(-\eta_1)}{\eta_1 - z}d\eta_1 &= \frac{i\pi}{\sinh \pi\alpha} z^{i\alpha}\ln z - \frac{\pi^2 \cosh \pi\alpha}{\sinh^2 \pi\alpha} z^{i\alpha} - \frac{1}{\alpha^2} \\
&\quad + O(\,|z|\,) \\
\int_{-\infty}^{0} \frac{(-\eta_1)^{i\alpha}}{\eta_1 - z}d\eta_1 &= -\frac{i\pi}{\sinh \pi\alpha} z^{i\alpha} + \frac{i}{\alpha} + O(\,|z|\,) \\
\int_{-\infty}^{0} \frac{\ln(-\eta_1)}{\eta_1 - z}d\eta_1 &= \frac{1}{2}(\ln z)^2 + \frac{\pi^2}{6} + O(\,|z|\,) \\
\int_{-\infty}^{0} \frac{1}{\eta_1 - z}d\eta_1 &= \ln z + O(\,|z|\,)
\end{aligned}\right\}, \text{ as } z \to 0. \tag{30}$$

Captions

Figure 1: Schematic of dynamic growth of a crack along a bimaterial interface.

Figure 2: Velocity dependence of mismatch parameter η for plane stress and plane strain. (Bimaterial combination: PMMA/steel)

Figure 3: Velocity dependence of mismatch parameter β for plane stress and plane strain. (Bimaterial combination: PMMA/steel)

Figure 4: Velocity dependence of mismatch parameter β for plane stress and plane strain at the vicinity of the shear wave speed of PMMA. (Bimaterial combination: PMMA/steel)

Figure 5: Velocity dependence of mismatch parameter ϵ for plane stress and plane strain. (Bimaterial combination: PMMA/steel)

Figure 6: Velocity dependence of the real part of mismatch parameter ϵ for plane stress and plane strain at the vicinity of the shear wave speed of PMMA. (Bimaterial combination: PMMA/steel)

Figure 7: Schematic of the optical set-up for CGS in transmission.

Figure 8: Selected sequence of CGS interferograms of a growing crack in a three point bend interfacial drop weight tower experiment. (Only PMMA side of PMMA/steel specimen is shown)

Figure 9: Velocity, (a) and acceleration, (b) time histories for the experiment shown in Figure 8.

Figure 10: Time histories of mismatch parameter ϵ, (a) and its time derivative, (b) for the experiment shown in Figure 8.

Figure 11: Comparison of digitized data points from the interferogram corresponding to $t = 9.5\mu$sec in Figure 8 with, (a) a K^d-dominant fit, equation (7.9); (b) a higher order transient analysis fit, equation (7.10). (Crack lies along the negative x_1-axis)

Figure 12: Comparison of digitized data points from the interferogram corresponding to $t = 23\mu$sec in Figure 8 with, (a) a K^d-dominant fit, equation (7.9); (b) a higher order transient analysis fit, equation (7.10). (Crack lies along the negative x_1-axis)

Figure 13: Selected sequence of CGS interferograms of a growing crack in an one point bend interfacial gas gun experiment. (Only PMMA side of PMMA/steel specimen is shown)

Figure 14: Velocity, (a) and acceleration, (b) time histories for the experiment shown in Figure 13.

Figure 15: Time histories of mismatch parameter ϵ, (a) and its time derivative, (b) for the experiment shown in Figure 13.

Figure 16: Comparison between the CGS fringe pattern and the fitted higher order transient stress field, equation (7.10), for a propagating crack in a PMMA/steel interface.

Figure 17: Velocity time history for the experiment shown in Figure 18.

Figure 18: Selected sequence of CGS interferograms of a growing crack in an one point bend interfacial gas gun experiment. (A blunt starter notch was used)

Figure 19: CGS interferograms providing visual evidence of the highly transient nature of dynamic interfacial crack growth.

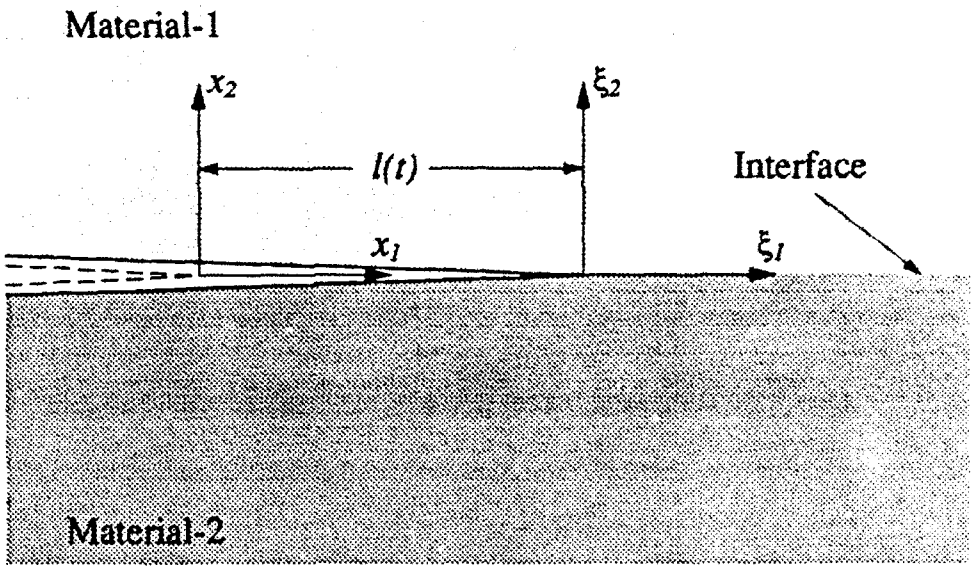

Figure 1: Schematic of dynamic growth of a crack along a bimaterial interface.

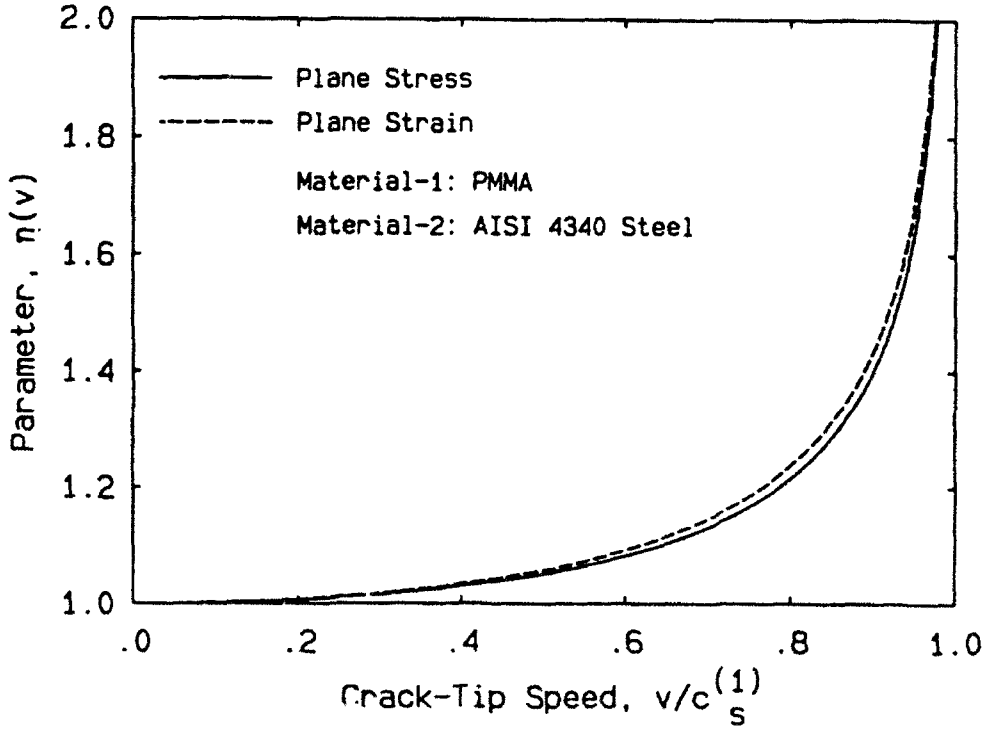

Figure 2: Velocity dependence of mismatch parameter η for plane stress and plane strain. (Bimaterial combination: PMMA/steel)

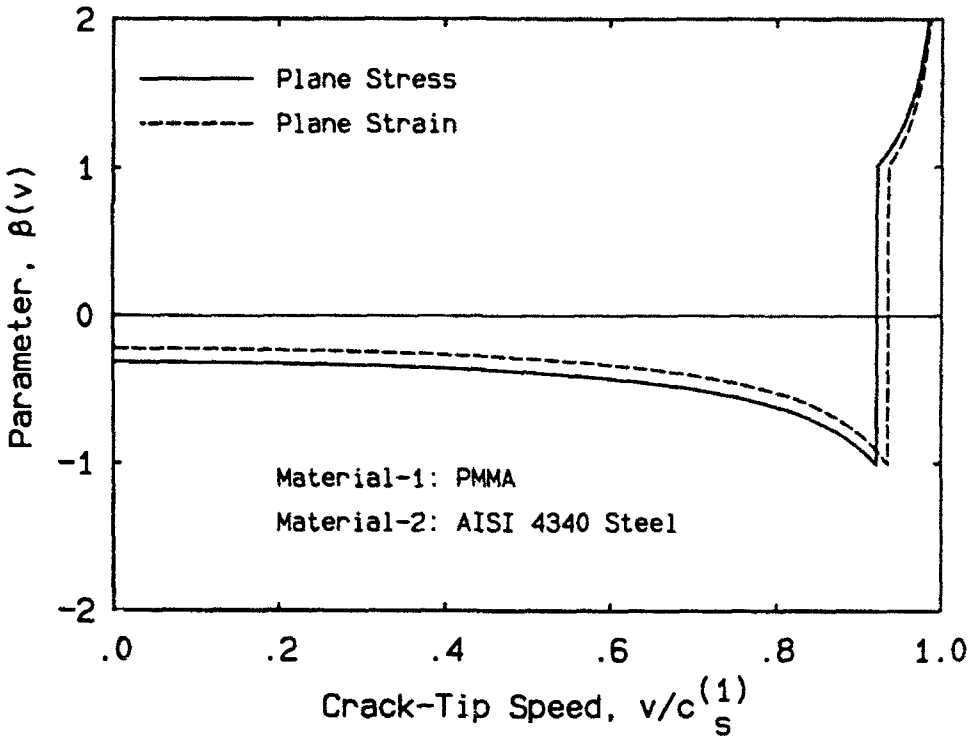

Figure 3: Velocity dependence of mismatch parameter β for plane stress and plane strain. (Bimaterial combination: PMMA/steel)

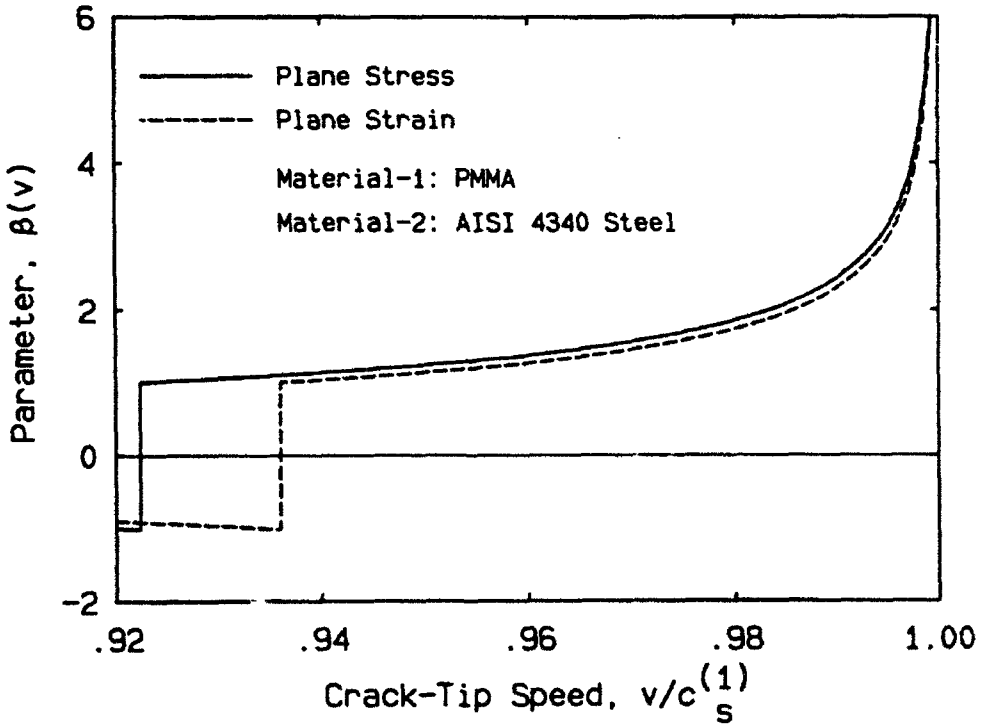

Figure 4: Velocity dependence of mismatch parameter β for plane stress and plane strain at the vicinity of the shear wave speed of PMMA. (Bimaterial combination: PMMA/steel)

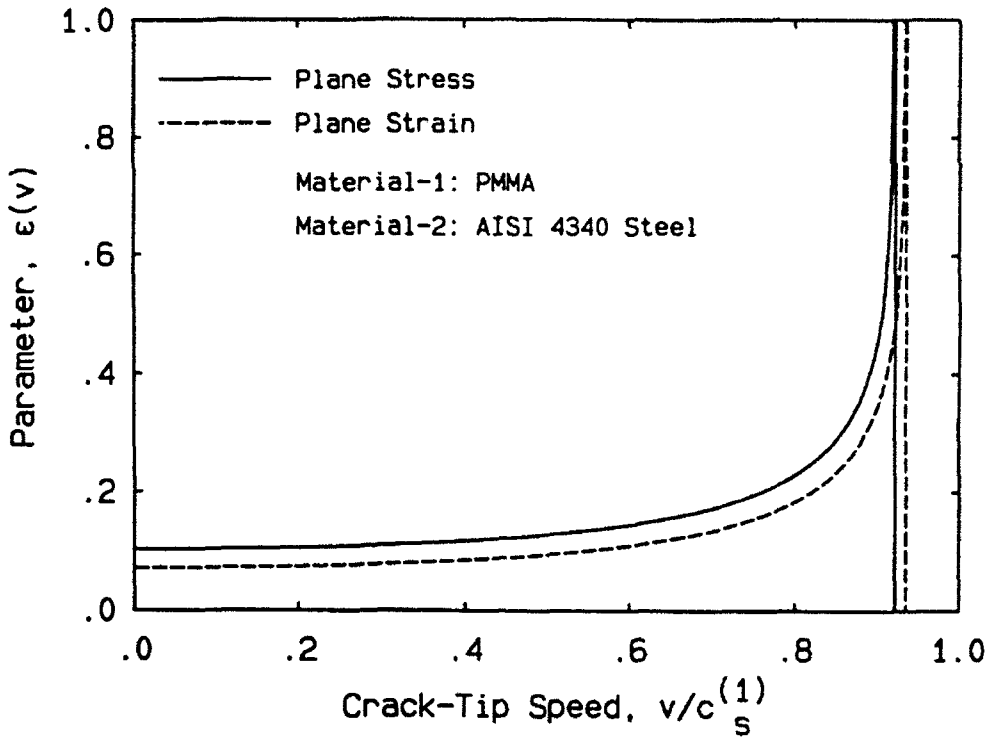

Figure 5: Velocity dependence of mismatch parameter ϵ for plane stress and plane strain. (Bimaterial combination: PMMA/steel)

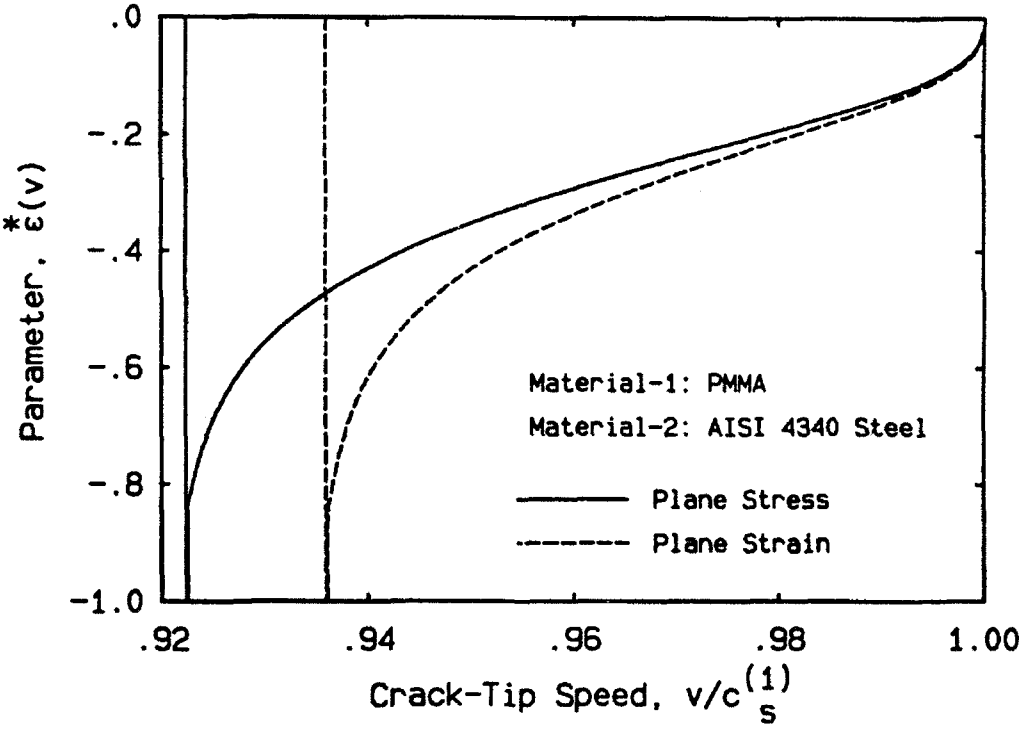

Figure 6: Velocity dependence of the real part of mismatch parameter ϵ for plane stress and plane strain at the vicinity of the shear wave speed of PMMA. (Bimaterial combination: PMMA/steel)

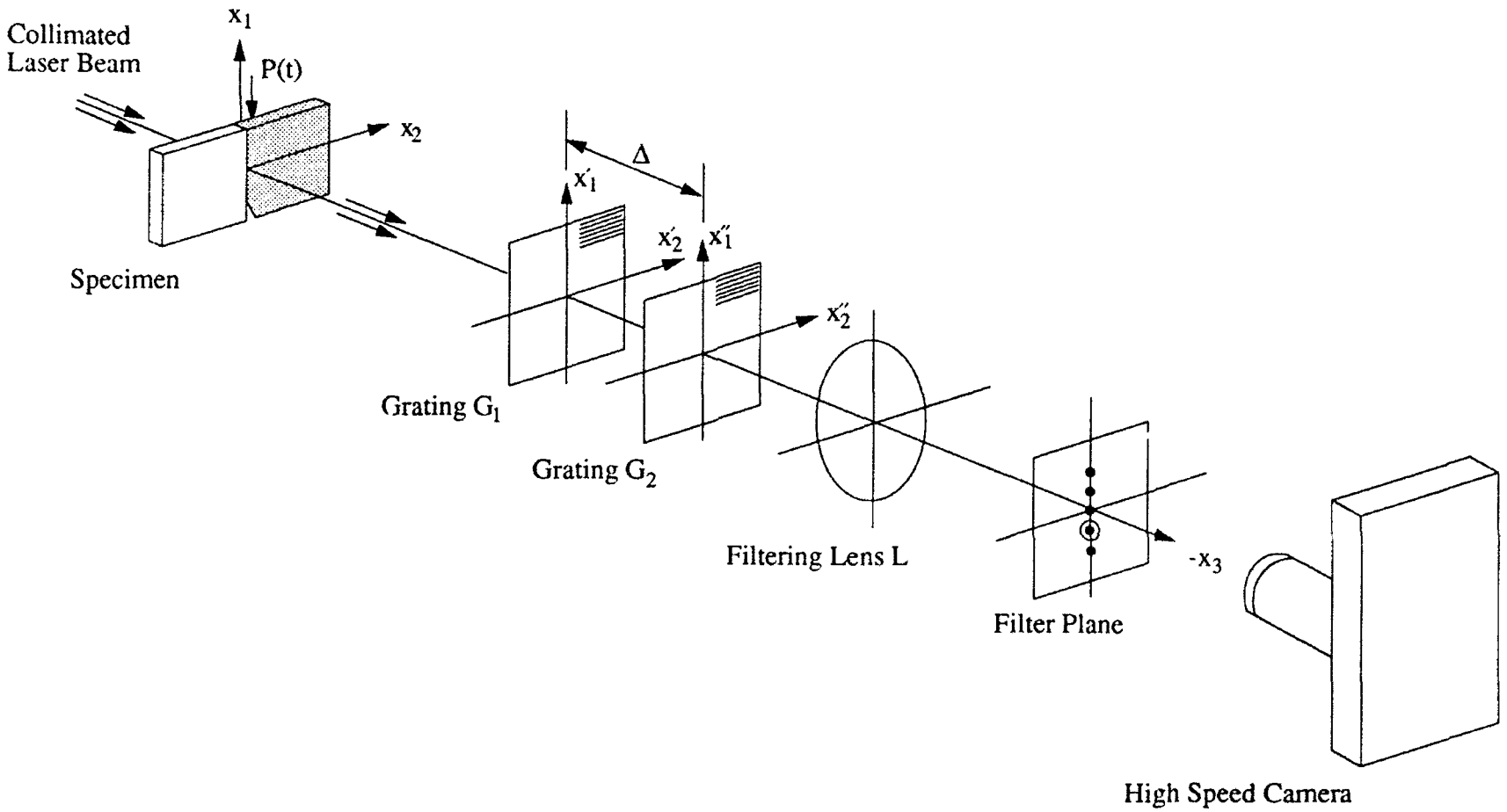

Figure 7: Schematic of the optical set-up for CGS in transmission.

t=9.5 μs
v=640 m/s

t=16.5 μs
v=790 m/s

t=23 μs
v=800 m/s

t=32 μs
v=880 m/s

Figure 8: Selected sequence of CGS interferograms of a growing crack in a three point bend interfacial drop weight tower experiment. (Only PMMA side of PMMA/steel specimen is shown)

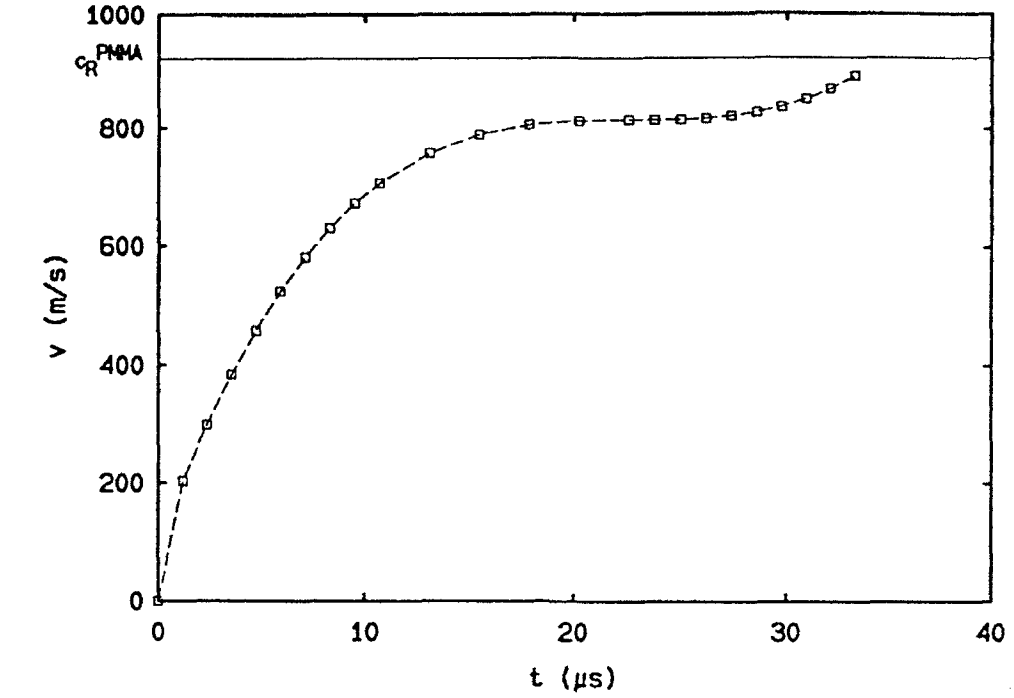

(a)

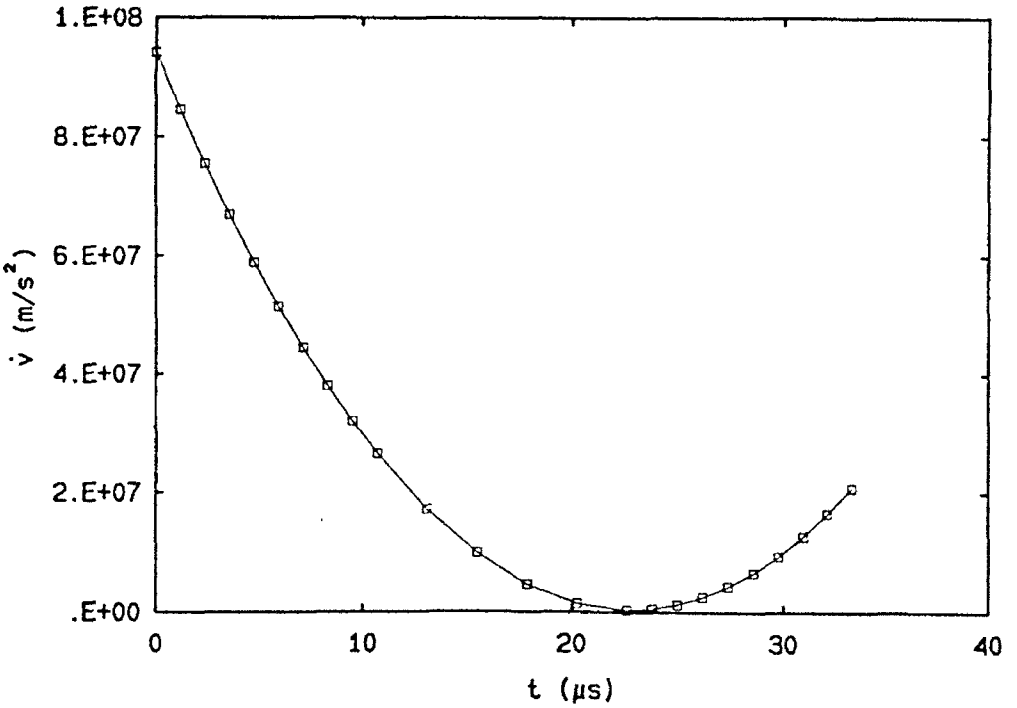

(b)

Figure 9: Velocity, (a) and acceleration, (b) time histories for the experiment shown in Figure 8.

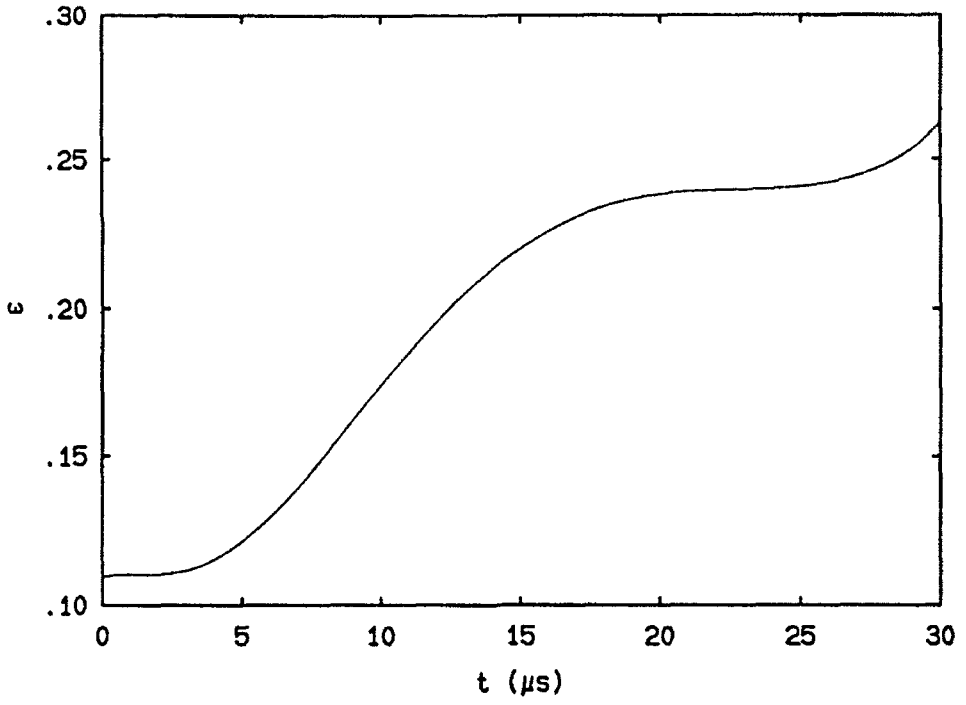

(a)

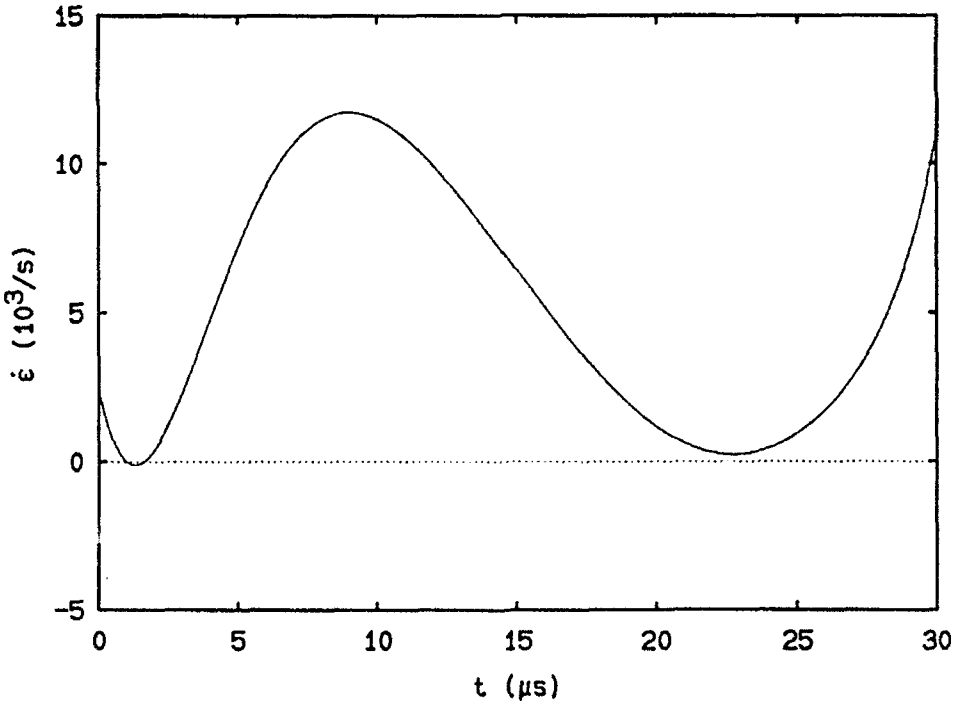

(b)

Figure 10: Time histories of mismatch parameter ϵ, (a) and its time derivative, (b) for the experiment shown in Figure 8.

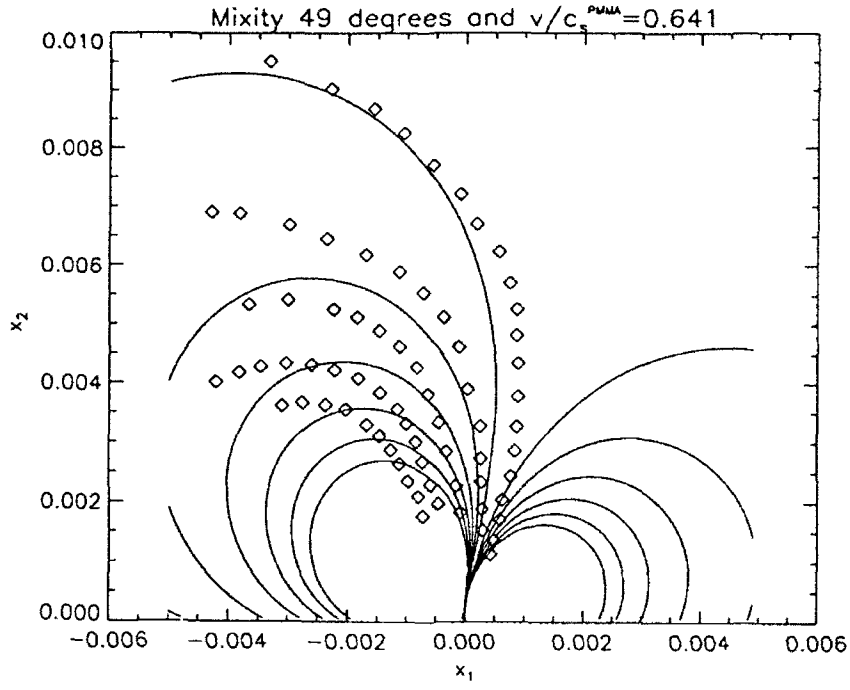

(a)

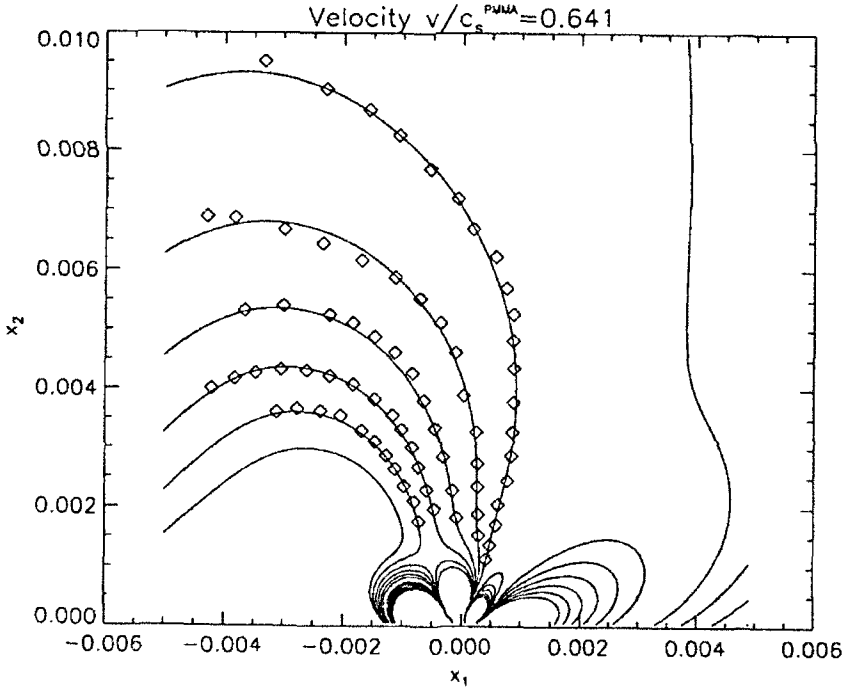

(b)

Figure 11: Comparison of digitized data points from the interferogram corresponding to $t = 9.5\mu$sec in Figure 8 with, (a) a K^d-dominant fit, equation (7.9); (b) a higher order transient analysis fit, equation (7.10). (Crack lies along the negative x_1-axis)

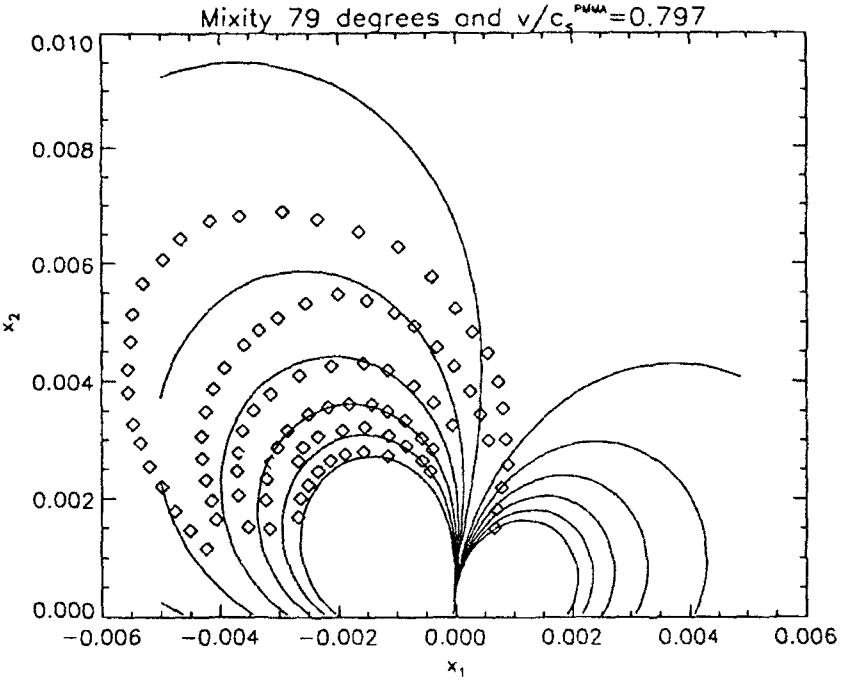

(a)

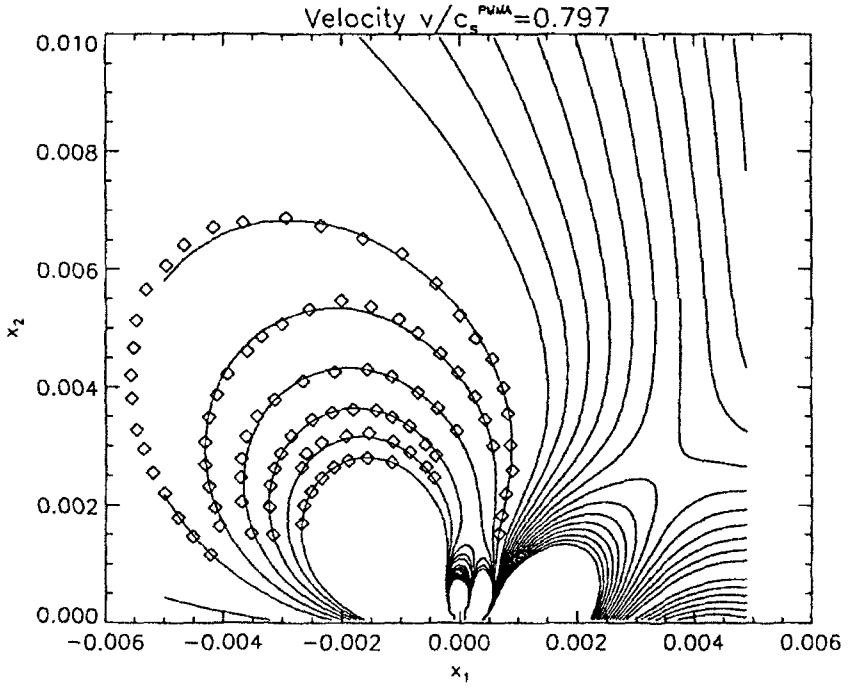

(b)

Figure 12: Comparison of digitized data points from the interferogram corresponding to $t = 23\mu$sec in Figure 8 with, (a) a K^d-dominant fit, equation (7.9); (b) a higher order transient analysis fit, equation (7.10). (Crack lies along the negative x_1-axis)

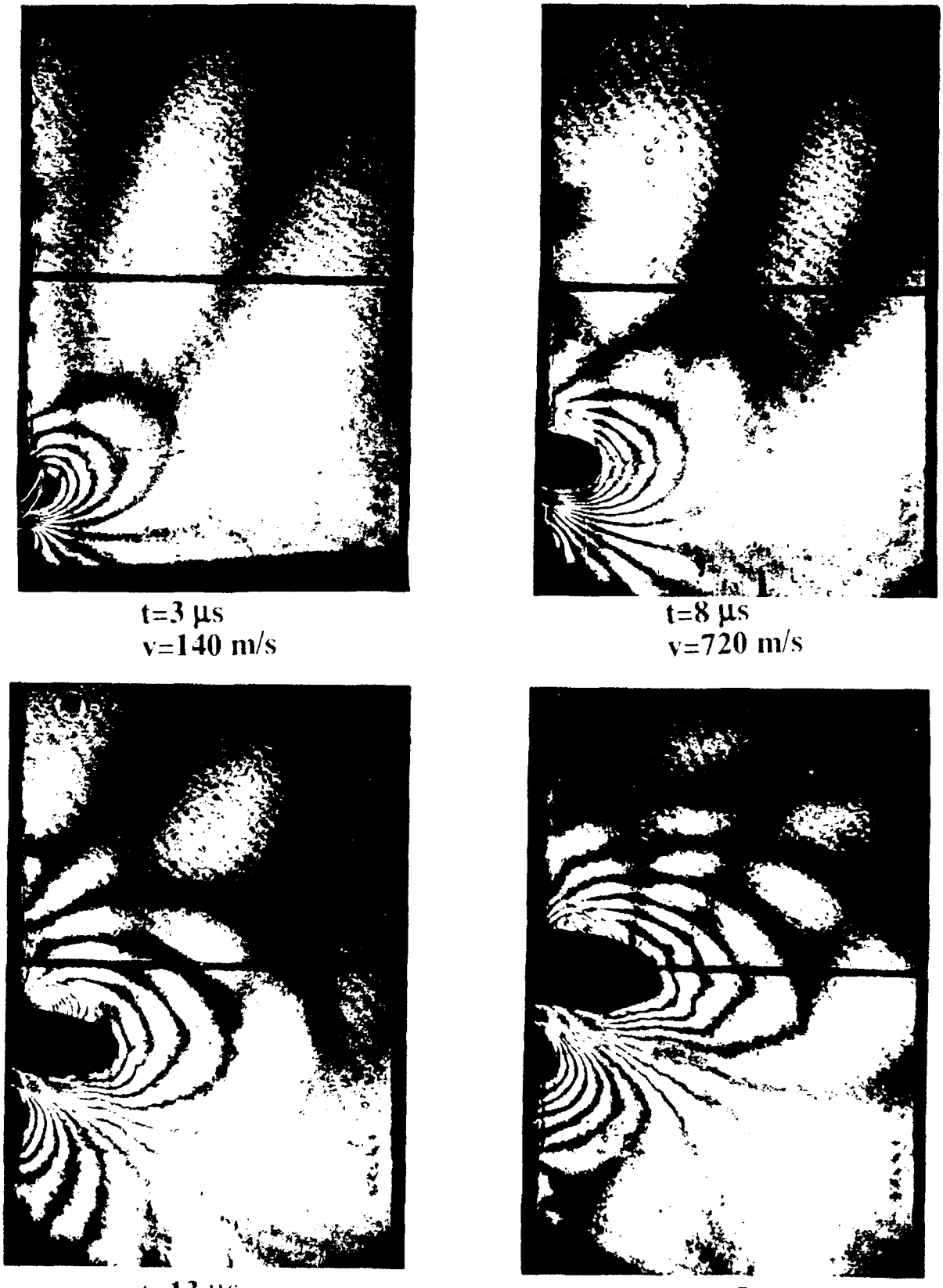

Figure 13: Selected sequence of CGS interferograms of a growing crack in an one point bend interfacial gas gun experiment. (Only PMMA side of PMMA/steel specimen is shown)

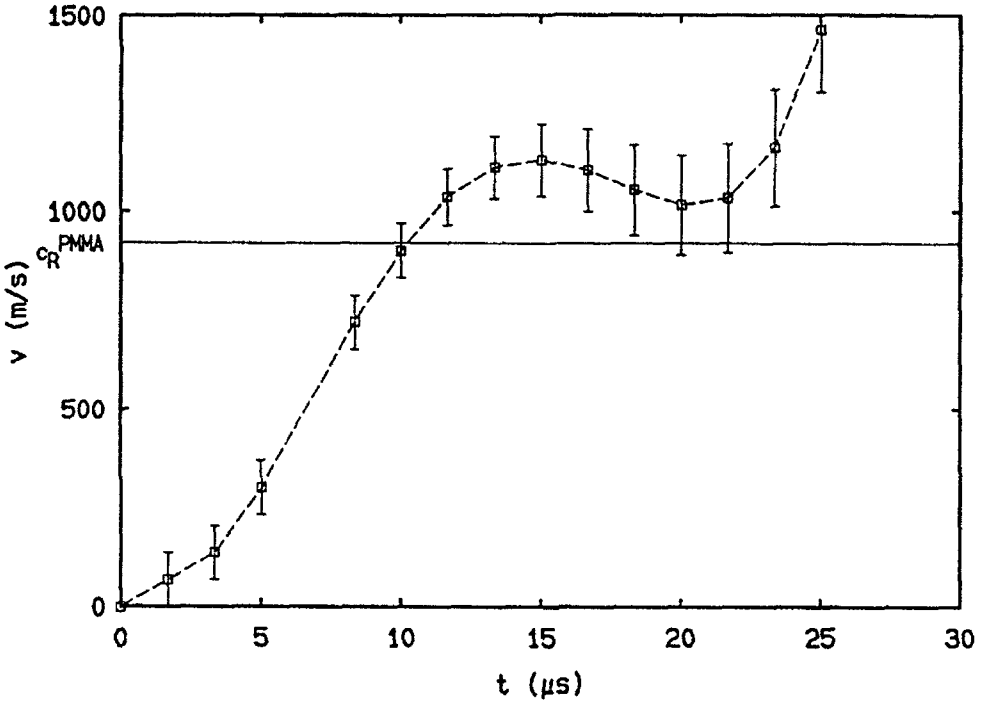

(a)

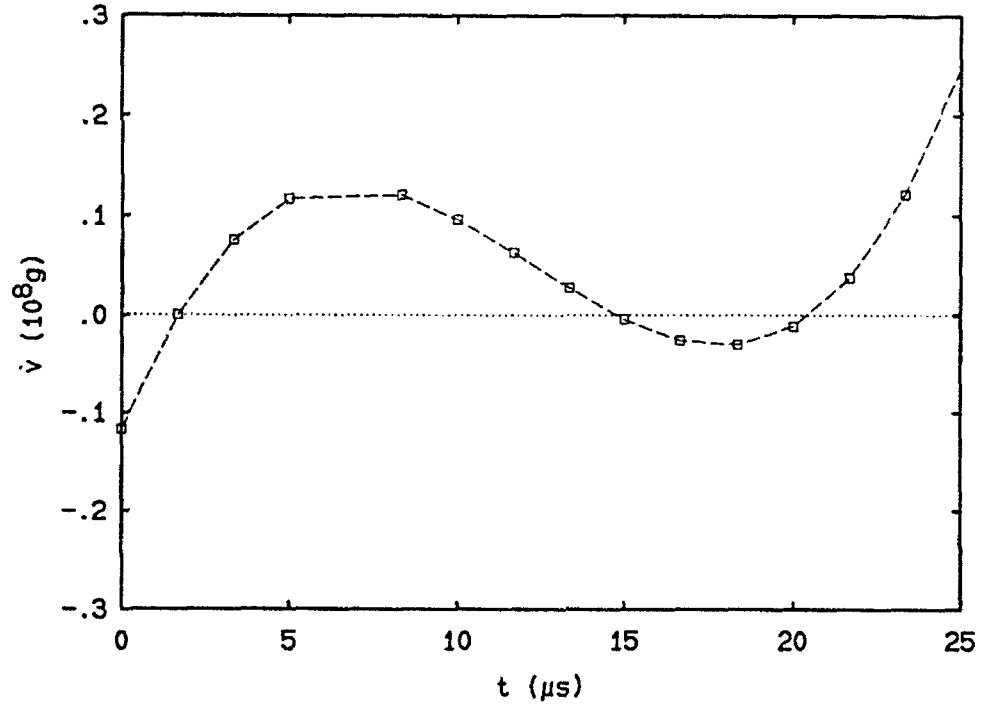

(b)

Figure 14: Velocity, (a) and acceleration, (b) time histories for the experiment shown in Figure 13.

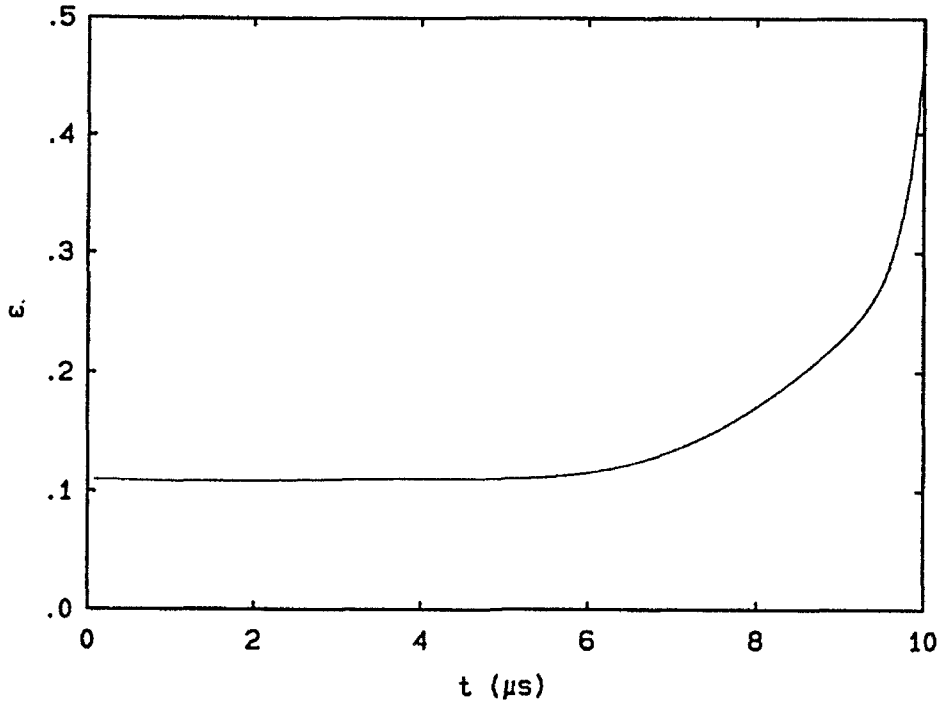

(a)

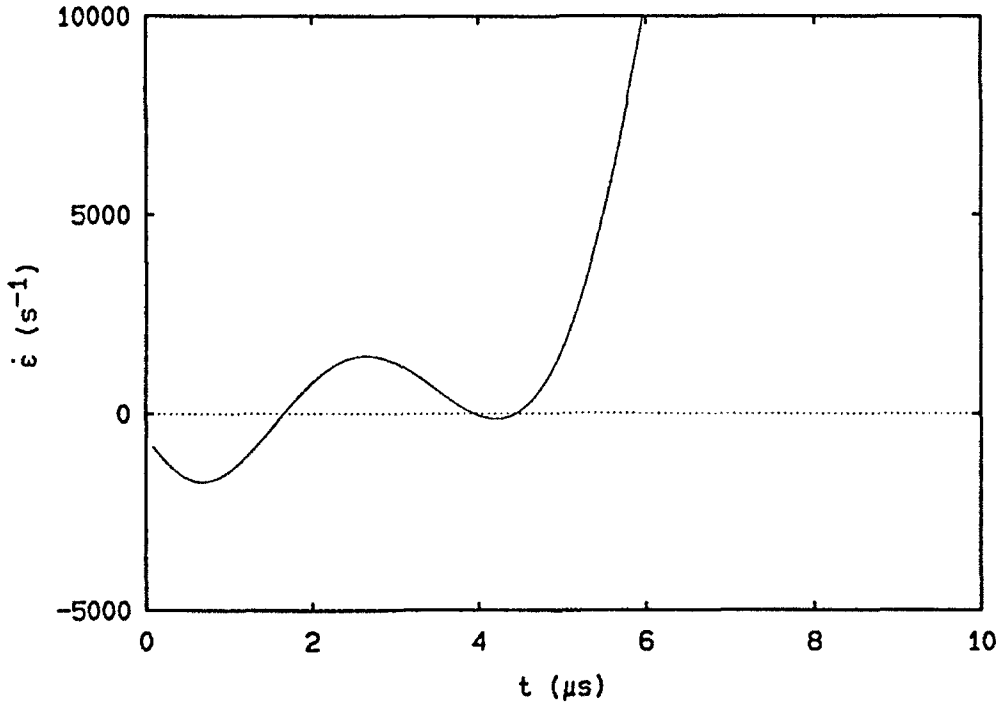

(b)

Figure 15: Time histories of mismatch parameter ϵ, (a) and its time derivative, (b) for the experiment shown in Figure 13.

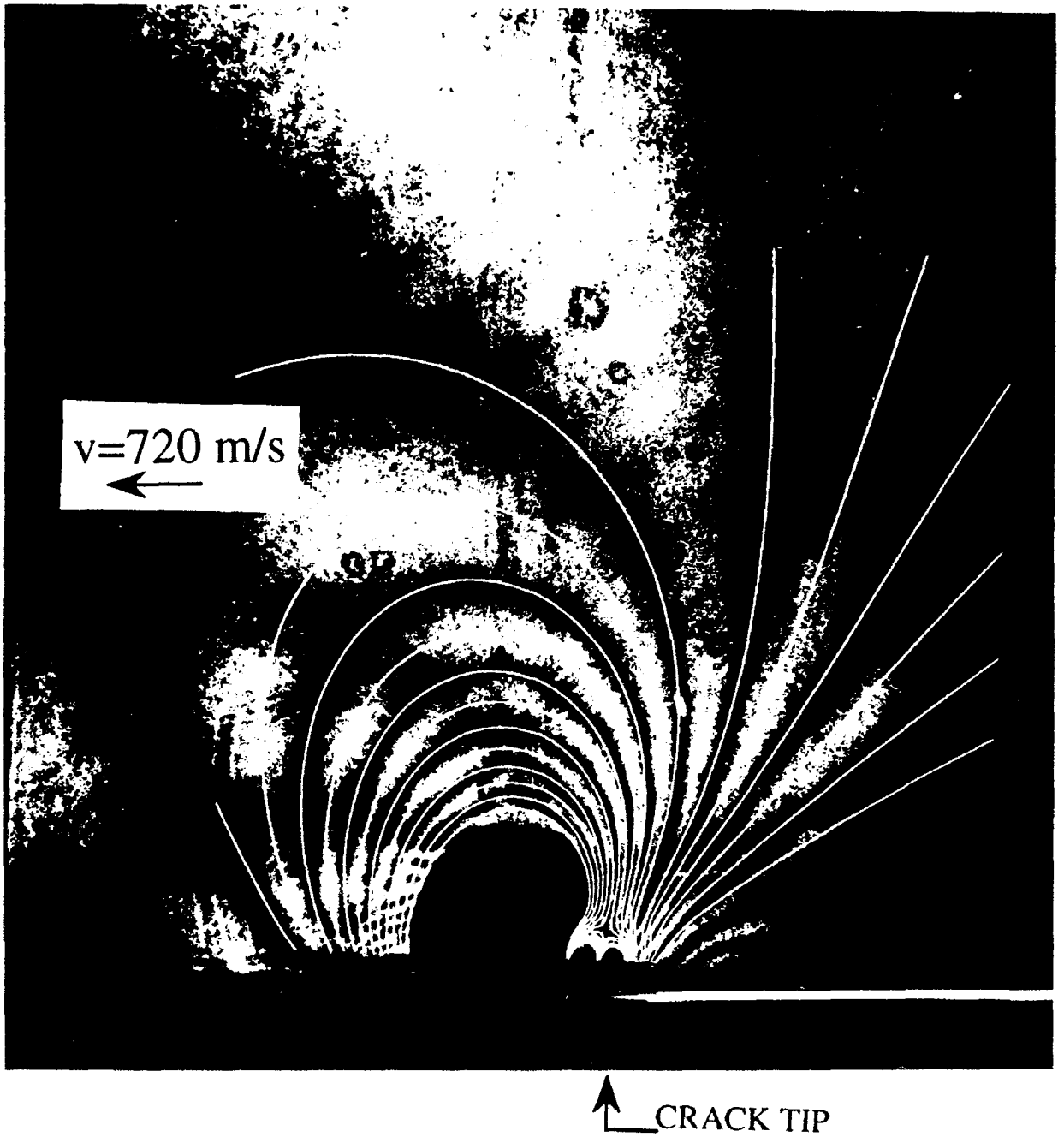

Figure 16: Comparison between the CGS fringe pattern and the fitted higher order transient stress field, equation (7.10), for a propagating crack in a PMMA/steel interface.

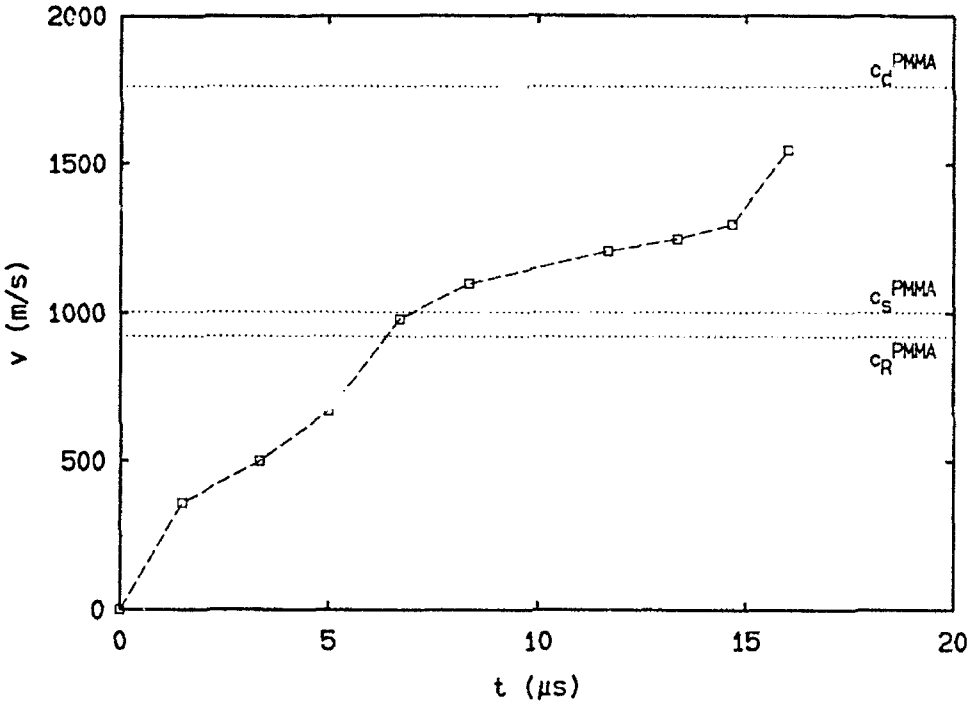

Figure 17: Velocity time history for the experiment shown in Figure 18.

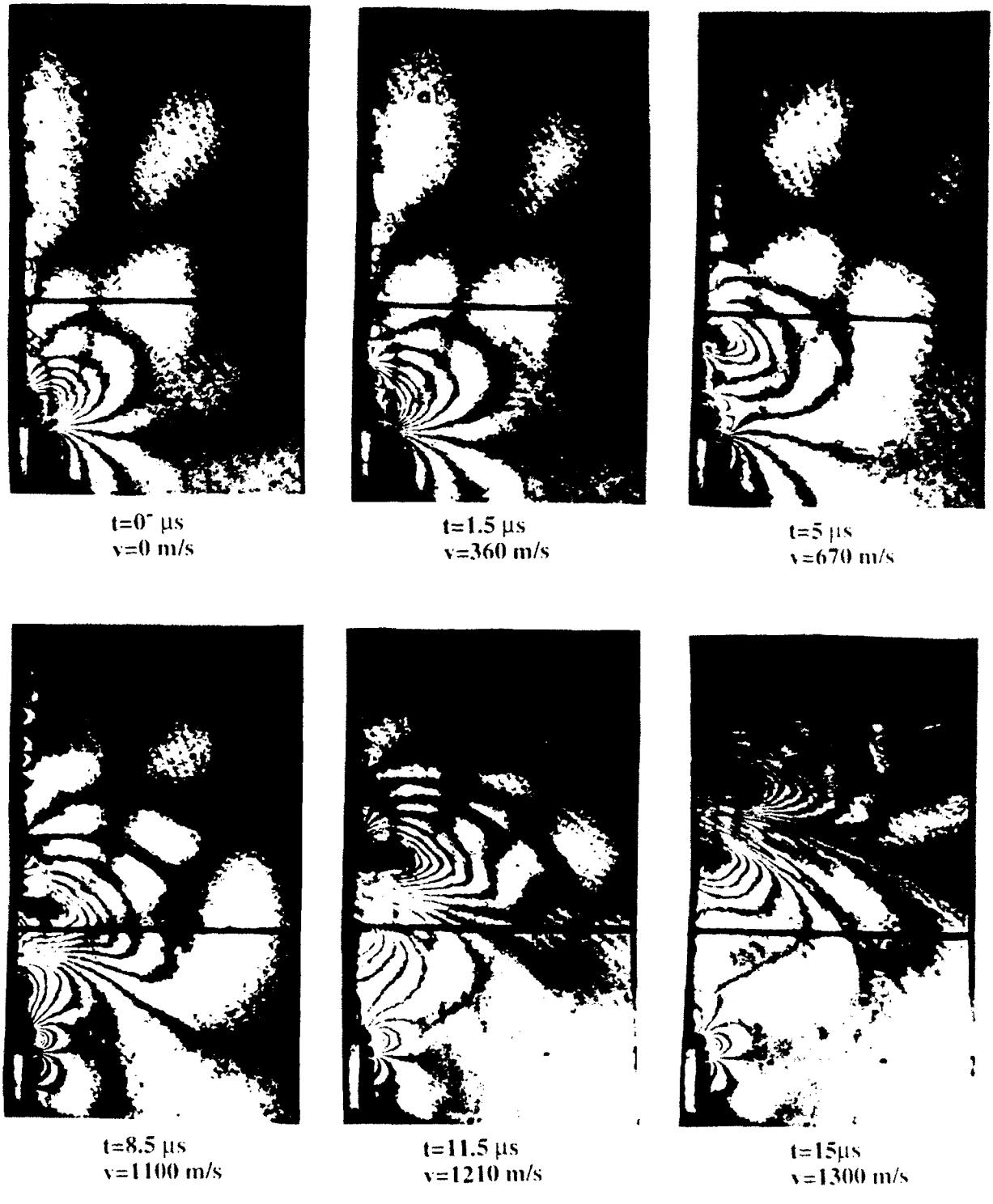

Figure 18: Selected sequence of CGS interferograms of a growing crack in an one point bend interfacial gas gun experiment. (A blunt starter notch was used)

t=10 μs
v=1000 m/s

t=12.5 μs
v=1170 m/s

t=15.5 μs
v=1190 m/s

t=18.5 μs
v=1470 m/s

Figure 19: CGS interferograms providing visual evidence of the highly transient nature of dynamic interfacial crack growth.